

# The Design, Development, and Evaluation of a Differential Pressure Gauge Directional Wave Monitor

by

Kevin R. Dodge

WHOI  
DOCUMENT  
COLLECTION

MISCELLANEOUS REPORT NO. 82-11

OCTOBER 1982



Approved for public release;  
distribution unlimited.

Prepared for

U.S. ARMY, CORPS OF ENGINEERS  
COASTAL ENGINEERING  
RESEARCH CENTER

Kingman Building  
Fort Belvoir, Va. 22060

03  
0581  
MR 82-11

Reprint or republication of any of this material shall give appropriate credit to the U.S. Army Coastal Engineering Research Center.

Limited free distribution within the United States of single copies of this publication has been made by this Center. Additional copies are available from:

*National Technical Information Service*  
ATTN: Operations Division  
5285 Port Royal Road  
Springfield, Virginia 22161

Contents of this report are not to be used for advertising, p...  
Citation of tr...  
endorsement or...  
products.

The finding...  
as an officia...  
so designated



UNCLASSIFIED

SECURITY CLASSIFICATION OF THIS PAGE (When Data Entered)

DD FORM 1 JAN 73 1473 EDITION OF 1 NOV 65 IS OBSOLETE

UNCLASSIFIED  
SECURITY CLASSIFICATION OF THIS PAGE (When Data Entered)

UNCLASSIFIED

- ii -

SECURITY CLASSIFICATION OF THIS PAGE(*When Data Entered*)

Wave height, period, and directional information as estimated from DPG data is compared with estimates from radar and Baylor gauge data at the field evaluation site.

Recommendations for future investigations and development of the DPG system are discussed.

UNCLASSIFIED

SECURITY CLASSIFICATION OF THIS PAGE(*When Data Entered*)

PREFACE

This report is published to provide engineers with a new technique and instrument to obtain directional wave data for use in coastal engineering design. A portion of the work discussed in this report was carried out under the U.S. Army Coastal Engineering Research Center's (CERC) Littoral Data Collection Methods and Engineering Applications work unit and the Field Research Facility's (FRF) Environmental Measurements and Analysis Work Unit under the Beach Restoration and Nourishment Program and the Coastal Flooding and Storm Protection Program of the Coastal Engineering area of Civil Works Research and Development.

The report is published as received from the author; results and conclusions are those of the author and are not necessarily accepted by CERC or the Corps of Engineers.

The report was prepared by Mr. Kevin Dodge while in graduate study at the University of Delaware and under the general supervision of Dr. Robert G. Dean.

CERC Technical Monitor for the work done under CERC Contract Number DACW72-81-C-0025 was Dr. Todd L. Walton, Jr.

Technical Director of CERC was Dr. Robert W. Whalin, Ph.D., P.E., upon publication of this report.

Comments on this publication are invited.

Approved for publication in accordance with Public Law 166, 79th Congress, approved 31 July 1945, as supplemented by Public Law 172, 88th Congress, approved 7 November 1963.



TED E. BISHOP  
Colonel, Corps of Engineers  
Commander and Director

ACKNOWLEDGEMENTS

Firstly, I would like to thank Dr. Robert Dean for his guidance and patience throughout this project.

I thank the other members of my graduate committee, Dr. Robert Anthony Dalrymple and Dr. Nobuhisa Kobayashi for their continuing interest and guidance, and especially Dr. Todd Walton whose assistance in the DPG project is greatly appreciated. I would also like to thank the U.S. Army Coastal Engineering Research Center and the Exxon Corporation for their support of the DPG study.

I would like to thank the many fine people who contributed to make the DPG project a success. Among them are the personnel of Setra Systems, Blake Cable, Brantner Connectors, Sea Data Corporation, Wilmington Valve and Fitting, and many other firms whose assistance is greatly appreciated. I am especially indebted to Curtis Mason and the excellent staff of the Field Research Facility, CERC, and to Jim Coverdale, Ed Green, and Rolin Essex for their dedicated technical assistance and advice.

I would like to give sincere thanks to my colleagues "Chip" Fletcher and Brian Jacobs who helped in the DPG installation and testing.

- 1 -

## TABLE OF CONTENTS

ACKNOWLEDGEMENTS . . . . .	iv
LIST OF FIGURES AND TABLES . . . . .	viii
LIST OF SYMBOLS . . . . .	xiii
CHAPTER I: INTRODUCTION . . . . .	1
CHAPTER II: CONCEPTS OF A DIFFERENTIAL PRESSURE GAUGE SYSTEM . . . . .	7
A. DPG Response to Surface Waves . . . . .	7
B. The Differential Pressure Gauge Directional Wave Monitor. . . . .	12
C. Selection of Transducers and Gage Length. . . . .	15
CHAPTER III: DPG HARDWARE . . . . .	20
A. Instrument, Service Box, and Cradle . . . . .	20
1. Introduction . . . . .	20
2. The Instrument Fuselage and Arms. . . . .	24
3. The Transducers . . . . .	25
4. The Isolation Sensor Diaphragms . . . . .	26
5. The Water-Tight Instrumentation Cylinder. . . . .	32
6. The Cable and Service Box . . . . .	32
7. The Electrical System . . . . .	33
8. The Instrument Cradle . . . . .	35
9. Biofouling and Corrosion Protection . . . . .	36
B. Data Retrieval. . . . .	37
C. Some Considerations of the Hardware Design. . . . .	37
1. Fuselage Isolation Diaphragms . . . . .	37
2. Height of Sensors . . . . .	38
D. Cost. . . . .	39
CHAPTER IV: DPG SOFTWARE. . . . .	40
A. Introduction. . . . .	40
B. Theory of Analysis. . . . .	41
C. Correction for Centering of Measurements. . . . .	47

TABLE OF CONTENTS (Continued)

D. Program Operation Notes . . . . .	50
1. Introduction . . . . .	50
2. Input and Screening of Data. . . . .	52
3. Conversion from Voltage to Pressure Signals. . . . .	52
4. Instrument Tilt Approximation. . . . .	53
5. Tide Calculation . . . . .	55
6. Development of Curvature Terms . . . . .	56
7. Significance of the Signals in Linear Theory . . . . .	56
8. FFT and Conversion to Water Surface Terms. . . . .	57
9. Failure of the Absolute Channel. . . . .	59
10. Failure of 3 Differential Channels . . . . .	62
11. Effective Period . . . . .	63
12. The Directional Fourier Coefficients . . . . .	63
13. Block-averaging. . . . .	64
14. Frequency Bands of Greatest Energy . . . . .	65
E. DPG Simulation and Error . . . . .	66
 CHAPTER V: LABORATORY DEVELOPMENT, CALIBRATION, AND TESTING OF THE INSTRUMENT . . . . .	76
A. Introduction . . . . .	76
B. Fluid Back-Filling the Sensors (System Modifications) . . . . .	76
C. Bench Calibration. . . . .	85
1. The Calibration Technique. . . . .	85
2. Testing for Air Bubbles. . . . .	88
3. Static Calibration Results . . . . .	90
4. Power Supply Sensitivity . . . . .	92
5. Transducer Drift . . . . .	92
6. Temperature Effect . . . . .	93
7. Absolute Sensor Back-Fill Pressure . . . . .	94
D. CERC Wave Tank Tests . . . . .	94
1. Introduction . . . . .	94
2. Installation . . . . .	95
3. Tests and Results. . . . .	97
E. The Second DPG Prototype . . . . .	105
 CHAPTER VI: FIELD INSTALLATION AND EVALUATION. . . . .	107
A. Installation at the FRF. . . . .	107
B. Instrument Orientation . . . . .	113
C. First Month's Inspection . . . . .	118

TABLE OF CONTENTS (Continued)

D. Results of DPG Data Analysis . . . . .	119
1. Introduction . . . . .	119
2. Time Domain Signal Analysis . . . . .	119
3. Record Length . . . . .	124
4. Capability of the DPG System . . . . .	134
5. Directional Spectra Smoothing . . . . .	135
6. Redundancy of DP2 and DP4 Measurements . . . . .	137
7. Energy Spectra from Differential Pressure Gauges . . . . .	140
8. Directional Estimates without the Absolute Pressure Gauge . . . . .	144
9. Arithmetic Development of the Curvature Terms . .	145
CHAPTER VII: RECOMMENDATIONS . . . . .	149
CHAPTER VIII: CONCLUSIONS . . . . .	155
REFERENCES . . . . .	160
APPENDIX A: Sample DPG Analysis Results; June 8-11, 1982 . . .	163
APPENDIX B: Typical Strip Chart Recordings from Bench Calibration . . . . .	183
APPENDIX C: A Partial List of DPG Dimensions . . . . .	189
APPENDIX D: Assembly and Maintenance of the DPG . . . . .	191
APPENDIX E: The Estimation of Higher Order Directional Fourier Coefficients . . . . .	200
APPENDIX F: Fortran Analysis Program for DPG Data . . . . .	207

LIST OF FIGURES AND TABLES

Figure

I-1,2,3	Approach of a long-crested wave to two adjacent pressure sensors. . . . .	4
II-1,2,3	Instrument response to a five-foot surface wave in varying water depths . . . . .	10
II-4	Differential pressure transducer response to a five-foot surface wave in twenty-five feet of water with varying deployment depths . .	11
II-5	Schematic representation of the DPG. . . . .	13
II-6	Differential pressure response with water depth and frequency. . . . .	19
III-1	The DPG Instrument . . . . .	21
III-2	The DPG instrument secured to the steel cradle .	22
III-3	Rendering of the DPG fuselage, arms, sensors, and water-tight instrumentation cylinder . . . . .	23
III-4	Assembly drawing of an isolation sensor diaphragm	27
III-5	Isolation sensor diaphragms shown attached by flexible and nylon tubing through the top of the water-tight instrumentation cylinder and into the transducers . . . . .	28
III-6	Assembled water-tight instrumentation cylinder with sensors penetrating the top plate . . . . .	30
III-7	The transducer stack before insertion into the instrumentation cylinder . . . . .	31
III-8	Wiring diagram for the DPG . . . . .	34

LIST OF FIGURES AND TABLES (Continued)

IV-1	Coordinate system adopted for DPG analysis. . . . .	41
IV-2	Flow chart of DPG analysis program. . . . .	51
IV-3	Instrument tilt above the seafloor. . . . .	54
IV-4	Four roots of tangent ( $2\theta$ ). . . . .	61
IV-5	Simulated time record of water surface elevation. .	67
IV-6	Raw energy spectra; Simulation Case 1. Illustrates presence of three distinct wave trains. . . . .	68
IV-7	Non-weighted 7-coefficient Fourier series direc- tional energy distribution. Simulation Case 1. Illustrates presence of three distinct wave trains with different directions. .	69
IV-8	Raw energy spectra; Simulation Case 2 . . . . .	71
IV-9	Non-weighted 7-coefficient Fourier series directional energy distribution. Simulation Case 2. Illustrates good directional spectra agreement with slight differences due to leakage. . . . .	72
IV-10	Non-weighted 7-coefficient directional energy spectra; Simulation Case 3. Illustrates software inability to clearly define two directions per frequency - waves of equal height. .	73
IV-11	Non-weighted 7-coefficient directional energy spectra; Simulation Case 4. Illustrates software inability to clearly define two directions per frequency - waves of unequal height	73
IV-12	Non-weighted directional energy spectra using the first seven directional Fourier coefficients compared to the first five . . . . .	75

LIST OF FIGURES AND TABLES (Continued)

V-1	Schematic representation of differential pressure transducer and isolation sensors . . . . .	78
V-2	Cross-section of isolation diaphragm with an object load applied. . . . .	85
V-3	The DPG bench calibration system . . . . .	87
V-4	Strip chart recording illustrating possible existence of air in arm side of dP4. . . . .	89
V-5	DPG transducer calibration curves. . . . .	91
V-6	Orientation of the DPG during CERC wave tank tests. . . . .	95
V-7	Sample strip chart recording; CERC test. Configuration I. DP3 arm end-cap left accidentally on. . . . .	98
V-8	Sample strip chart recording; CERC test. Configuration I. . . . .	100
V-9	Sample strip chart recording; CERC test. Configuration II . . . . .	101
V-10	Comparison of DPG absolute pressure gauge and CERC resistance wave probe . . . . .	102
VI-1	Site of the DPG field evaluation . . . . .	108
VI-2	Nearshore bathymetry of installation site. .	109
VI-3	Preparing for field installation: the DPG suspended underneath the operator's platform of the CRAB . . . . .	110
6-1	Orientation Headings of the DPG Arms (Table). . . . .	114

LIST OF FIGURES AND TABLES (Continued)

VI-4	Typical influence of the steel cradle upon the magnetic compasses used for orientation measurements . . . . .	115
6-2	Comparison of Tide Level (Table) . . . . .	121
VI-5	Portion of time record from DPG signals. . .	122
VI-6	DPG analysis results using the full record length of 17 minutes with effective 2 Hertz sampling . . . . .	126
VI-7	DPG analysis results using the first 8.5 minutes of the record, (4 Hertz sampling . . . . .	127
VI-8	DPG analysis results using the last 8.5 minutes of the record, (4 Hertz sampling . . . . .	128
VI-9	Block-averaged energy spectra of water surface displacement for a 17 minute long record and 8.5 minute long records. . .	129
VI-10	Non-weighted directional spectra of peak energy band (11.0 seconds) for a 17 minute long record and 8.5 minute long records . . . . .	130
6-3	Comparison of DPG Results with FRF Observations (Table) . . . . .	131
VI-11	Photographs of CERC radar screen illustrating wave activity from June 8 - June 11, 1982. .	132
VI-12	Non-weighted directional spectra of the first two peak energy bands:ABS, dP2, and dP3 gauge combination and ABS, dP4, and dP3 gauge combination. Well-defined swell .	138
VI-13	Non-weighted directional spectra of the first two peak energy bands:ABS, dP2, and dP3 gauge combination and ABS, dP4, and dP3 gauge combination. Poorly-defined sea. .	139

LIST OF FIGURES AND TABLE (Continued)

VI-14	Block-averaged energy spectra of water surface displacement and water surface slope. . . . .	141
VI-15	Wave crest approximately aligned with dP2 arm . . . . .	142
VI-16	Typical portion of time series of dP2 and dP4 "slope" signals with the associated dP4-dP2 "curvature" signals. . . . .	145
VI-17	Block-averaged power spectra of water surface displacement and curvature terms . . .	147
A-1	Comparison of Other Directional Estimates (Table). . . . .	182
D-1	Back-filling the center sensors. . . . .	194
D-2	Back-filling the arm sensors . . . . .	195

LIST OF SYMBOLS

ABS	absolute pressure (signal or transducer)
$a_o, a_n, b_n$	directional Fourier coefficients
$B_n$	$\pi D_n^4 / \mu_n l_n$
$c'$	normalized co-spectra
D	inner tubing diameter; distance between gauges
$dP_n$	differential pressure along arm n
$F(\delta, \theta)$	complex directional amplitude spectrum
FS	full scale
h	water depth
H	wave height
$H_{1/3}$	significant wave height
J	number of wave trains present in simulated record
$J_n$	Bessel function
$K_D^{-1}$	folding time of sensor response
$K_p$	pressure response function
$K_u$	current response function
$k_x$	wavenumber in the x direction
$k_y$	wavenumber in the y direction
l	length of tubing
$l_{bf}$	height of sensor above transducer
N	number of sample points analyzed; maximum number of Fourier coefficient pairs
P	pressure
$P_{atm}$	atmospheric pressure

LIST OF SYMBOLS (Continued)

$P_{bf}$	sensor back-fill pressure
$P_{dyn}$	dynamic pressure
$P_{mean}$	mean pressure of record
$P_x$	pressure differential in x direction
$P_y$	pressure differential in y direction
$Q$	difference in water column height above sensors; volumetric flow rate in sensor line
$q'$	normalized quad-spectra
$R$	rated capacity of transducer
$s$	sensor height above bottom
$S(\delta)$	unidirectional spectral density
$S(\delta, \theta)$	directional energy spectrum
$S^*(\delta, \theta)$	measured directional energy spectrum
$t$	time
$U$	current
$x$	x-axis location
$y$	y-axis location
$z_s$	water column height above sensor
$\alpha$	instrument tilt; transducer diaphragm volumetric change proportionality constant to pressure differential
$\beta$	angle between gauges
$\beta_n'$	apparent heading of DPG arm n
$\beta_n$	actual heading of DPG arm n
$\Delta P_f$	frictional pressure drop along circular pipe
$\Delta t$	data sampling interval
$\Delta V_c$	volume displaced by transducer diaphragm
$\Delta x$	gage length
$\epsilon$	phase angle
$\epsilon_n$	error in compass measurement of DPG arm n
$\eta$	water surface displacement
$\eta_x$	water surface slope in x direction

LIST OF SYMBOLS (Continued)

$\eta_y$	water surface slope in y direction
$\eta_{xx}$	water surface curvature in x direction
$\eta_{yy}$	water surface curvature in y direction
$\eta_{xy}$	water surface curvature in x-y direction
$\mu$	coefficient of dynamic viscosity
$\gamma'$	specific weight of seawater
$\gamma'_{bf}$	specific weight of back-filling fluid
$\delta$	wave frequency
$\bar{\delta}$	effective frequency
$\delta_n$	spectral frequency
$\theta$	wave direction
$\bar{\theta}_n$	mean direction



CHAPTER I  
INTRODUCTION

The need for widespread wave data of improved quality has been recognized by the ocean science and engineering community for some time. In an editorial in *Shore and Beach* (October, 1974), M. P. O'Brien noted that:

Observations and measurements of ocean waves have been made at points along the coasts of the United States -- at some locations over a considerable period of time -- but the accumulated data fall short of the need in geographical distribution, duration of the records, and detail of wave characteristics.... [Data]...suffers from a number of deficiencies, notably the lack of wave direction measurements....

Significant strides have been made in the measurement and recording of wave amplitude and period since Dean O'Brien's commentary, but the success of these systems has not been matched by the development of numerous reliable wave sensors with directional capability. Despite the importance of directional wave information to offshore and coastal engineers as well as ocean scientists, the development of directional wave sensors has lagged behind other ocean

instrumentation advancements. Indeed, a recent conference of scientists and engineers skilled in wave measurement cited the improvement of the measurement, analysis, and reporting technology of directional wave spectra as the first priority of future ocean wave research and development (Dean, 1982).

Some directional wave data are available today using both remote sensing and in-situ techniques. Remote sensing, a promising alternative for the future because of its capability to monitor large ocean surface areas, presently suffers from the expense and lack of availability of air and space craft platforms as well as sometimes lengthy and expensive data analysis. Further, the development of remote sensing still requires dependable ground verification. Although in-situ systems are single point sensors, they offer some advantages over remote sensing techniques. In-situ instruments can monitor the sea surface continuously, are composed of less expensive and less complex hardware, and can generally offer relatively inexpensive data reduction that approaches real-time. Although more difficult to install and service, submerged in-situ systems offer advantages over surface riding or piercing instruments in that submerged hardware is less prone to loss, does not interfere with the propagating wave field, and is more likely to operate without malfunction during extreme wave events. Such underwater systems, however, are generally limited to use in near-shore applications or at a shallow depth from a fixed platform in deep water.

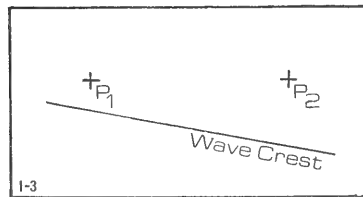
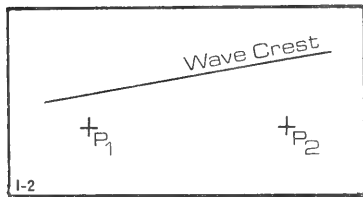
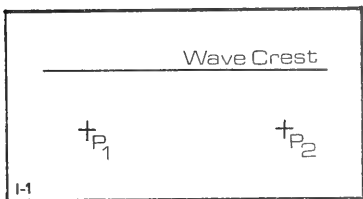
Several types of underwater in-situ systems have been suggested; some of which are operational presently. Such instruments include tri-axial current meters (van Heteren and Keyser, 1981), bi-axial current meters with one pressure transducer or wave staff (Aubrey, 1981; Nagata, 1964; Bowden and White, 1966; Simpson, 1969), arrays of pressure transducers (Peacock, 1974; Seymour, 1978; Mobarek, 1965; Chakrabarti, 1971; Chakrabarti and Snider, 1973; Panicker and Borgman, 1970; Ploeg, 1972), and measurement of the bi-axial components of the force on a sphere together with bottom pressure fluctuations (Suzuki, 1969). A review of many procedures that have been used to make directional wave measurements is presented by N. N. Panicker (1974), K. Rikiishi (1977), and more recently within the Proceedings of the National Research Council Workshop on Wave Measurement Technology (1982).

Data from some current meter systems is often suspect after deployment because of the susceptibility of the instrumentation to bias from bio-fouling and corrosion. Bottom-mounted pressure transducers, on the other hand, have been used with considerable success for wave sensing for several years (Forristall, 1981).

The concept of measuring the directional characteristics of waves is fairly straightforward. If one considers a long wave crest approaching parallel to the alignment of two pressure sensors, as in Figure I-1, it is easy to imagine both sensors recording the crest passage simultaneously. If the wave crest approaches obliquely to

the pressure sensors, as in Figure I-2, one could imagine that one sensor would report the passage of the crest before the other. The difference in pressure over time between the sensors' records can be analyzed by well-known techniques and a first estimate of the wave direction calculated, (Longuet-Higgins, Cartwright, and Smith, 1963). There is, of course, a directional ambiguity with only two sensors

since a wave approaching as in Figure I-3 would create the same pressure record over time as in Figure I-2. Such ambiguities may be resolved by additional sensors.



FIGURES I-1,2,3: Approach of a long-crested wave to two adjacent pressure sensors.

Presently, the analysis of data from bottom-mounted arrays of pressure sensors usually develops pressure differences through the subtraction of individually measured absolute pressures. However, instantaneous differences in the transducers' records due to wave action are typically very small when compared to the large pressure values that they

are required to record. Hence, the pressure difference across an array is calculated by subtracting two large numbers in order to generate a very small number. Such a system lends itself to inherent inaccuracies. For example, a bottom-mounted transducer in twenty feet of water records the passage of a three foot wave crest of nine second period with a value of 24.78 psia compared to the 23.64 psia reading under still water. A similar transducer placed twenty feet away at a 45 degree angle to the wave crest would report 24.69 psia at the moment the crest passes its neighboring gauge. (Linear wave theory is utilized for this example.) The arithmetic difference calculated between the transducers, 0.09 psia, is less than one half of one per-cent of the still water value each transducer would record or less than nine percent of the dynamic pressure caused by the passing wave. The difference can be improved by increasing the distance between transducers -- at the expense of a more physically unmanageable array, greater error in the assumption of linear water surface slope, and introduction of directional ambiguities for the higher frequencies present.

It is the contention of this thesis that the accuracy of the directional wave spectrum calculated from such small differences between large pressure values is questionable. The accuracy and physical size of the pressure sensor array can be improved by utilizing differential pressure transducers designed to record small pressure differences between two points. This thesis will document

the design, installation, and performance of such an instrument as carried out at the University of Delaware and the Coastal Engineering Research Center's test and field research facilities in Fort Belvoir, Virginia, and Duck, North Carolina.

Since the majority of industries and machinists associated with the project's instrumentation work in the English system of units in the United States, the English system was used in the development and reporting of this project.

## CHAPTER II

### CONCEPTS OF A DIFFERENTIAL PRESSURE GAUGE SYSTEM

#### A. DPG Response to Surface Waves

As previously mentioned, it is the difference in pressure between points that must be considered in the determination of wave direction. Differential pressure transducers generate an electrical voltage proportional to the fluid pressure difference on opposite sides of a mechanical diaphragm. Absolute (or gage) pressure transducers report only the fluid pressure at one point. Using absolute (or gage) transducers, the difference in pressure between two points must be arithmetically created by subtracting the pressures reported at each of the two points of interest. Since the differential transducer measures pressure differences directly, the differential gauge can be considered to be an inherently more effective instrument for determining wave direction. Furthermore, the response with depth of the differential pressure is a maximum over a range of frequencies that is more representative of typical ocean gravity waves. For a pressure transducer located at height  $s$

above bottom, the dynamic pressure at the sensor can be expressed over time  $t$  as:

$$P_{dyn}(x, y, s; t) = \gamma \frac{H}{2} K_p \cos(k_x x + k_y y - \sigma t + \epsilon) \quad (2.1)$$

where  $K_p = \frac{\cosh ks}{\cosh kh}$

and  $H$  = wave height

$k_x = k \cos \theta$  = wavenumber in the x-direction

$k_y = k \sin \theta$  = wavenumber in the y-direction

$\theta$  = wave direction

$\sigma$  = wave frequency

$h$  = water depth

$\gamma$  = specific weight of water

$\epsilon$  = phase angle

The components of differential pressure differs in phase and by a factor of wavenumber:

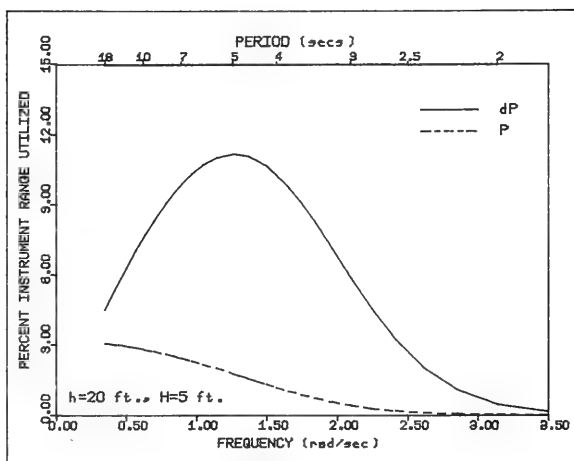
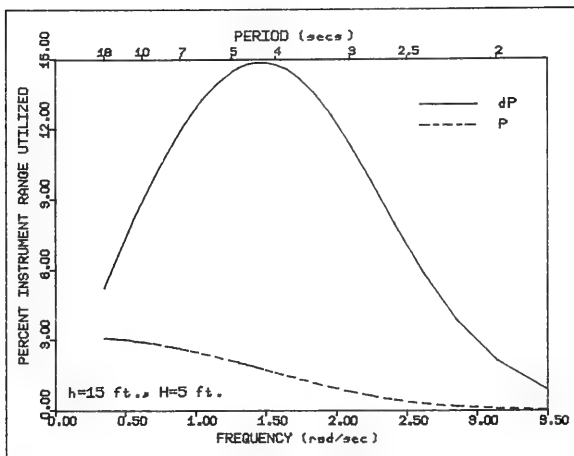
$$dP(x, t, s; t) = - \gamma \frac{H}{2} k \begin{bmatrix} \cos \theta \\ \sin \theta \end{bmatrix} K_p \sin(k_x x + k_y y - \sigma t + \epsilon) \begin{bmatrix} \frac{\partial x}{\partial y} \end{bmatrix} \quad (2.2)$$

A current meter similarly located at a depth  $s$  will record a signal under waves such as:

$$U(x, y, s; t) = \frac{H}{2} \sigma K_u \cos(k_x x + k_y y - \sigma t + \epsilon) \quad (2.3)$$

where:  $K_u = \frac{\cosh ks}{\sinh kh}$

Although the magnitude of both the pressure and current decreases steadily over increasing frequency, the differential pressure signal reaches a maximum at an intermediate frequency. This is illustrated graphically in Figure II-1, which depicts the dynamic response of pressure and differential pressure gauges located near the bottom with a wave crest of 2.5 foot amplitude. In the upper-most curves, the differential gauge is assumed to sample two points separated by three feet coincident with the wave ray. The lower curve represents the difference in pressure monitored by two absolute pressure gauges separated by twenty feet along the wave ray. Each curve is normalized by typical values of the rated capacity of the instruments, (35 psia for the pressure transducer, and  $\pm 0.5$  psid for the differential transducers). Figure II-1 represents a water depth of fifteen feet, while Figures II-2 and II-3 represent twenty and twenty-five feet water depths respectively. In each case, the transducers are located three feet off the seafloor. It is clear that the differential pressure signal utilizes a greater portion of



FIGURES II-1,2: Instrument response to a five-foot surface wave in varying water depths. Sensors are three feet from the seafloor.

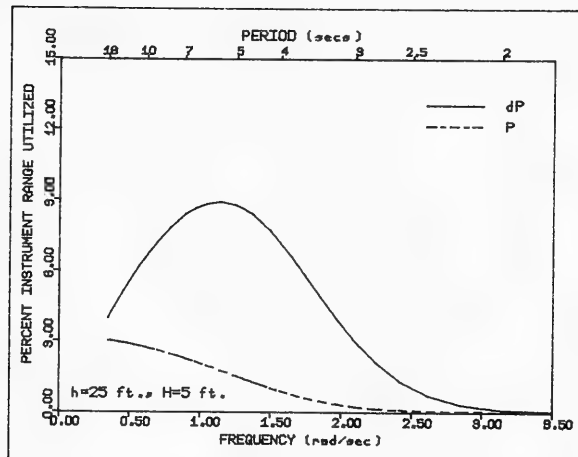


FIGURE III-3: Instrument response to a five-foot surface wave, (continued from previous page).

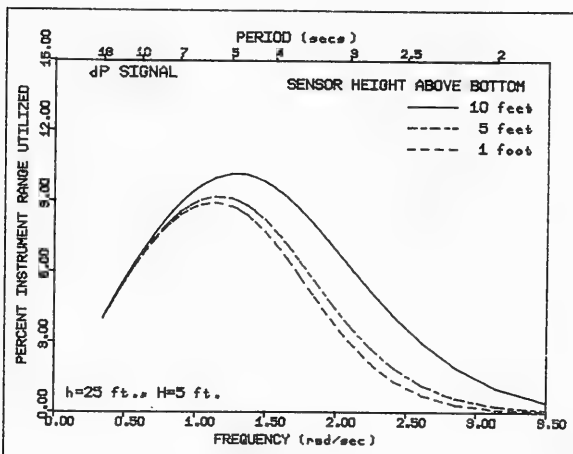


FIGURE II-4: Differential pressure transducer response to a five-foot surface wave in twenty-five feet of water with varying deployment depths.

the instrument's dynamic range and reaches its greatest response level for waves between four and six second periods. Sensitivity to longer period waves increases with increasing water depth. Differential pressure response increases as the transducers are raised off the seafloor, as expected, and the greatest sensitivity shifts to waves of higher frequency (Figure II-4).

In Figures II-1 through II-4, the response of the differential transducer was developed over a pressure sample spacing of only three feet -- less than one-sixth of the gage length of conventional pressure sensor array systems. Typical arrays generally develop two orthogonal measurements of water surface slope by sampling points separated by twenty to thirty feet. The differential pressure gauge concept, then, suggests that more efficiently measured directional information can be obtained with a considerably smaller instrument than is presently used.

#### B. The Differential Pressure Gauge Directional Wave Monitor

To test the effectiveness of an array using differential pressure transducers, the differential pressure gauge directional wave monitor (DPG) was developed. Using small distances between differential pressure sampling points, it was possible to design a system which directly measures the water surface slope yet is physically smaller, more manageable, and potentially more accurate

than conventional pressure sensor arrays.

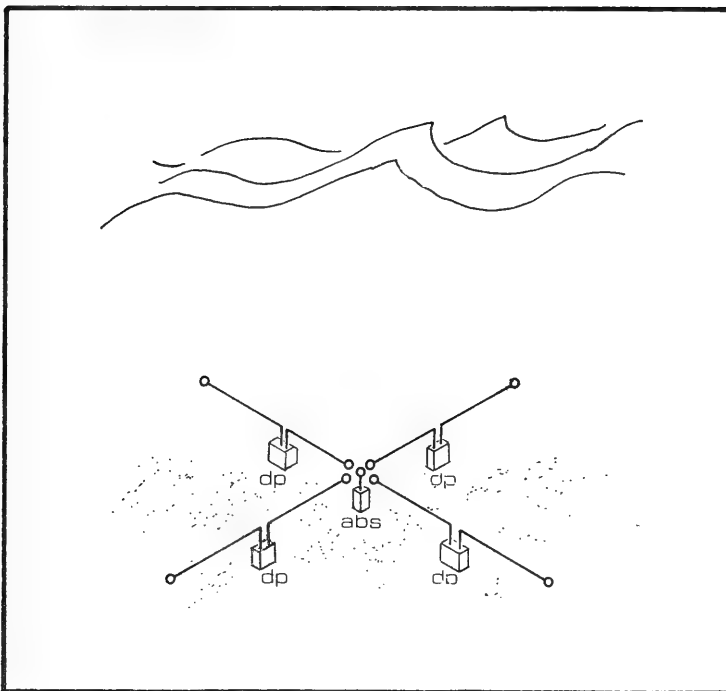


FIGURE II-5: Schematic representation of the DPG.

The DPG samples the pressure about its center using an absolute pressure transducer and simultaneously samples the differential pressures on the bow, port, aft, and starboard sides of

the instrument center using four differential pressure gauges, (Figure II-5). The differential gauges directly infer water surface slope, and since there are two such measurements along two axes through the instrument center, it is possible to arithmetically develop the water surface curvature along each axis. It will be demonstrated in Chapter IV that these measurements permit the estimation of the first seven Fourier coefficients of the directional wave spectrum. Conventional analysis from submerged pressure sensor arrays arithmetically develops one measurement of the water surface slope along each of two axes. Typical surface riding buoys similarly measure the slope along each of the two axes. This data, along with the water surface displacement record, permits the generation from these systems of the first five directional Fourier coefficients. The cloverleaf buoy, a cluster of three surface riding buoys, is capable of estimating the first nine Fourier coefficients, (Mitsuyasu, 1973; Cartwright and Smith, 1964).

It can be shown that it is possible to generate up to the first  $M(M-1)+1$  directional Fourier coefficients for an array with  $M$  number of gauges (Borgman, 1969). Using this technique, pressure sensor arrays such as the Scripps Sxy gauge (Seymour, 1978) could generate the first nine directional Fourier coefficients. The DPG, in the configuration described, could develop the first eleven coefficients. The DPG could potentially develop the first twenty-one coefficients with the same number of transducers in a different

configuration. This analysis technique is discussed in Appendix E.

#### C. Selection of Transducers and Gage Length

The selection of the gage length between the two points to be compared by the differential pressure transducers is dependent upon three criteria: (1) the characteristics of the transducer, (2) the error in approximating the water surface slope as a linear function between two sampled points, and (3) reasonable size limitations of the instrument. The third criterion limits the gage length per transducer to a maximum of about five feet if one imposes a design constraint of easy instrument manageability. At such small spacings, the maximum error in linearly approximating the water surface slope between sample points is less than one and one-half percent for the shortest waves of interest, (say, 3.2 seconds).

Having satisfied the second and third criteria, the first criterion remains. In the selection of the differential transducers, one must consider the physical size, ruggedness, cost, and availability of a transducer that can measure small "wet" bidirectional pressure fluctuations. The desired rated capacity of the transducer is a function of the maximum wave height expected and the ability of the transducer to detect and report a pressure difference of a minimum wave condition beyond the ambient and electrical noise level. One might determine the rated capacity by

first selecting an instrument deployment depth according to the site and the wave frequencies that are of most interest or are most likely to be encountered -- remembering that deeper installations require more sensitive transducers. A maximum wave height at the most sensitive frequency for the chosen depth is then considered with the manageable gage length restriction in mind. The maximum differential pressure is then calculated from Equation 2.2. The result is an estimate of the rated capacity of the transducer needed. This estimate is then used to select a transducer available from industry. One next considers the noise level of the system to determine whether the selected instrument is capable of reporting the minimum differential pressure of interest, (i.e., a small amplitude wave of frequency higher or lower than that of the instrument's most sensitive range at the chosen depth). Satisfied with the results, the gage length,  $\Delta x$ , is fine-tuned based on the rated capacity of the transducer,  $R$ , and the maximum wave of interest. From Equation 2.2,

$$\Delta x = \frac{R}{\gamma H k \cos \theta K_p} \quad (2.4)$$

The instrument's response to a minimum wave condition is checked again using the newly calculated gage length to ensure that a reasonable signal to noise ratio is maintained for small amplitude, long period waves.

The installation site of the DPG was proposed as the United States Army Corps of Engineers Field Research Facility (FRF) at Duck, North Carolina, operated by the Coastal Engineering Research Center (CERC). The instrument was to be placed near and hard-wired to the Facility research pier. After examining the bathymetry near the pier and considering the high cost of underwater cable, a nominal deployment depth of 20 feet was selected. This indicated that the instrument would be most sensitive to waves of about 5 second period, (Figure II-2). This was considered acceptable at the time since the mean monthly nearshore wave periods for this site were reported between 4.8 and 6.5 seconds (SPM, Figure 4-11, 1977). (It was discovered much later that this estimate was poor. A better estimate is given as about 7.5 seconds from Birkemeier, et.al., (1981).) A design wave height of 16 feet was chosen and considered with a gage length of five feet. This suggested the use of a  $\pm 0.6$  psid transducer which was unavailable. A  $\pm 0.5$  psid transducer was selected instead, mandating a gage length of 4.15 feet (1.27 meters) using Equation 2.3.

The overall dimensions of the final instrument, then, became 9 feet - 9 inches (2.97 m) along each axis (including protective caps on the ends of each arm) and 40 inches (1 m) in height to accomodate the electronics package.

The response of an instrument of this configuration in varying depths of seawater is illustrated in Figure II-6. The contours represent lines of equal transducer response per  $\sqrt{foot}$  of wave height normalized by the rated capacity of the transducer. The fields of highest value indicate the environmental conditions conducive to greatest instrument performance.

The absolute transducer was selected with a rated capacity of 50 psia (because of cost and availability) which provides the DPG the capability to measure a pressure head of over 75 feet.

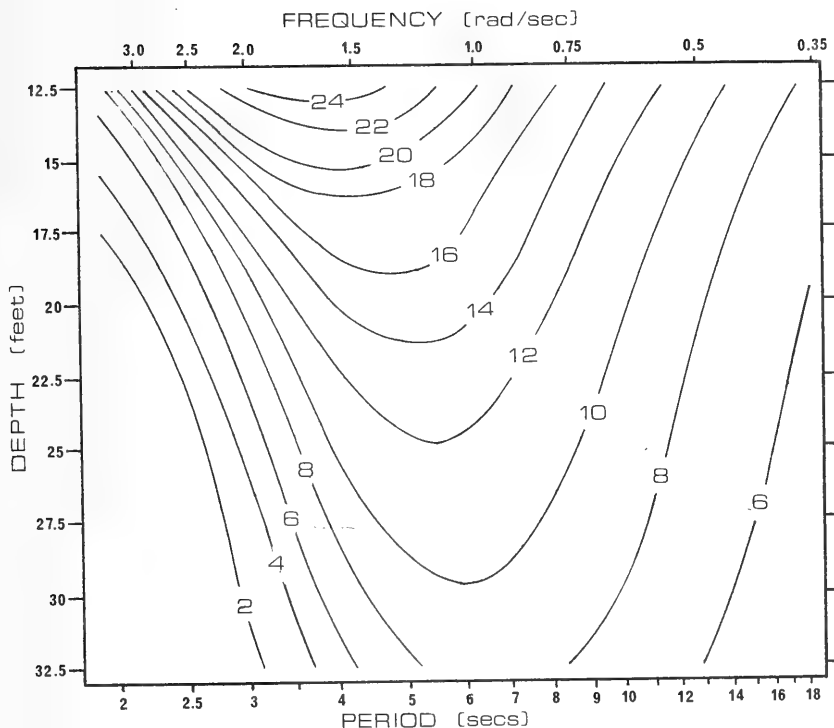


FIGURE II-6: Differential pressure response with water depth and frequency. Contours are lines of equal  $dP$  response normalized by the rated capacity of the instrument, (1.0 psid). (Sensors are 3.875 feet from the seafloor; differential gage length = 4 feet along wave ray; wave height = 5 feet.)

CHAPTER III  
DPG HARDWARE

A. INSTRUMENT, SERVICE BOX, AND CRADLE

1. Introduction

The in-situ instrumentation is contained in a poly-vinyl chloride (PVC) structure that is secured to a steel cradle moored to the seafloor. The PVC structure, or "instrument", as it is hereafter called, consists of a central tube, or "fuselage", and four "arms" that extend from near the top of the fuselage. A plexiglass service box, also attached to the cradle, provides storage for eighty feet of unarmored cable at the installation site. Figure III-1 illustrates the instrument and Figure III-2 depicts the steel cradle with the instrument in place suspended under the Field Research Facility's CRAB vehicle.

This chapter describes the DPG system as installed at the FRF, Duck, N.C. Several components of the system were altered from the original design during DPG assembly and laboratory testing. The discussion of these modifications is presented in Chapter V.

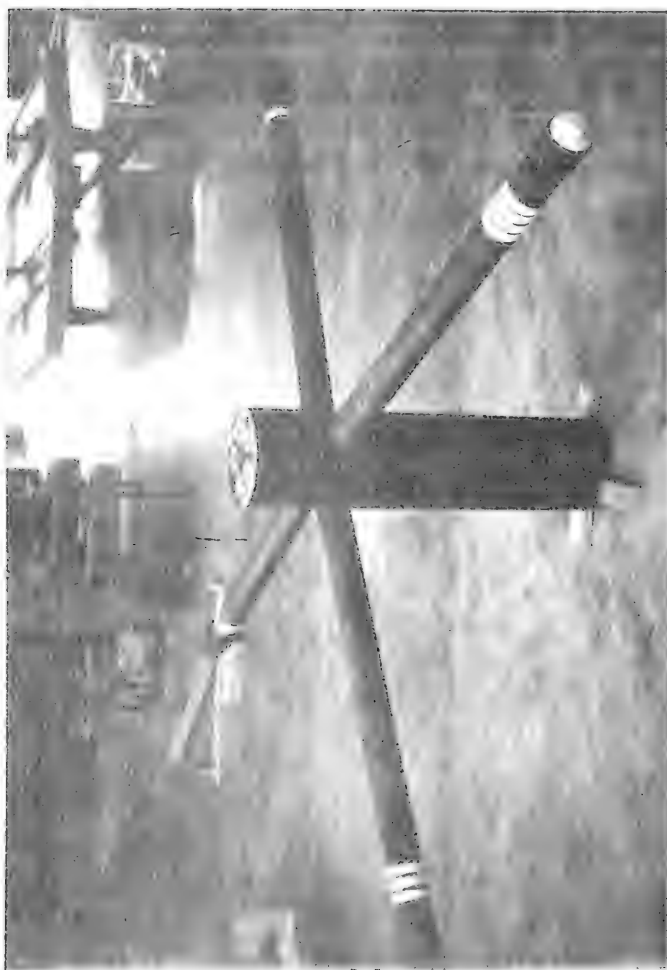


FIGURE III-1: The DPG Instrument.



FIGURE III-2: The DPG instrument secured to the steel cradle. The assembly is suspended beneath the Coastal Research Amphibious Buggy (CRAB) operated by the CERC Field Research Facility.

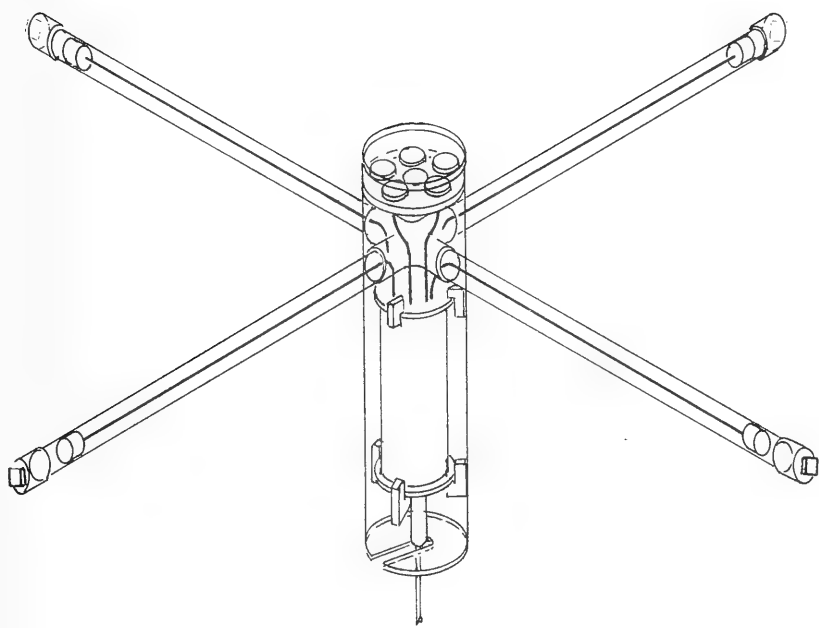


FIGURE III-3: Rendering of the DPG fuselage, arms, sensors, and water-tight instrumentation cylinder.

## 2. The Instrument Fuselage and Arms

The fuselage section of the instrument is ten inches in diameter and forty inches in length, (Figure III-3). It secures a circular plate with five pressure-sensing "isolation" diaphragms and a water-tight cylinder that contains the pressure transducers. Both ends of the fuselage are covered by plexiglass plates to prevent large marine animals from entering the inside of the instrument. The top plate contains a number of 5/8 inch holes to allow the fuselage to flood and ensure that the pressure-sensing diaphragms therein are communicating with the outside. The bottom plate has a one inch wide slit cut across its radius to allow the cable entry to the fuselage and water-tight cylinder. Both plates are secured to the cylinder by titanium bolts attached to PVC blocks on the inside of the fuselage. The blocks are made fast to the fuselage by adhesives and nylon screws.

Each of the four arms penetrate the fuselage and are held therein by a PVC "spider." A spider is a common plumbing junction which connects four pieces of tubing at ninety degree angles to one another. Four bolts are tapped through the spider to secure the arms. In this way, any or all of the arms can be disconnected for greater ease in transportation, or potentially, a change in arm orientation.

The arms are three-inch diameter PVC pipe and fifty-two inches in length. Each contains a pressure-sensing diaphragm near its end. The extreme end of each arm is covered by a threaded pipe-cap which can be removed to inspect the diaphragm and replace copper scouring pads placed near the diaphragm to reduce biological fouling. The arms are punctured with 11/16 inch diameter holes about their ends to allow diaphragm communication with the environment. Each arm is labelled with strips of white cloth tape to identify the differential transducer channel corresponding to that arm.

### 3. The Transducers

A typical differential pressure gauge senses the pressure difference between the diaphragm at the end of an arm and one of the five diaphragms mounted inside the fuselage. The differential pressure transducers are located inside the water-tight cylinder. The differential transducers are Setra Systems Model 228. They are a high line, low-differential wet-wet capacitance type sensor with infinite resolution and a  $\pm 0.5$  psid range. Transducer output noise is rated as below 100 microvolts RMS. Burst pressure is 2500 psid (either side) such that there is less danger of catastrophic failure during construction or installation. The differential transducers require 28 volts DC nominal excitation and feature 0 to 5 volt positive output. The transducer circuits have internal protection against reversed excitation voltage for at least 5 minutes,

short-circuit of signal output leads, and short duration power line transients up to 150 volts. Each is supplied with independent remote zero adjustment, although this feature is not used in the present DPG model.

The fifth pressure-sensing diaphragm in the fuselage supplies a signal measured by an absolute pressure transducer also located inside the cylinder. The absolute gauge is a Setra Systems Model 205-2 of 50 psia range. It also operates on 28 volt DC nominal excitation for a 0 to 5 volt positive output.

#### 4. The Isolation Sensor Diaphragms

The stainless steel diaphragms of the transducers are protected from the harsh marine environment by the nine "isolation" diaphragms located within the fuselage and arms, (Figure III-4). The isolation diaphragms are made of 13 mil DuPont Fairprene<sup>®</sup> elastomer mounted on an acrylic housing. Fairprene<sup>®</sup> is a durable nylon material, coated with neoprene, that is flexible perpendicular to the plane of the fabric. The elastomer is sealed to its acrylic housing by a 90-10 copper-nickel alloy ring. The 90-10 alloy was picked for its anti-fouling properties. Bio-fouling across the diaphragm ring could puncture the elastomer or restrict its ability to deflect and thereby introduce a bias. The rings are designed to last at least five years assuming a corrosion rate of 1.0 mpy, (Dexter, 1979). The ring is secured to the diaphragm housing with six Monel 1/4 inch

bolts. Diaphragm housings are 2-7/8 and 3 inches in outside diameter within the arms and fuselage respectively, and 2-5/16 inches long, including the Cu-Ni ring. The diameter of the elastomer exposed by the ring is 1-5/8 inches on all diaphragms. The acrylic housings behind the elastomers are hollowed to a conical shape that funnels to

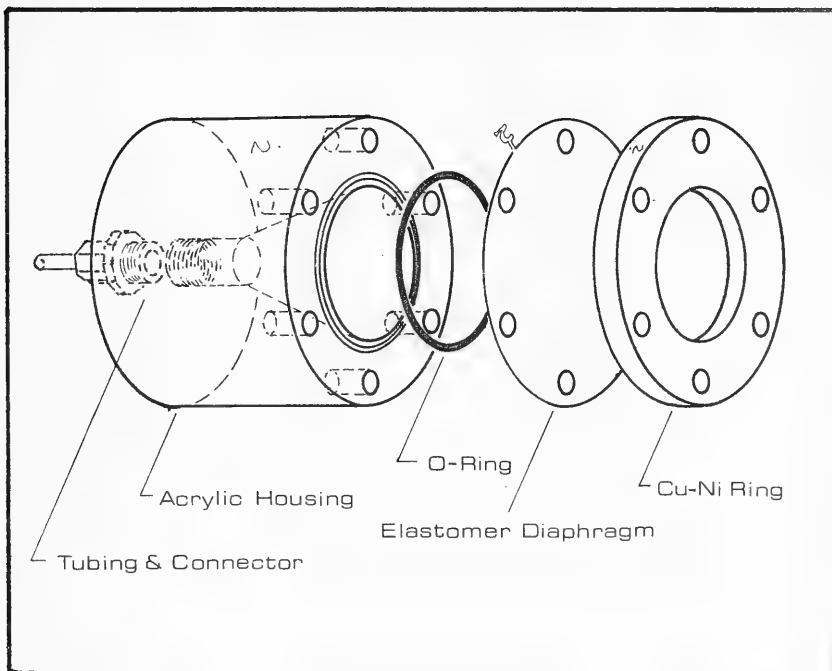


FIGURE III-4: Assembly drawing of an isolation sensor diaphragm.



FIGURE III-5: Isolation sensor diaphragms shown attached by flexible and nylon tubing through the top of the water-tight instrumentation cylinder and into the transducers.

a small opening in the back. This opening mates with 1/4 inch (1/8 inch I.D.) flexible teflon tubing which leads to the sensing ports on the pressure transducers inside the water-tight cylinder. The flexible tubing, manufactured by Cajon®, is armored with stainless steel braid. Specifically, it connects to the back of the isolation diaphragm chamber and is fastened to the top of the water-tight cylinder with Swage-Lock® connectors, (Figure III-5). The connectors penetrate the top of the cylinder and connect to nylon tubing inside. Nylon tubing is used inside the cylinder because of its partial flexibility and transparency. (Nylon is easily impregnated and hardened by seawater and is used outside the cylinder only as a permanent fastener, (Dexter, 1979).) The nylon tubing is heated and bent to shape to mate with the transducer pressure ports. The housing and tubing assembly is filled with fluid which transmits the deflections of the elastomer to the stainless steel transducer diaphragms. The fluid is dyed with food coloring for ease of identification and inspection for air bubbles that might be seen in the nylon tubing or acrylic housings.

During assembly, the isolation diaphragm housings are drawn through the arms and secured inside them by brass screws which penetrate the arm walls from the outside. The five isolation diaphragms inside the fuselage fit snugly through three-inch holes in a circular plate positioned just above the spider. A two-inch hole is cut in the center of the plate for ease in assembly.



FIGURE III-6: Assembled water-tight instrumentation cylinder with sensors penetrating the top plate.



FIGURE III-7: The transducer stack before insertion into the instrumentation cylinder.

## 5. The Water-Tight Instrumentation Cylinder

The water-tight cylinder, located underneath the spider, is an anodized aluminum pressure-tested housing developed by Sea-Data Corporation. Four sacrificial zinc anodes are positioned about the top of the cylinder. All of the pressure tubing penetrates the top (removable) section of the cylinder, while the power and data cable connects to the bottom via Brantner underwater XSL-20 connectors, (Figure III-6). The cylinder is held in place within the fuselage by PVC blocks bolted to the fuselage walls with Monel fasteners.

The transducers are held inside the cylinder by a series of five wafers separated by acrylic rods. The bottom two wafers support two of the differential transducers, the middle two support the remaining two differential and one absolute transducer, and the upper attaches to the underside of the cylinder top and suspends the wafer assembly. The wafer and transducer stack is shown in Figure III-7.

## 6. The Cable and Service Box

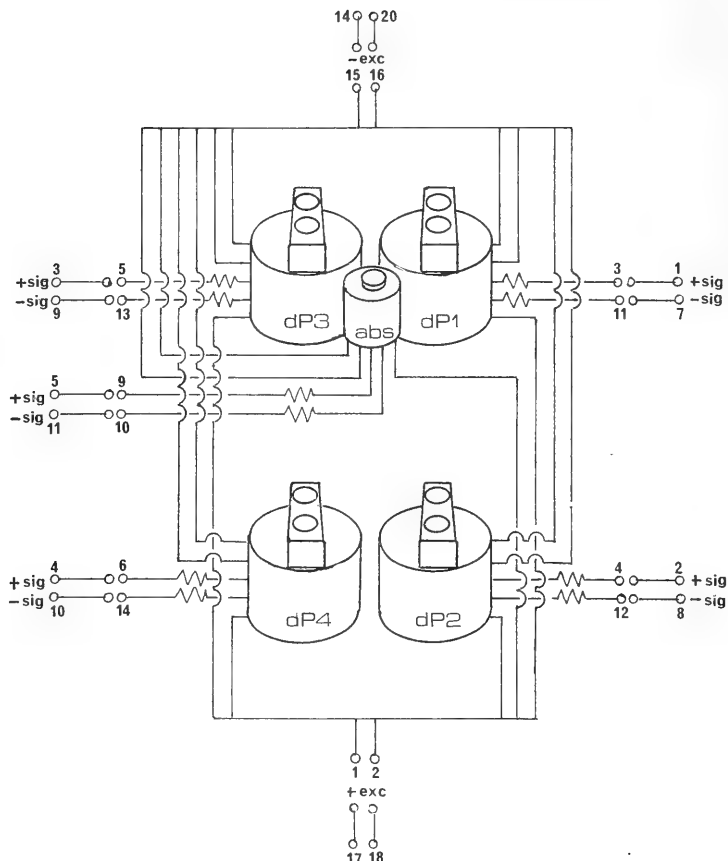
The instrument is cabled to shore for power requirements and data delivery. Eleven hundred feet of Blake BC 4960-1 double armored cable is laid between the instrument and the land-based recording facility. The cable is an eighteen conductor (18 gage - tin/copper) strand wrapped around a polypropylene filler. The conductors are water-blocked, wrapped in mylar tape, and sheathed under a

polyurethane jacket with double steel armoring and an external polyurethane jacket. The cable weighs 0.98 pounds per foot in air.

Eighty feet of the seaward end, stripped of its armoring, is stored in an 18 inch square by 9 inch plexiglass service box just before mating with the instrument. The top plate of the box is removable by unthreading four titanium nuts. This accesses the spare cable if the instrument is to be moved or taken to the surface. If the instrument requires service in the boat or on shore, the cable may be disconnected above water, sealed with a dummy connector, and released. A dummy connector is then attached to the instrument for safety. For re-installation at some later time, the cable is recovered, re-connected in the boat, and the instrument is brought underwater. It is hoped that operating the underwater connectors only above water will help alleviate some of the flooding and corrosion problems experienced in the past with underwater-pluggable connectors.

#### 7. The Electrical System

Fourteen of the available twenty conductors are utilized. Ten carry the five transducers' signal outputs, two carry the positive excitation voltage (one for back-up), and two carry the negative excitation ground, (one for back-up). Each of the transducers share the excitation positive and negative leads. A simple RC network can be installed at the landward end of each signal



Pin numbers are internal AMP 16 and BRANTNER XSL 20 Connectors  
Resistors are 100 ohm (1/8 watt)

FIGURE III-8: Wiring diagram for the DPG.

output as a passive low-pass filter. The network is easily designed for 3 dB attenuation at 50 cycles per second with the aim of eliminating 60 hertz noise from the power supply and local electrical systems. Such high frequency noise would alias into the calculated water wave spectra and bias the analysis results. An active filter is, however, more strongly recommended. To guard against the possibility of unwanted output oscillation caused by the capacitance introduced by the long cable to shore, 100 ohm resistors are installed in series in each of the output leads inside the water-tight cylinder. Since the electrical circuitry of the transducers is equivalent to a 4-terminal network which can be grounded at only one point, it is essential that the negative output leads of the transducers not be commoned since the negative excitation leads are already commoned inside the instrument.

A complete wiring diagram is presented in Figure III-8.

#### 8. The Instrument Cradle

Both the instrument and the service box are mounted onto a steel cradle secured to the seabed. The cable is constructed of C4x5.4 steel channel and 3/4 inch thick steel plate, two inch steel pipe legs and L1x1x1/8 angle iron stringers. The channel is connected primarily by the steel plate. A break is made in one plate to allow the cable to slip through the structure when the instrument is pulled out of the cradle. This is closed by a plate which bolts

over this area to retain structural integrity after the instrument is installed. The legs are welded onto the underside of the channel such that they balance the cradle about its center when no instrumentation is installed upon it. Onto the bottom of the forty inch legs are welded 10 by 12 inch thin steel plates to reduce burial into the seafloor. The cradle is secured to the bottom using 5/16 inch galvanized chain that attaches underneath each channel and cinches tight with a chain binder to one of four screw anchors driven into the seafloor.

The instrument arms lay into the steel channel and the fuselage slips into the center of the cradle. The arms are made fast to the cradle with heavy electrical cable ties. The service box is mounted onto the cradle by four titanium bolts secured through the bottom of the box. Attaching plates and rings are welded throughout the cradle for buoy markers, flotation devices, pingers, diver-assist lines, and weights to balance the asymmetrically placed service box if necessary.

#### 9. Biofouling and Corrosion Protection

The cradle was sandblasted, primed, undercoated, and then covered with anti-fouling paint. All surfaces of the plexiglass service box and the PVC instrument structure (with the exception of the fuselage end-cover plates) were sanded and also coated with anti-fouling paint. The paint used was red PETIT BIOGUARD 1665 with

19.14% active ingredient bis(tributyltin)adipate.

B. Data Retrieval

At the FRF installation site, the cable interfaces with Facility equipment at the seaward end of the pier. The power supply board is located inside a trailer at the seaward end and the transducer output leads are hard-wired down the length of the pier and recorded on a NOVA computer system located inside the facility's main building on shore. The computer digitally records the transducer signals at 1/4 second sampling for a 17 minute period every six hours.

C. Some Considerations of the Hardware Design

1. Fuselage Isolation Diaphragms

The absolute pressure measurement and one side of each of the differential pressures are all to be taken at the instrument center. Five individual diaphragms in the fuselage are employed for this task. Since not all of the diaphragms can occupy the center of the instrument in one plane, there is a small error inherent when saying that the differential measurements are exactly adjacent and share an endpoint with the absolute measurement. The midpoint of the fuselage isolation diaphragms are each about two inches (7.1 cm) from the

actual fuselage center. Further, the arrangement of the dP3, dP2 and dP4 diaphragms within the fuselage is such that they are not precisely aligned with the x- or y- axes respectively. This design was the result of space allocation problems within the top of the fuselage. The errors are such that the sensor alignment of dP2 is  $91^\circ$ ,  $178^\circ$  for dP3, and  $269^\circ$  for dP4 with respect to dP1 =  $0^\circ$ . It was considered that these one and two degree errors were negligible for the present investigation.

## 2. Height of Sensors

Once again due to practical space allocation, the instrument was designed such that the center isolation diaphragms are nine inches (22.9 cm) above the arm diaphragms. The pressure response function is developed during data analysis for the mean of these two elevations above the seafloor. In 20 feet of water, the error between the pressure response function for the actual sensor height and the mean sensor height is less than two-and-one-half percent for the highest wave frequencies of interest (periods of 3.14 seconds) and less than one percent for wave periods greater than four seconds.

D. Cost

The hardware used to construct and install the final DPG prototype at the Field Research Facility cost approximately \$13,000. Machine shop fees for the entire project were \$3090. The total project cost, including design, development, laboratory testing, hardware, travel, computer time, salaries, and indirect costs was approximately \$31,000.

CHAPTER IV  
DPG SOFTWARE

A. Introduction

The theory of data analysis and computer software for the original design of the DPG were developed during the drafting and machining stages of the project. The complete theory and software to directly develop the first seven directional Fourier coefficients for a fully functioning 4-arm DPG are presented in this chapter. After initial evaluation of the instrument's first sets of field data, it was considered that only one differential pressure gauge on each axis was reliably accurate. Hence the software package, as used at the FRF installation site, analyzes only two orthogonal differential pressure channels along with the absolute signal. The FRF package, then, is an abridged version of the program described herein. It develops only water surface slope in the x and y directions and vertical displacement, and the first five directional Fourier coefficients.

## B. Theory of Analysis

Selecting the x-y coordinate system in the horizontal with the origin at the instrument's center as in Figure IV-1, the DPG is assumed to faithfully record the water surface displacement  $\eta(x, y, t)$  at the center, the slopes  $\eta_x$  at A and C and  $\eta_y$  at B and D. The curvatures  $\eta_{xx}$  and  $\eta_{yy}$  across the center can be arithmetically approximated by  $(\eta_x(A) - \eta_x(C))/\Delta x$  and  $(\eta_y(B) - \eta_y(D))/\Delta y$  respectively. With the present DPG configuration, it is not possible to arithmetically create the cross curvature term  $\eta_{xy}$ . An additional measurement would be necessary to define such a term.

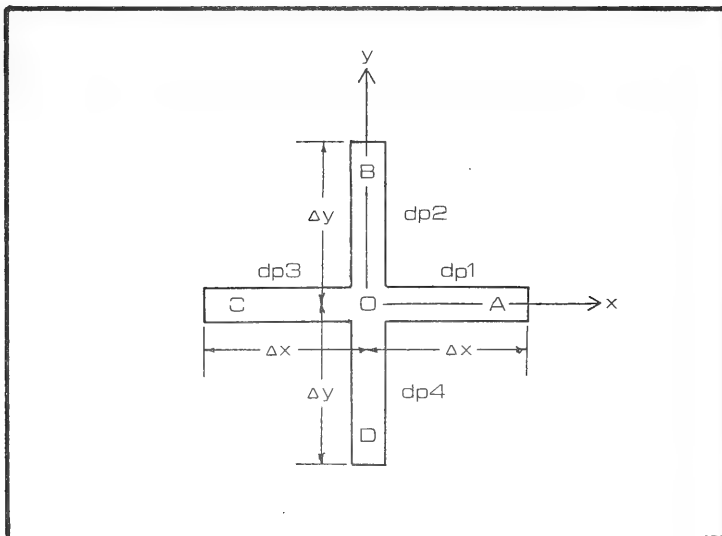


FIGURE IV-1: Coordinate system adopted for DPG analysis.

The analysis procedure follows from Longuet-Higgins, Cartwright, and Smith (1963). The water surface displacement is expressed in terms of the complex directional amplitude spectrum,  $F(\sigma, \theta)$ , as:

$$\eta(x, y, t) = \int_{-\infty}^{\infty} \int_0^{2\pi} F(\sigma, \theta) e^{i(\sigma t - k_x x - k_y y)} \partial \theta \partial \sigma \quad (4.1)$$

where  $\sigma$  = frequency

$\theta$  = direction (assuming  $\theta$  measured counter-clockwise from the positive x-axis)

$k_x = k \cos \theta$ , wave-number in the x-direction

$k_y = k \sin \theta$ , wave-number in the y-direction,

and  $\sqrt{i} = -1$ .

The water surface slope and curvature follow from (4.1) as:

$$\frac{\partial \eta}{\partial x}(x, y, t) = \int_{-\infty}^{\infty} \int_0^{2\pi} -ik \cos \theta F(\sigma, \theta) e^{i(\sigma t - k_x x - k_y y)} \partial \theta \partial \sigma \quad (4.2)$$

$$\frac{\partial \eta}{\partial y}(x, y, t) = \int_{-\infty}^{\infty} \int_0^{2\pi} -ik \sin \theta F(\sigma, \theta) e^{i(\sigma t - k_x x - k_y y)} \partial \theta \partial \sigma \quad (4.3)$$

$$\frac{\partial^2 \eta}{\partial x^2}(x, y, t) = \int_{-\infty}^{\infty} \int_0^{2\pi} -k^2 \cos^2 \theta F(\sigma, \theta) e^{i(\sigma t - k_x x - k_y y)} \partial \theta \partial \sigma \quad (4.4)$$

$$\frac{\partial^2 \eta}{\partial y^2}(x, y, t) = \int_{-\infty}^{\infty} \int_0^{2\pi} -k^2 \sin^2 \theta |F(\sigma, \theta)|^2 e^{i(\sigma t - k_x x - k_y y)} d\theta d\sigma \quad (4.5)$$

Information providing a partial description of the directional energy spectrum  $S(\sigma, \theta)$ , (equal to  $|F(\sigma, \theta)|^2$ ), is contained in the auto- and cross- spectra of the water surface displacement, slope, and curvature terms. These spectra are obtained through Fast Fourier Transform procedures using:

$$S_{\eta\eta}(\sigma) = \int_0^{2\pi} |F(\sigma, \theta)|^2 d\theta \quad (4.6)$$

$$S_{\eta\eta_x}(\sigma) = -ik \int_0^{2\pi} \cos \theta |F(\sigma, \theta)|^2 d\theta \quad (4.7)$$

$$S_{\eta\eta_y}(\sigma) = -ik \int_0^{2\pi} \sin \theta |F(\sigma, \theta)|^2 d\theta \quad (4.8)$$

$$S_{\eta_x\eta_y}(\sigma) = k^2 \int_0^{2\pi} \sin \theta \cos \theta |F(\sigma, \theta)|^2 d\theta \quad (4.9)$$

$$S_{\eta_x\eta_x}(\sigma) = k^2 \int_0^{2\pi} \cos^2 \theta |F(\sigma, \theta)|^2 d\theta \quad (4.10)$$

$$S_{\eta_Y \eta_Y}(\sigma) = k^2 \int_0^{2\pi} \sin^2 \theta |F(\sigma, \theta)|^2 d\theta \quad (4.11)$$

$$S_{\eta_X \eta_{XX}}(\sigma) = ik^3 \int_0^{2\pi} \cos^3 \theta |F(\sigma, \theta)|^2 d\theta \quad (4.12)$$

$$S_{\eta_Y \eta_{YY}}(\sigma) = ik^3 \int_0^{2\pi} \sin^3 \theta |F(\sigma, \theta)|^2 d\theta \quad (4.13)$$

The directional spectrum at a frequency  $\sigma$  is then expressed as a partial Fourier series in terms of the wave direction  $\theta$  as:

$$S(\sigma, \theta) = a_0 + \sum_{n=1}^N a_n \cos n\theta + \sum_{n=1}^N b_n \sin n\theta \quad (4.14)$$

The Fourier coefficients are determined in the usual manner as:

$$a_0(\sigma) = \frac{1}{2\pi} \int_0^{2\pi} S(\sigma, \theta) d\theta \quad (4.15)$$

$$a_n(\sigma) = \frac{1}{2\pi} \int_0^{2\pi} S(\sigma, \theta) \cos n\theta d\theta \quad (4.16)$$

$$b_n(\sigma) = \frac{1}{\pi} \int_0^{2\pi} S(\sigma, \theta) \sin n\theta \, d\theta \quad (4.17)$$

The first seven Fourier coefficients in the Fourier series representation of the directional spectrum, Equation 4.14, (i.e.,  $N=3$ ), are obtainable from the auto- and cross-spectra, (Equations 4.6 through 4.13):

$$a_0 = \frac{1}{2\pi} S_{\eta\eta}(\sigma) \quad (4.18)$$

$$a_1 = \frac{-1}{i\pi k} S_{\eta\eta_x}(\sigma) \quad (4.19)$$

$$a_2 = \frac{1}{\pi k^2} [S_{\eta_x\eta_x}(\sigma) - S_{\eta_y\eta_y}(\sigma)] \quad (4.20)$$

$$a_3 = \frac{4}{i\pi k^3} \left[ \frac{3}{4} k^2 S_{\eta\eta_x}(\sigma) + S_{\eta_x\eta_{xx}}(\sigma) \right] \quad (4.21)$$

$$b_1 = \frac{-1}{i\pi k} [S_{\eta\eta_y}(\sigma)] \quad (4.22)$$

$$b_2 = \frac{2}{\pi k^2} [s_{\eta_x \eta_y}(\sigma)] \quad (4.23)$$

$$b_3 = \frac{-4}{i\pi k^3} \left[ s_{\eta\eta}(\sigma) + \frac{3}{4} k^2 s_{\eta\eta}(\sigma) \right] \quad (4.24)$$

The truncated Fourier series directional spectrum is now easily developed from Equation 4.14.

If two measurements each are accurately made of  $\eta_x$  and  $\eta_y$ , it would be possible to generate all of the first and third coefficients four different ways and the second coefficients two different ways using various combinations of the differential gauges in auto- and cross-spectra. The instrument software, (re-printed in Appendix F), generates each of the possible coefficients. There are two advantages here. The program will use the mean value of each calculated angular Fourier coefficient in generating the directional spectrum if it is decided that each transducer is working correctly. If it is concluded that a transducer is malfunctioning during a sampling interval, the program will disallow that transducer's signal during the final coefficient calculation. The redundancy of the transducers' measurements, then, would offer a potentially more accurate estimate of the directional Fourier coefficients as well as a first-stage failsafe mechanism if one of the differential

transducers fails. This was indeed the case in the field evaluation.

### C. Correction for Centering of Measurements

The analysis theory used herein assumes that all of the water surface measurements are taken about one point in the generation of the first five directional Fourier coefficients. However, the physical orientation of the instrument is such that the water surface slopes are each taken about a point midway along each arm (approximately two feet from the instrument center in the present design). This analysis difficulty can be overcome by averaging the two slope measurements along each axis and using the resulting mean slope values in the analysis. This is done in the present program if both transducers along an axis are deemed operational.

The measured slope values could be transferred to the center of the instrument using a complex response function. If one considers, for example, the absolute pressure signal to be monitored at the instrument center  $(x_0, y_0)$ , and an  $x$ -axis differential pressure signal measured at  $(x_1, y_1)$ , the water surface and displacement terms could be expressed (from Equations 4.1 and 4.2) as:

$$\eta(x_0, y_0, t) = \int_{-\infty}^{\infty} \int_0^{2\pi} F(\sigma) e^{i(\sigma t - k_x x_0 - k_y y_0)} \partial \theta \partial \sigma \quad (4.25)$$

$$\eta_x(x_1, y_1, t) = -ik \int_{-\infty}^{\infty} \int_0^{2\pi} \cos\theta F(\sigma) e^{i(\sigma t - k_x x_1 - k_y y_1)} d\theta d\sigma \quad (4.26)$$

The cross-spectrum of water surface displacement and slope as measured, then, would be

$$S_{\eta\eta_x}^*(\sigma) = -ik \int_0^{2\pi} \cos\theta |F(\sigma, \theta)|^2 e^{-i[k_x(x_1 - x_0) + k_y(y_1 - y_0)]} d\theta \quad (4.27)$$

However, the analysis requires that

$$S_{\eta\eta_x}(\sigma) = -ik \int_0^{2\pi} \cos\theta |F(\sigma, \theta)|^2 d\theta \quad (4.28)$$

Hence, the measured spectrum is corrected using

$$S_{\eta\eta_x}(\sigma) = S_{\eta\eta_{x_1}}^*(\sigma) \int_0^{2\pi} e^{i[k_x(x_1 - x_0) + k_y(y_1 - y_0)]} d\theta \quad (4.29)$$

Similarly, the correction for a slope measurement along the y-axis at  $(x_2, y_2)$  would be

$$S_{\eta\eta_y}(\sigma) = S_{\eta\eta_{y_2}}^*(\sigma) \int_0^{2\pi} e^{i[k_x(x_2 - x_0) + k_y(y_2 - y_0)]} d\theta \quad (4.30)$$

and for the cross-correlation of slope:

$$S_{\eta_x \eta_y}(\sigma) = S_{\eta_x \eta_y}^*(\sigma) \int_0^{2\pi} e^{i[k_x(x_2-x_1)+k_y(y_2-y_1)]} d\theta \quad (4.31)$$

where the starred spectra are those measured by the instrument.

The transfer function alters only the phase, not the amplitude, and is a function of wave frequency, direction, and gage length of the instrument arms. The corrections require one to know the wave direction of each frequency component a priori. These can be calculated (if two transducers along an axis are functioning properly) using the simultaneous solution of a set of equations such as:

$$S_{\eta \eta_x}(\sigma) = S_{\eta \eta_{x_1}}^*(\sigma) \int_0^{2\pi} e^{i[k_x(x_1-x_0)+k_y(y_1-y_0)]} d\theta$$
$$S_{\eta \eta_x}(\sigma) = S_{\eta \eta_{x_3}}^*(\sigma) \int_0^{2\pi} e^{i[k_x(x_3-x_0)+k_y(y_3-y_0)]} d\theta \quad (4.32)$$

or

$$S_{\eta \eta_y}(\sigma) = S_{\eta \eta_{y_2}}^*(\sigma) \int_0^{2\pi} e^{i[k_x(x_2-x_0)+k_y(y_2-y_0)]} d\theta$$
$$S_{\eta \eta_y}(\sigma) = S_{\eta \eta_{y_4}}^*(\sigma) \int_0^{2\pi} e^{i[k_x(x_4-x_0)+k_y(y_4-y_0)]} d\theta \quad (4.33)$$

where  $(x_1, y_1)$ ,  $(x_3, y_3)$ , and  $(x_2, y_2)$ ,  $(x_4, y_4)$  are the known positions of the x- and y-axis slope measurements, respectively. Alternatively, the analysis could be carried out with the non-corrected spectra, the directions at each frequency estimated, and the process repeated using spectra corrected by the previously estimated direction to yield continually more accurate directional information. This analysis, however, can correct only for the principal direction.

Such corrections are assumed small enough to be neglected in the present analysis. For the worst case of small period waves, (say, 3.2 seconds), the phase shift is less than 1 degree.

#### D. Program Operation Notes

##### 1. Introduction

The FORTRAN analysis program, presented in Appendix F, accesses and analyzes the five raw digitized voltages received from the DPG data storage tape. A crude flow chart of the program is shown in Figure IV-2.

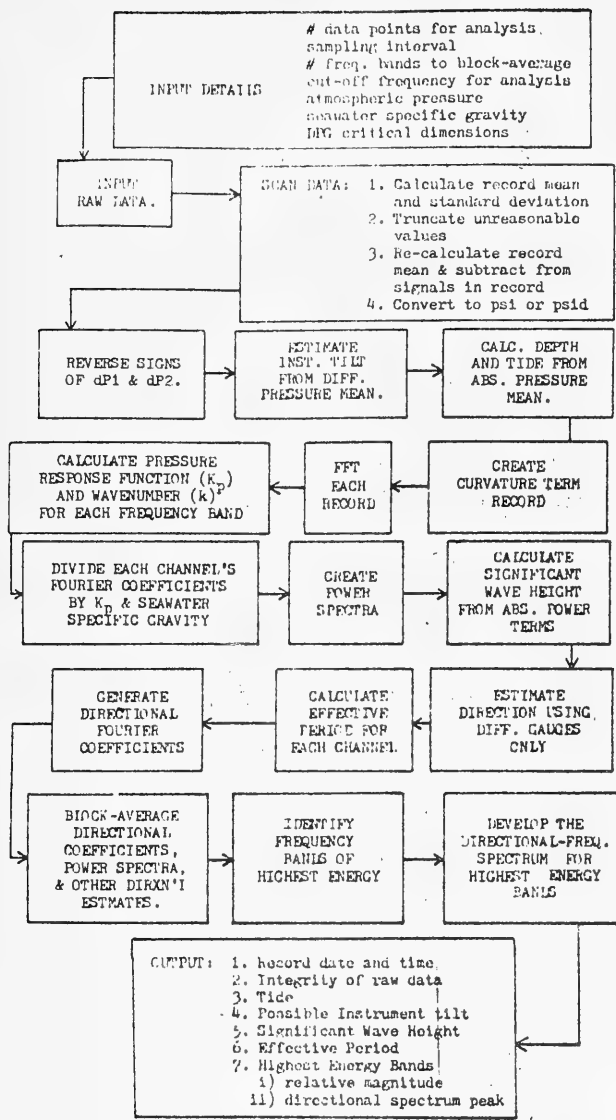


FIGURE IV-2: Flow chart of DPG analysis program.

## 2. Input and Screening of Data

A preliminary scan of the voltage records is made to calculate the mean and standard deviation of each. In each record, sampled points that are greater or less than 3 standard deviations from the mean are truncated to the average value of their two neighboring points. The number and magnitude of high and low truncations made in each record are reported at the terminal. If an unusually large number of alterations are necessary for a record, the operator may choose to disallow the particular record from further spectral analysis. The mean of each record is recalculated and is then subtracted from each of the transducer signals.

## 3. Conversion from Voltage to Pressure Signals

The differential signals are converted from volts to pounds per square inch differential (PSID) which corresponds to  $P(\text{arm}) - P(\text{center})$ . These values are then divided by the distance between the sensor positions for each arm to yield the pressure differential per inch of length along an arm. To maintain a consistent sign convention among the pressure differences across the instrument, the signs of the dP1 and dP2 signals are reversed. The four differential channels' signals are now in the form:

$$\begin{aligned} dP1 &= (P(\text{center}) - P(\text{arm1})) / \Delta x1 \\ dP2 &= (P(\text{center}) - P(\text{arm2})) / \Delta x2 \\ dP3 &= (P(\text{arm3}) - P(\text{center})) / \Delta x3 \\ dP4 &= (P(\text{arm4}) - P(\text{center})) / \Delta x4 \end{aligned}$$

With this convention, the program as written will generate the directional distribution with the greatest energy concentrated about the compass heading to which the waves are moving towards with DPG arm 1 = 0 degrees. (The heading is later adjusted to represent the compass direction from which the waves propagate with respect to true north.)

The absolute signal is then reduced to pounds per square inch absolute (PSIA).

#### 4. Instrument Tilt Approximation

The mean of each differential pressure record is compared to the zero-wave condition tare as determined in the laboratory. If the mean of a differential record is assumed to represent a zero-wave condition in the field, then a discrepancy between the mean and the laboratory tare could indicate instrument tilt above the seabed. An approximation of the tilt of each arm is calculated using this difference between the mean and tare for each transducer record. If the arm tilts about the horizontal an angle  $\alpha$ , as shown in Figure IV-3, then a pressure difference between the sensors is detected. This pressure differential is converted to a pressure head,  $Q$ , and the tilt  $\alpha$  approximated from the arctangent of  $Q/\Delta x$ . Specifically,

$$\alpha = \tan^{-1} \left[ \frac{\Delta P}{(\gamma - \gamma_{bf})} \cdot \frac{1}{\Delta x} \right] \quad (4.34)$$

where  $\Delta P = dP(\text{record mean}) - dP(\text{horizontal})$  and  $\Delta x = \text{gage length of arm}$ . The specific gravity of the fluid back-filling the sensor diaphragms,

$\gamma_{bf}$  must be different than that of the surrounding seawater,  $\gamma$ . If both differential transducers along an axis are operating correctly, the angle of tilt calculated for colinear arms should agree with opposite

signs. The direction of tilt is defined after considering

the manner in which the differential pressures are reported by the instrument, (i.e.,  $dP = P(\text{arm}) - P(\text{center})$ ). An increase in the mean value of a differential transducer indicates that the end of the corresponding arm is slanting upwards (neglecting any changes in temperature).

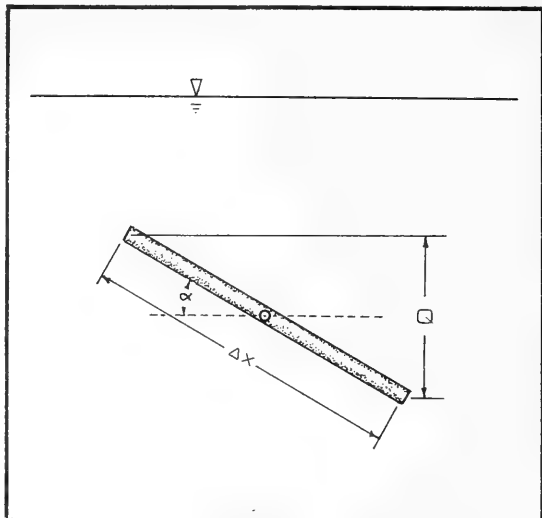


FIGURE IV-3: Instrument tilt above the seafloor.

If it is decided that the instrument is stable over time, (i.e., there is no further settlement), then changes in the mean of the differential gauge signals could be used to calculate the ambient seawater temperature. This estimate could then be used to develop the temperature-corrected specific gravity of the seawater and back-fill fluid. (This calculation is not included in the present software package.) Temperature estimates could not be made if the back-fill fluid volumes on both sides of the differential pressure transducers were equal. (See Section V.C.6.)

## 5. Tide Calculation

The mean voltage of the absolute transducer record is converted to pressure and is used to calculate the tide level. The total average water column above the sensor,  $z_s$ , can be found from

$$z_s = \frac{1}{\gamma} (P_{\text{mean}} - P_{\text{atm}} - \gamma_{\text{bf}} l_{\text{bf}} - P_{\text{bf}}) \quad (4.35)$$

where  $P_{\text{mean}}$  = mean absolute pressure

$P_{\text{atm}}$  = atmospheric pressure

$\gamma$  = specific weight of seawater

$\gamma_{\text{bf}}$  = specific weight of back-filling fluid

$l_{\text{bf}}$  = height of sensor above the transducer

$P_{\text{bf}}$  = back-fill pressure.

Both the specific fluid weights should be temperature corrected. The

difference between  $z_s$  and the measured water column above the sensor at mean water represents the average tide level during the record.

## 6. Development of Curvature Terms

As the next step, the curvature terms are created by subtracting the colinear slope terms and dividing by the distance between the center of the slope measurements.

## 7. Significance of the Signals in Linear Theory

The absolute pressure transducer signal can then be considered to be in the form:

$$P(x, y, t) = \gamma \frac{H}{2} K_p \cos (k_x x + k_y y - \sigma t) \quad (\text{psia}) \quad (4.36)$$

and the differential signals in the form:

$$P_x(x, y, t) = - \gamma \frac{H}{2} k_x K_p \sin (k_x x + k_y y - \sigma t) \quad (\text{psid}) \quad (4.37)$$

$$P_y(x, y, t) = - \gamma \frac{H}{2} k_y K_p \sin (k_x x + k_y y - \sigma t) \quad (\text{psid}) \quad (4.38)$$

The wavenumber,  $k$ , and the pressure response function are generated for the frequencies

$$\sigma(n) = \frac{2\pi}{N\Delta t} (n-1) ; \quad n = 2, 3, \dots, N/2 \quad (4.39)$$

where  $N$  is the number of sample points analyzed and  $\Delta t$  is the sampling interval. The water depths used in the calculations include the tidal variation computed earlier.

#### 8. FFT and Conversion to Water Surface Terms

The absolute record, the four differential records, and the two curvature records are processed by the Fast Fourier Transform (FFT) and the resulting Fourier coefficients divided by the pressure response function and specific weight of the seawater. Frequency bands greater than 2 rad/sec (wave periods less than 3.14 seconds) are disregarded because of the error inherent in dividing these high frequency bands by their respectively small  $K$  values.

The absolute record is then comparable to:

$$\eta(x, y, t) = \frac{H}{2} \cos (k_x x + k_y y - \sigma t) \quad (\text{in.}) \quad (4.40)$$

and the differential records to:

$$\eta_x(x, y, t) = -\frac{H}{2} k \cos \theta \sin (k_x x + k_y y - \sigma t) \quad (\text{in./in.}) \quad (4.41)$$

and

$$\eta_y(x, y, t) = -\frac{H}{2} k \sin \theta \sin (k_x x - k_y y - \sigma t) \quad (\text{in./in.}) \quad (4.42)$$

while the curvature, or acceleration, terms are as:

$$\eta_{xx}(x, y, t) = -\frac{H}{2} k^2 \cos^2 \theta \cos(k_x x + k_y y - \sigma t) \quad (\text{in.}^{-1}) \quad (4.43)$$

and

$$\eta_{yy}(x, y, t) = -\frac{H}{2} k^2 \sin^2 \theta \cos(k_x x - k_y y - \sigma t) \quad (\text{in.}^{-1}) \quad (4.44)$$

Twice the sum of the squares of the modified Fourier coefficients represents the power spectrum of the displacement, slope components, and curvature components. The significant wave height is determined from four times the square root of the sum of the absolute channel's power spectrum:

$$H_{1/3} = 4\sqrt{S_{\eta\eta}} \quad (4.45)$$

## 9. Failure of the Absolute Channel

If it is decided that the absolute transducer has failed, the water surface displacement and power spectrum can theoretically be estimated from the x- and y-axis differential transducers that are deemed as operational. This procedure necessarily assumes that there is only one wave direction per frequency. The record of the absolute transducer has been developed in the time domain to that of Equation (4.40):

$$\eta(x, y, t) = \frac{H}{2} \cos(k_x x + k_y y - \sigma t)$$

so that the power spectrum of the absolute transducer is as:

$$S_{\eta\eta}(\sigma) = \frac{H^2}{4} \overline{\cos^2(k_x x + k_y y - \sigma t)} = \frac{H^2}{8} \quad (4.46)$$

and the power spectrum of the x and y differential gauges are correspondingly:

$$S_{\eta_x\eta_x}(\sigma) = \frac{H^2}{8} k^2 \cos^2 \theta \quad (4.47)$$

$$S_{\eta_y\eta_y}(\sigma) = \frac{H^2}{8} k^2 \sin^2 \theta \quad (4.48)$$

The power spectrum of the absolute record, then, might be developed from the sum of the x and y differential power spectra divided by the

square of the wavenumber. Such a module, however, is not part of the software as presented in Appendix F.

Theoretically, it is also possible to estimate the principal wave direction without the absolute transducer signal similarly assuming that there is only one wave direction per frequency. From Equations 4.9, 4.10, and 4.11 the differential cross-correlations are as:

$$S_{n_x n_x} = k^2 S_{nn} \cos^2 \theta = \frac{1}{2} k^2 S_{nn} (1 + \cos 2\theta) \quad (4.49)$$

$$S_{n_y n_y} = k^2 S_{nn} \sin^2 \theta = \frac{1}{2} k^2 S_{nn} (1 - \cos 2\theta) \quad (4.50)$$

$$S_{n_x n_y} = k^2 S_{nn} \sin \theta \cos \theta = \frac{1}{2} k^2 S_{nn} (\sin 2\theta) \quad (4.51)$$

for some frequency  $\theta$ , so that an estimate of the wave direction might be found from:

$$\tan 2\theta = \frac{2S_{n_x n_y}}{S_{n_x n_x} - S_{n_y n_y}} \quad (4.52)$$

for some frequency  $\theta$ . There exists four roots in the arctangent of 2, as can be seen in Figure IV-4. It can be shown that two of these roots are associated with maxima (and separated by  $180^\circ$ ) and the

other two (also separated by  $180^\circ$ ) are associated with minima and separated from the first two roots by  $90^\circ$ . Two of these roots can be

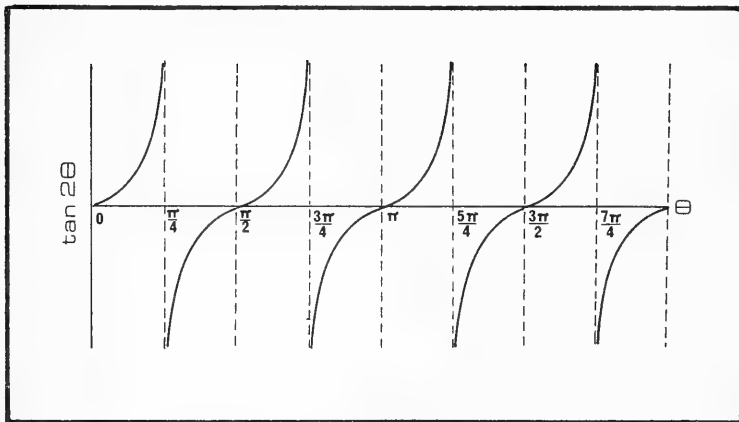


FIGURE IV-4: Four roots of tangent( $2\theta$ ).

eliminated by considering the signs of the numerator and denominator. The remaining two might be resolved by considering the physical environment of the deployment site. One does not expect, for example, incident swell to approach a straight shoreline at angles much greater than 45 degrees to the shore normal. This directional estimate is calculated in the software package and displayed optionally.

## 10. Failure of 3 Differential Channels

If only the absolute and one differential pressure channels are considered operational, another estimate of the wave direction might be made with a 180 degree ambiguity. With the power spectra of the absolute and differential channels in the form of Equations 4.46 through 4.48;

$$\frac{S_{\eta\eta}(\sigma)}{S_{\eta_x\eta_x}(\sigma)} = \frac{1}{k^2 \cos^2 \theta}$$

So that

$$\theta = \cos^{-1} \frac{1}{k} \sqrt{\frac{S_{\eta_x\eta_x}(\sigma)}{S_{\eta\eta}(\sigma)}} \quad (4.53)$$

or similarly

$$\theta = \sin^{-1} \frac{1}{k} \sqrt{\frac{S_{\eta_y\eta_y}(\sigma)}{S_{\eta\eta}(\sigma)}} \quad (4.54)$$

for some frequency  $\sigma$ .

## 11. Effective Period

The non-block-averaged frequency band corresponding to the centroid of each power spectrum is then calculated from:

$$\bar{\sigma} = \frac{\sum_n \sigma_n S_{xx}(\sigma_n)}{\sum_n S_{xx}(\sigma_n)} \quad (4.55)$$

where  $S_{xx}(\sigma)$  is the auto-spectrum of a transducer signal. This is an estimate of the "effective wave period" during the record as determined by each transducer.

## 12. The Directional Fourier Coefficients

The directional (or angular) Fourier coefficients are calculated for each frequency band using Equations 4.18 through 4.24. The coefficients are taken as the mean of all those calculated with different combinations (or cross-spectra) of operating channels. These angular coefficients, as well as the water surface displacement power spectrum, are block-averaged over a specified number of adjacent frequency bands. Since an ocean wave time series is composed of random functions, the Fourier coefficients of each channel must not be block-averaged before generation of the angular coefficients. The average of a random function exhibits zero correlation with the average of another, so that the angular coefficients must be calculated from the raw cross-spectra terms and

then averaged. Similarly, the directional estimates obtained from Equations 4.52, 4.53, and 4.54 are block-averaged.

### 13. Block-Averaging

The stability of the generated spectra is enhanced by block-averaging over adjacent frequency bands. If the water surface displacements are assumed to be Gaussian, the Fourier coefficient spectral estimates are distributed according to the chi-square distribution with two degrees of freedom. The block-averaged, or smoothed, Fourier coefficient spectral estimates are represented by the chi-square distribution with the number of degrees of freedom equal to two times the number of adjacent frequencies averaged (Borgman, 1972). When the analysis program operates upon records from computer simulation or a controlled laboratory environment, each spectral estimate is considered separately; that is, there is no block-averaging. This is equivalent to two degrees of freedom and is done to retain the highest resolution possible for the narrow spectra and shorter time records generated in simulation and the laboratory. When the program operates upon a record from the ocean environment, each signal is block-averaged over four to eight adjacent spectral frequencies to yield eight to sixteen degrees of freedom respectively. It is assumed that the frequency resolution thereby lost in the block-averaged analysis of the ocean's broader spectra is balanced by the increased stability of the record.

#### 14. Frequency Bands of Greatest Energy

The block-averaged frequency bands of maximum energy are then identified from one of the operative channels (generally the absolute) and the amount by which each exceeds the average energy in the spectrum is calculated. The truncated Fourier series directional spectrum (Equation 4.14) is then calculated for each of these high energy bands. The direction of peak energy for each spectrum is reported as that band's direction of wave propagation -- adjusted accordingly to instrument orientation relative to true north.

The "mean direction" of each band can also be calculated as:

$$\pi \overline{\theta_n} = \tan^{-1} \frac{b_n}{a_n} \quad (4.56)$$

where  $n=1,2,3$ . (If no water surface curvature terms are developed, then  $n=1,2$ .) There exists a directional ambiguity for  $n>1$  since there exists more than one peak in  $\sin n\theta$  for  $n>1$  (from which the  $b_n$  terms are developed).

Since the ultimate intent of the DPG as a tool is to report predominant wave characteristics at the installation site, the presentation of wave information at the dominant energy levels is considered to be the preferred data display.

#### E. DPG Simulation and Error

A simple simulation program was utilized to test the capabilities of the software. A directional wave-pressure field over water depth  $h$ , at transducer depth  $s$ , was considered using

$$P(x, y, s; t) = \gamma h + \sum_{j=1}^J \gamma \frac{H_j}{2} K_{p_j} \cos (k_x x + k_y y - \sigma t)_j \quad (4.57)$$

where  $J$  = number of wave trains present. Multiple wave trains of different frequencies and/or directions were simulated by superimposing all of the dynamic water surface elevations at  $(x, y, t)$  onto the static water column,  $h$ . The pressure at those  $(x, y)$  points corresponding to the five DPG diaphragm locations were generated over time. (It was assumed that the five diaphragms in the center of the instrument occupy the same point.) From these values, four differential signals and one absolute signal were developed at  $\Delta t$  intervals for a record length of  $N\Delta t$  to simulate DPG in-situ performance. Non-linear wave-wave interactions were not considered in this simple model.

The integrity of the FFT analysis was first tested by simulating a single wave train at a principal frequency of the FFT. Results of the analysis of the simulated record indicated acceptable FFT performance since all of the energy was indeed found to be

concentrated at the simulated wave frequency.

The ability to discriminate a number of different wave trains was next tested. Two wave trains of frequencies within one spectral bandwidth of one another and of different energy and direction were superimposed upon a train of lower frequency. Analysis was carried

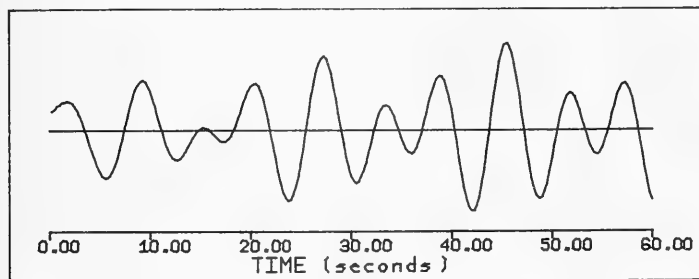


FIGURE IV-5: Simulated time record of water surface elevation. Case 1.  $H = 4$  ft.,  $\theta = 46$  deg., 5.98 sec. pd.;  $H = 3$  ft.,  $\theta = 180$  deg., 6.33 sec. pd.;  $H = 4$  ft.,  $\theta = 300$  deg., 9.00 sec. pd.

out for 512 sample points of 0.25 second interval. A portion of the simulated time record of the water surface displacement generated over each of the five sampling points of the DPG is shown in Figure IV-5. The raw spectral energy distribution, or energy spectra, presented in Figure IV-6, illustrates the presence of three distinct frequencies well. Although the simulated lowest and highest frequency waves were of the same wave height, the higher frequency wave demonstrates a smaller energy spike due to the spectral leakage between the lower frequency bands. The non-smoothed 7-coefficient

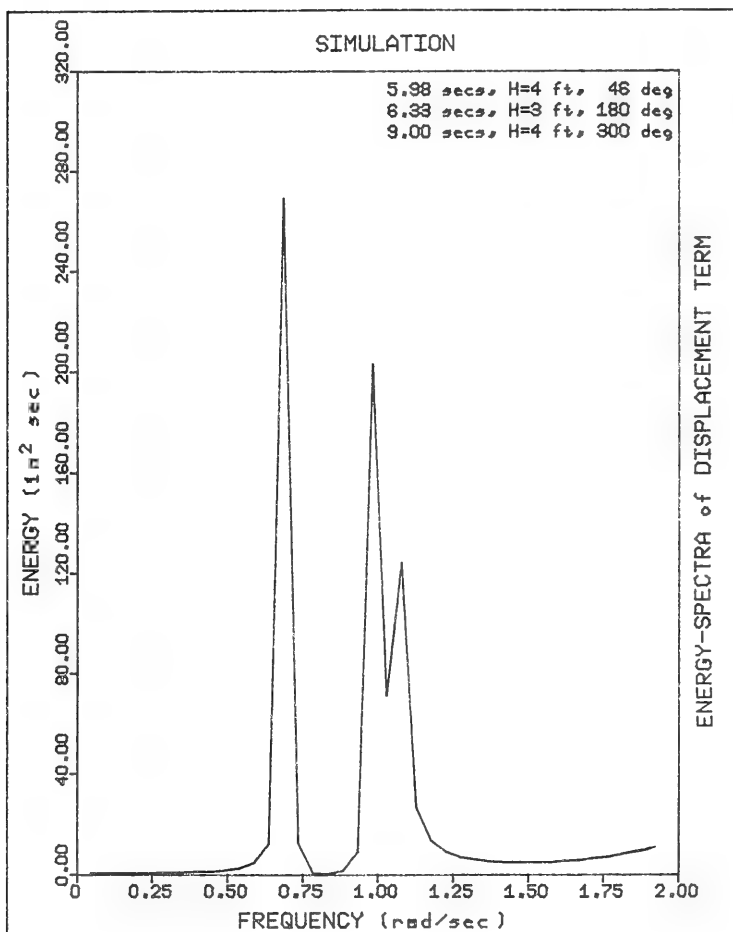


FIGURE IV-6: Raw energy spectra; Simulation Case 1. Illustrates presence of three distinct wave trains.

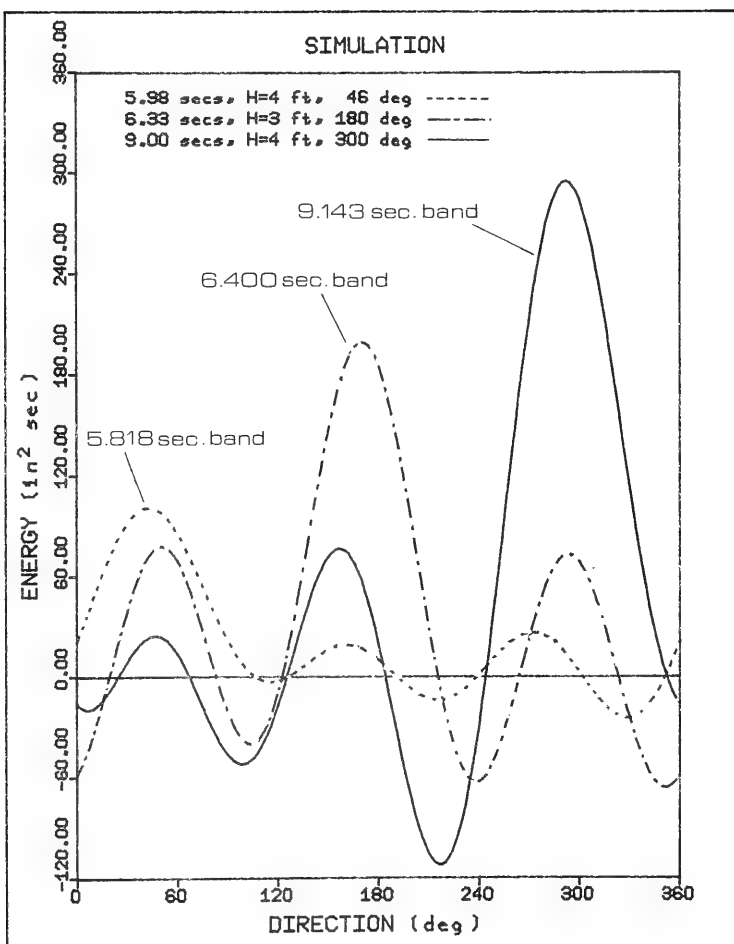


FIGURE IV-7: Non-weighted 7 coefficient Fourier series directional energy distribution. Simulation Case 1. Illustrates presence of three distinct wave trains with different directions.

Fourier series directional distribution was plotted over two degree increments for the three bands of highest energy and is presented in Figure IV-7. The analysis program demonstrates its ability to define each wave train's direction accurately by presenting the maximum energy at the correct simulated wave direction. The half-power directional width of each is approximately 60 degrees. These curves, of course, do not contain all of the simulated wave energy since only three major spectral bands are plotted.

Two wave trains of different frequency but with identical height and direction were next simulated over 512 points of 0.25 second interval. The frequency of each was selected to fall exactly between two spectral frequencies. The higher frequency bands were 0.1184 rad/sec apart and the lower were 0.464 rad/sec apart. The raw energy spectra, shown in Figure IV-8, depicts the two wave trains' energy distribution over frequency. Slight differences in leakage between the two simulated wave frequencies can be detected. The non-smoothed directional distributions of the two waves, shown in Figure IV-9, agree well with each other as expected. The very slight differences are the result of differences in spectral leakage for each wave.

The analysis procedure, however, is unable to differentiate between two waves of identical frequency and different direction. Two waves of the same height and non-spectral frequency were simulated with a 130 degree difference in direction. The

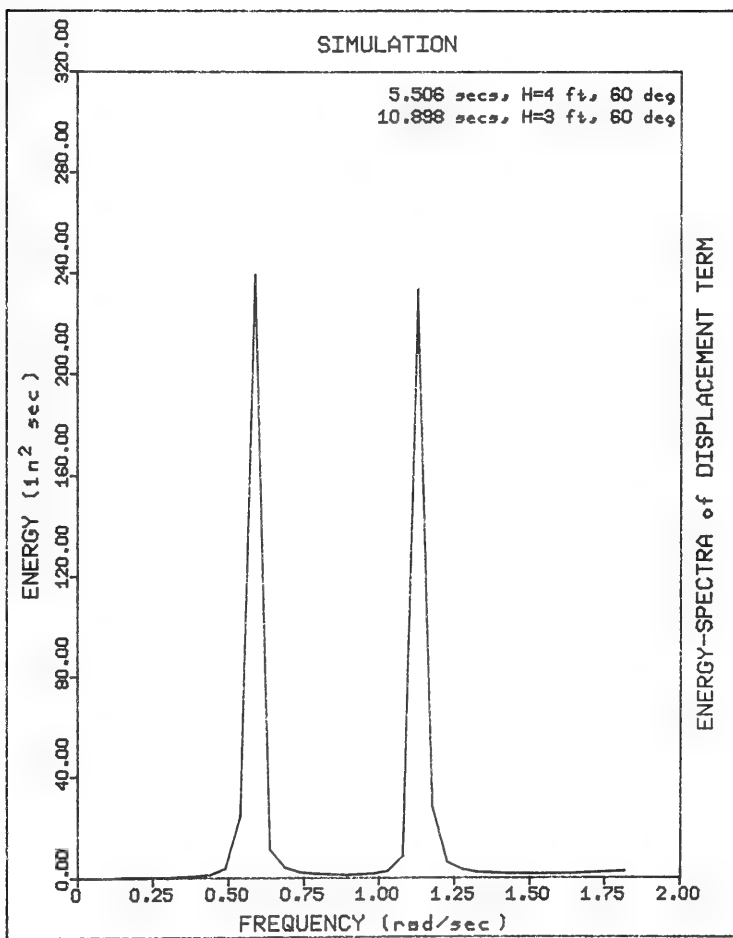


FIGURE IV-8: Raw energy spectra; Simulation Case 2.

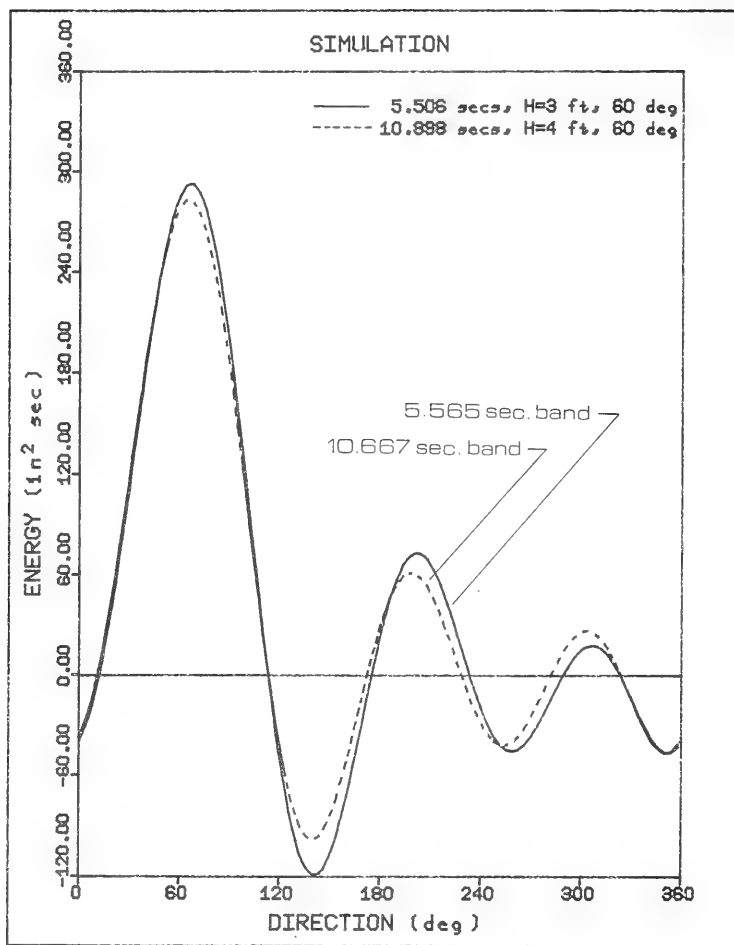
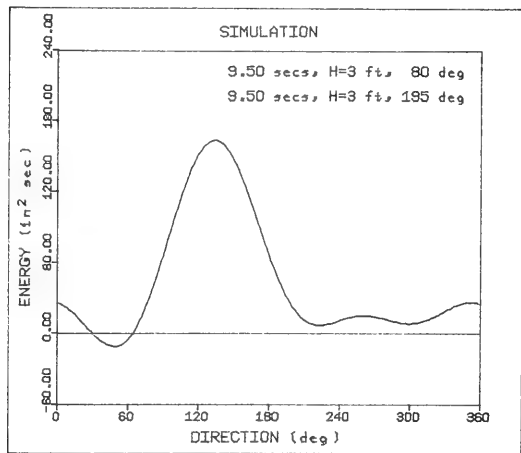
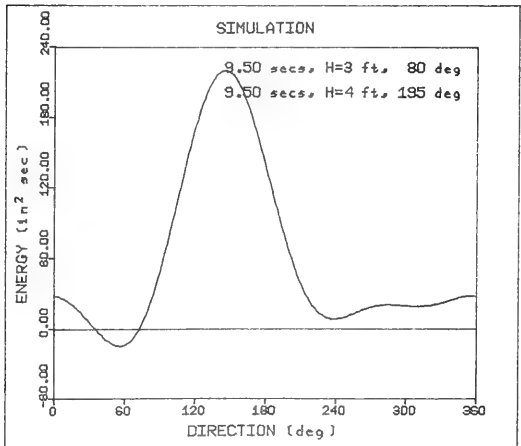


FIGURE IV-9: Non-weighted 7-coefficient Fourier series directional energy distribution; Simulation Case 2. Illustrates good directional spectra agreement with slight differences due to leakage.



FIGURES IV-10,11: Non-weighted 7-coef-  
ficient directional spectra; Simu-  
lation Cases 3 and 4. Illustrates  
software inability to clearly define  
two directions per frequency, (waves of  
equal and unequal height).



non-smoothed seven-coefficient Fourier series directional distribution, presented in Figure IV-10, demonstrates a wide peak of 80 degree half-power bandwidth. The distribution suggests omnidirectional wave power, but with a maximum at the mean of the two simulated directions, 80 and 195 degrees.

The identical case was re-simulated with the 80-degree wave retaining its three foot height and the 195-degree wave assuming a four foot height. The directional distribution, shown in Figure IV-11, is asymmetrical with peak energy at the weighted average value of the two wave directions.

Inclusion of higher order terms in the partial Fourier series representation of direction should increase the accuracy of the series representation. Figure IV-12 illustrates the heightened directional resolution of a simulated wave train at a principal frequency using the first seven directional Fourier coefficients, (N=3), compared to the first five, (N=2). The non-smoothed half-power bandwidth for seven coefficients is 66 compared to 76.3 for five.

In the simple simulation analysis, the software appears to be non-sensitive to wave direction -- at least for the presence of only one wave train. Four waves of equal energy and frequency, but different direction, were each simulated individually over the DFG. The directional distribution for each was overlaid upon one another

and excellent agreement readily seen.

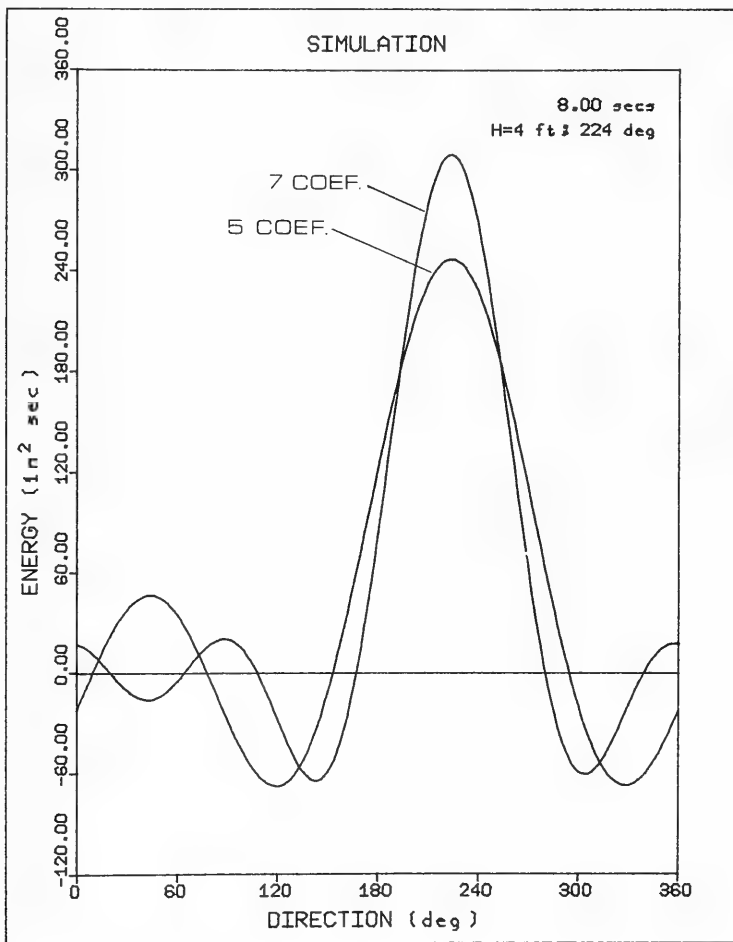


FIGURE IV-12: Non-weighted directional spectra using the first seven directional Fourier coefficients compared to the first five. Single simulated wave of spectral frequency.

## CHAPTER V

### LABORATORY DEVELOPMENT, CALIBRATION, AND TESTING OF THE INSTRUMENT

#### A. Introduction

Some modifications to the instrument were made during the fluid back-filling of the sensors. These changes, as well as the static bench calibration of the DPG instrument are documented and discussed in this chapter. The preliminary wave-tank tests carried out at the Coastal Engineering Research Center (CERC), Fort Belvoir, Virginia, are also described.

#### B. Fluid Back-Filling the Sensors

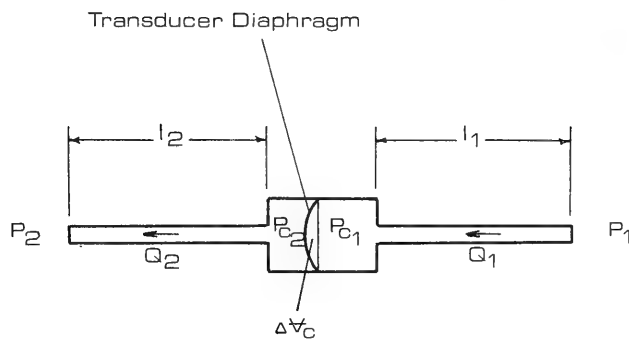
##### System Modifications

Certainly the most difficult problem encountered during the assembly of the DPG was the fluid back-filling of the sensing diaphragms. The frustration and numerous failures during the very intense six-week period of back-filling attempts led to two changes each of the type of fluid and tubing used.

The original design called for 1/16 inch inner diameter stainless steel tubing between the water-tight cylinder and isolation diaphragms. The fuselage, or center, tubings were 14 inches in length, while the arm tubings were 44 inches in length. Methanol was first tried as the back-filling fluid, but then discarded because of the poisonous hazard it presented. Standard automobile transmission fluid was next used as the back-filling agent. Although much safer, it easily contaminates laboratory tools and work areas.

Hundreds of attempts were made to back-fill the sensors and eliminate all air in the system. An air bubble of appreciable size could compress under a dynamic load and thereby prevent the transducer from sensing the full pressure exerted upon the isolation diaphragm. The back-filling fluid itself is assumed incompressible so that with no air in the system the fluid transmits the pressure sensed by the isolation diaphragm immediately to the transducer. The final technique used to back-fill the DPG is outlined in Appendix D.

Once satisfied that air was removed from the system, more problems arose when the transducers, sensing through the 1/16 inch I.D. tubing filled with transmission fluid, failed to respond to a load faster than five to twelve seconds. It was decided that the frictional head loss caused by the high viscosity of the fluid and long, small diameter tubing might be responsible for such large response times. It was also considered possible that small bubbles might still be lodged in the system or that impurities in the fluid



$P_n$  = Pressure at Sensor  $n$

$P_C$  = Transducer Chamber Pressure

FIGURE V-1: Schematic representation of differential pressure transducer and isolation sensors.

may have blocked the transducer filter screens and diaphragm.

The frictional pressure gradient along the inside length  $l$  of a circular pipe is (Peerless, 1967):

$$\frac{\Delta P_f}{l} = \frac{128 \mu Q}{\pi D^4} \quad (5.1)$$

where  $\Delta P_f$  = frictional pressure drop

$\mu$  = coefficient of dynamic viscosity

$Q$  = volumetric flow rate

$D$  = inner diameter of tubing.

Figure V-1 presents a schematic representation of the differential transducer and sensors. The fluid flow along each arm,  $Q_1$  and  $Q_2$ , that results from difference in pressure between the system's sensors may be expressed from Eq. 5.1 as:

$$Q_1 = B_1 (P_1 - P_{C_1}) \quad (5.2a)$$

$$Q_2 = B_2 (P_{C_2} - P_2) \quad (5.2b)$$

where

$$B_n = \frac{\pi D_n^4}{128 \mu_n l_n} \quad (5.3)$$

Re-writing;

$$P_1 - P_{c_1} = Q_1/B_1 \quad (5.4a)$$

$$P_{c_2} - P_2 = Q_2/B_2 \quad (5.4b)$$

And, from continuity;

$$Q_1 = Q_2 \equiv Q \quad (5.5)$$

Adding Equations 5.4a and 5.4b;

$$P_1 - P_2 = P_{c_1} - P_{c_2} + Q \left( \frac{1}{B_1} + \frac{1}{B_2} \right) \quad (5.6)$$

The transducer diaphragm displaces a volume  $\Delta V_c$  proportional to the change in pressure across the transducer chamber:

$$\Delta V_c = \alpha \Delta P_c = \alpha (P_{c_1} - P_{c_2}) \quad (5.7)$$

Re-writing Equation 5.7 and expressing the change in volume in terms of the fluid flow  $Q$ ;

$$\Delta P_c = P_{c_1} - P_{c_2} = \frac{1}{\alpha} \Delta V_c = \frac{1}{\alpha} \int Q \, dt \quad (5.8)$$

Differentiating both sides;

$$Q = \alpha \frac{d}{dt} (\Delta P_C) \quad (5.9)$$

Substituting (Equations 5.8 and 5.9 into 5.6, one obtains:

$$\Delta P = P_1 - P_2 + \Delta P_C + \alpha \left( \frac{1}{B_1} + \frac{1}{B_2} \right) \frac{d}{dt} \Delta P_C \quad (5.10)$$

where  $\Delta P$  is the difference in pressure between the two sensors. If the change,  $\Delta P$ , occurs instantaneously, it can be shown that the solution to Eq. 5.10 is

$$\Delta P_C = \Delta P (1 - e^{-K_D t}) \quad (5.11)$$

substitution into Eq. 5.10 yields:

$$\Delta P = \Delta P_C + \alpha \left( \frac{1}{B_1} + \frac{1}{B_2} \right) K_D \Delta P e^{-K_D t} \quad (5.12)$$

where  $K_D^{-1}$  is the "folding time" of the response. Solving,

$$\begin{aligned} K_D^{-1} &= \frac{\alpha (B_1 + B_2)}{B_1 B_2} \\ &= \frac{128 \alpha \mu_1 \mu_2 \ell_1 \ell_2}{\pi D_1^4 D_2^4} \left( \frac{D_1^4}{\mu_1 \ell_1} + \frac{D_2^4}{\mu_2 \ell_2} \right) \end{aligned} \quad (5.13)$$

If the fluid and tubing diameter are the same on both sides of the transducer, Eq. 5.13 reduces to:

$$K_D^{-1} = \frac{128 \alpha \mu \ell_1 \ell_2}{\pi D^4} \left( \frac{1}{\ell_1} + \frac{1}{\ell_2} \right) \quad (5.14)$$

The form of Eq. 5.11 was verified qualitatively by examining the strip chart output of a differential transducer and sensor system loaded in an approximately instantaneous manner.

It is clear that the response time is proportional to the fluid viscosity and inversely proportional to the fourth power of the tubing diameter. Changing the tubing length was not considered since the lengths were pre-determined by the DPG configuration as described in Chapter II.

It was first thought that the response time could be sufficiently decreased by reducing the fluid viscosity. A number of fluids were considered but all discarded because of their degrading effects on the system's materials, (i.e., acrylic, neoprene, Buna-n, nylon, and stainless steel). After two hundred and eighty hours of nearly continuous laboratory work, it was decided to use gin as the back-filling fluid. It is inexpensive, easily obtainable, safe, and has a dynamic viscosity coefficient one and one half orders of magnitude less than transmission fluid. The transducers and sensors were drained of transmission fluid and flushed briefly with hexane, then methanol, then back-filled with gin. A 50-50 combination of 40 proof McCall's and 80 proof Gilbeys gin was used. The water content of the gin required that the fluid rest in the system for twenty-four hours during rising temperatures so that air released from the water could be collected and removed.

Although the system response time improved, it remained unacceptably high. It is crucial for each of the five DPG transducers to respond quickly and simultaneously to ensure proper instantaneous measurement of the sub-surface dynamic pressure.

Otherwise, an artificial phase lag may be introduced between the sensors' readings.

It was next decided to double the diameter of the long arm tubings. This tactic decreased response time to about 0.12 seconds, but the new 1/8 inch I.D. tubing was quite rigid. It was mated to the original connectors by Swage-Lock® reducers with very short 1/16 inch I.D. tubings. The severe handling of the arm tubings during back-filling and instrument assembly eventually led to the fracture of at least two, and possibly three, of the reducers. Before the failures occurred, the instrument was calibrated (Section V.C), assembled (Appendix D), and brought to CERC under the pressure of time for initial wave-tank testing.

When the DPG was returned to the laboratory at the University of Delaware, the arm tubing failures were confirmed and all of the connectors and external tubing were replaced with flexible 1/8 inch I.D. line and again back-filled with gin. The 1/16 inch I.D. nylon tubing within the water-tight cylinder was not replaced. Response time was recorded consistently as an acceptable 0.12 seconds, (Section V.C), and the flexible tubing proved very easy to work with.

### C. Bench Calibration

#### 1.. The Calibration Technique

An extremely simple calibration was first considered to statically determine the static response of the transducers to a known load. The isolation diaphragms were positioned facing upwards and were loaded with known weights. This technique was ineffective because of the physical nature of the diaphragms. The bottoms of the weights were rarely in full contact with the elastomer, as is depicted graphically in Figure V-2, so that the applied pressure to the sensor could not be easily calculated. If the weight was too heavy and large, some of the force of the weight would be exerted upon the top face of the

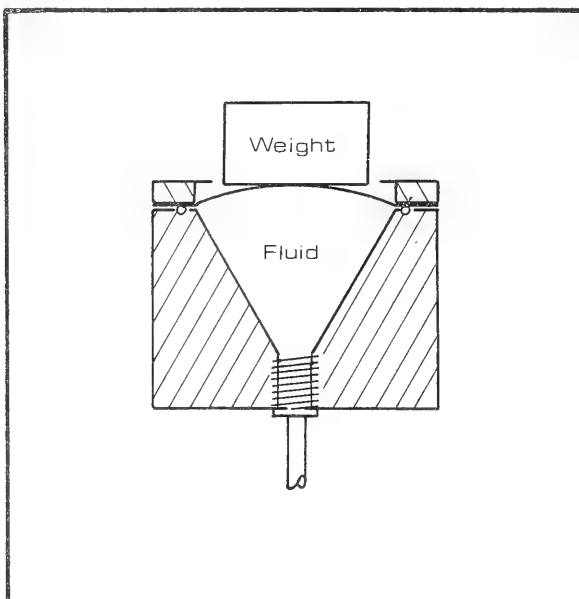


FIGURE V-2: Cross-section of isolation diaphragm with an object load applied.

acrylic housing and not upon the fluid. (Intuitively, one would expect this to happen even in the ideal case of force applied by the dynamic water column -- if the exposed elastomer area was so small that it could not deflect.)

A slightly more sophisticated calibration system was then designed. The system, as drawn in Figure V-3, consists of two pressure chambers which secure around each isolation diaphragm of a differential transducer, (only one is used with the absolute transducer). Each chamber is equipped with its own pressure transducer and a bicycle tire valve stem. The chambers are connected by tubing with a valve in the center to isolate, bleed, or allow the chambers to communicate with one another. The chambers are built of short steel cylinders with a plate welded on one end. Each chamber is secured to a sensor diaphragm with a short length of motorcycle tire inner tube that is glued to the chamber and hose-clamped to the isolation diaphragm housing. The system is pressured with a bicycle tire pump and the pressure sensed in each chamber and by the DPG transducer is reported on a multi-channel strip chart. The DPG transducers' response was interfaced with the strip chart using a short "bench cable" that mated with the instrumentation connector located within the DPG transducer stack.

The instrument was calibrated twice; once with the 1/8 inch arm and 1/16 inch I.D. center inflexible tubing used at CERC, and two weeks later, with the 1/8 inch I.D. flexible tubing used on the

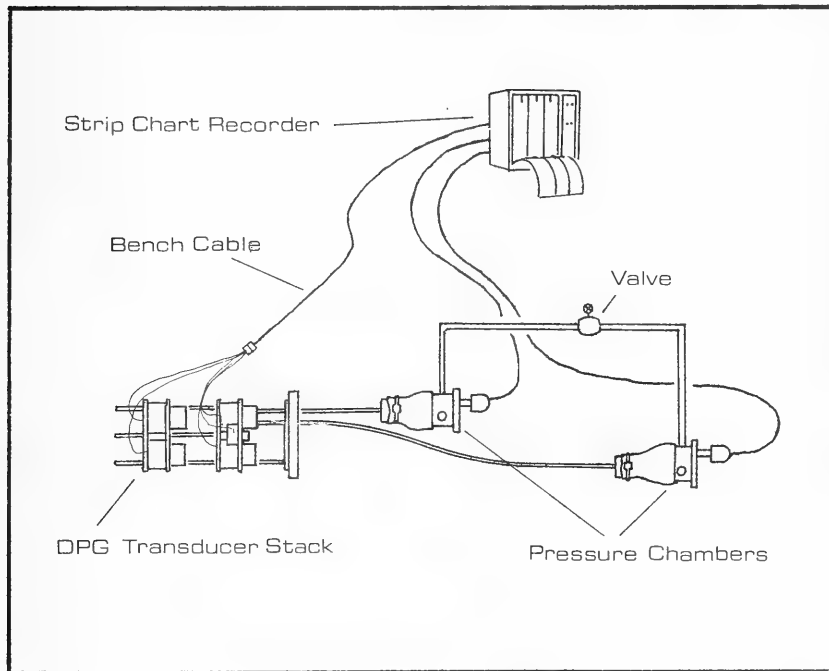


FIGURE V-3: The DPG bench calibration system. One pair of sensors shown for clarity.

final instrument installed at the FRF, Duck, NC. Early during the first calibration, one of the chamber transducers failed. This meant that only one side of a differential transducer could be loaded at a

time, while the other side was assumed to remain at atmospheric pressure. The calibration technique, then, was not able to simulate differential pressure loading while both sides were subjected to a pressure head as would be felt on the seafloor. (Both chambers leaked somewhat, so that it was not feasible to pressure each side to a particular head and then begin the differential loading.)

The calibration technique described herein entailed static loading whereas the operating instrument would be subjected to dynamic loading. This was not of great concern, however, since the in-situ loading is of relatively low frequency. The calibration technique could be improved by using an oscillating pump to pressure the chambers sinusoidally over time.

## 2. Testing for Air Bubbles

Theoretically the calibration system can be used to check for the presence of air bubbles in the transducer sensor lines. Firstly, air in a line will compress under a load and bias the pressure value that the transducer will report. Secondly, it is hypothesized that the loading and unloading of the air bubble will delay the response time of the system. If this is true, then it may be possible to detect an air bubble by loading each side of a differential transducer equally, then unloading them simultaneously. The side with the greater air volume will lag in response. (It is assumed that the inherent lag in arm-side response due to the longer arm

tubing length is negligible for large tubing diameters ( $\geq 1/8$  inch inner diameter). The length of small diameter nylon tubing is the same for each side of a transducer.) This effect was never tested exhaustively in the laboratory, but one possible such occurrence is

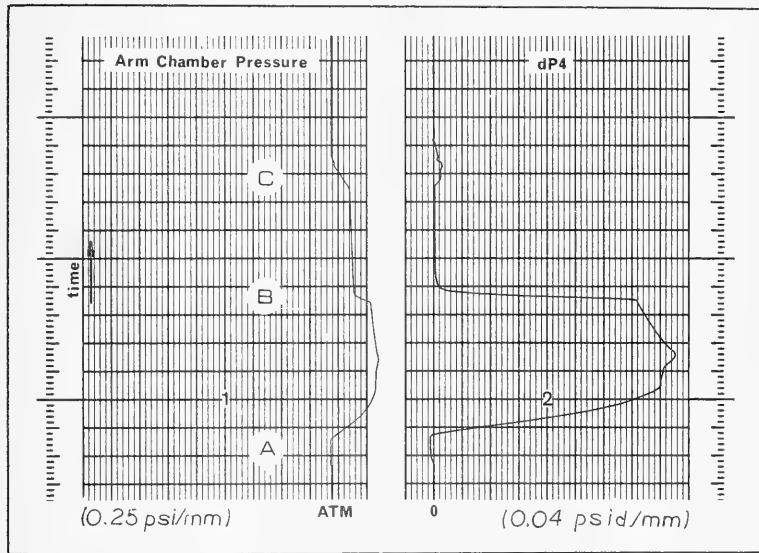


FIGURE V-4: Strip chart recording illustrating possible existence of air in arm side of dP4. A) arm sensor loaded; B) arm and center sensors communicate to establish zero differential pressure; C) both sensors bled simultaneously, arm side shows slight lag. Chart speed: 5 mm/sec.

shown in Figure V-4. The chamber on the arm sensor of dP4 was loaded (A) and then allowed to communicate with the center sensor chamber (B). The differential transducer correctly reported zero difference in pressure. When the entire system was bled (C), the transducer briefly indicated a greater pressure on the arm side. The arm was re-back-filled to be safe.

### 3. Static Calibration Results

The calibration results for each of the four differential pressure and the absolute pressure transducers as found during the pre-FRF calibration are shown in Figures V-5 (a) through (e). Differential transducers dP2, dP3, dP4, and the absolute transducer each demonstrated acceptable one-to-one reporting of the loads applied. DP1, however, is significantly biased. The problem was attributed to the transducer itself, since a similar error appeared during the first calibration. The zero-differential value of dP1 was also consistently high (5 to 7 volts as compared to 2.5 volts, as ordered); and unlike the other transducers, it demonstrated sensitivity to excitation voltage as is discussed in Section V.C.4. This malfunction did not appear until just before the scheduled testing was to begin at CERC and time limitations did not allow for its immediate repair. The calibration results of the first investigation for the absolute transducer and dP2, dP3, and dP4 are identical to those of the second.

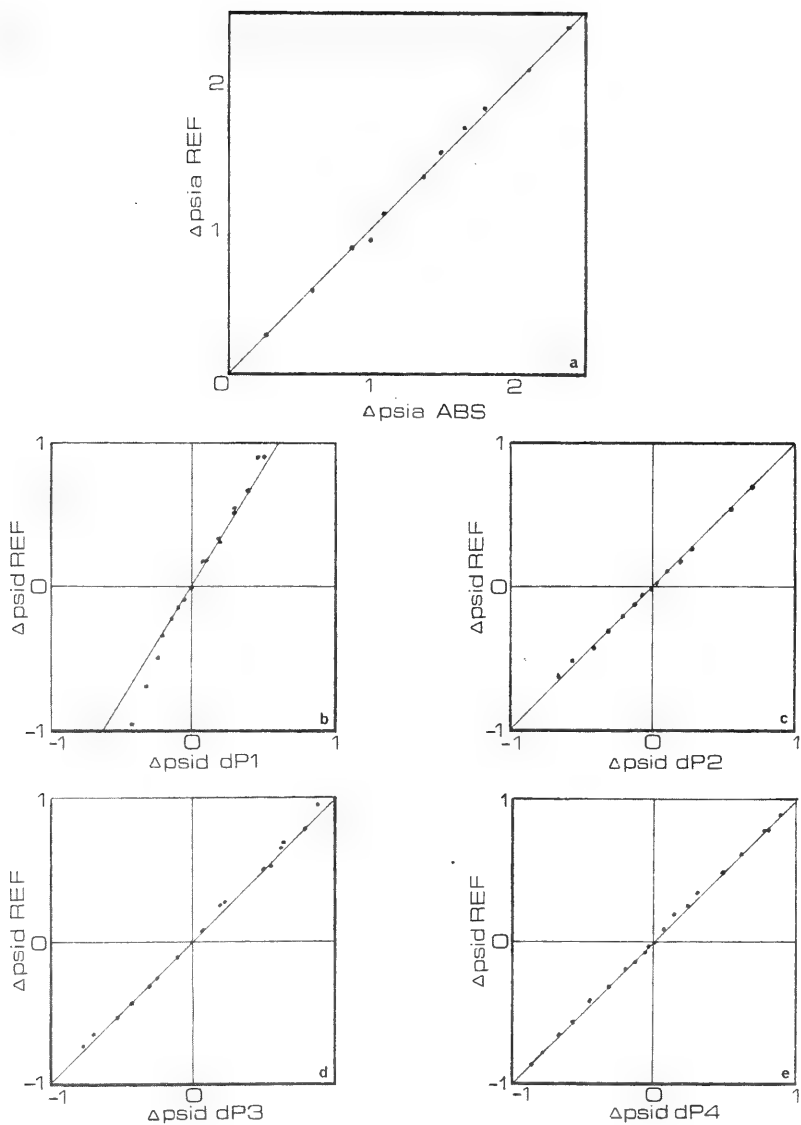


FIGURE V-5 (a) through (e): DPG transducer calibration curves.

The calibration curves were generated from the strip chart output reproduced in Appendix B. The calibration chamber was pressurized, allowed to leak slightly, and the chamber and DPG transducer readings taken from the strip chart at the point before the system was loaded again. The response time for the DPG transducers was determined by measuring the passage of time between loading events as reported by the chamber transducer and the DPG transducer on the strip chart. Each transducer appears to respond in an acceptably similar short time period.

#### 4. Power Supply Sensitivity

Each of the transducers demonstrated satisfactory insensitivity to power supply voltage fluctuations except dP1. Whereas the absolute and dP2, dP3, and dP4 transducers were unaffected by voltage changes from 20 to 26 volts, the output of dP1 decreased in an unexplained manner at excitation voltages below 22 volts.

#### 5. Transducer Drift

The absolute and dP1, dP2, and dP3 transducers proved steady in output with steady loading. However, dP4 intermittently and erratically drifted during the second set of bench calibration tests. It is assumed that such drift will be simply interpreted as a long period wave by the FFT analysis of the data. But the inability of

the transducer to establish a zero-differential tare value invalidates any calculations of instrument tilt or ambient temperature using dP4 signals (Section IV.C.4).

## 6. Temperature Effect

All transducers are temperature sensitive to some degree. The thermal sensitivity specifications of the DPG's Setra absolute and differential pressure transducers are less than  $\pm 0.02\%$  FS/ $^{\circ}\text{F}$  and  $\pm 0.03\%$  FS/ $^{\circ}\text{F}$  thermal zero shift with thermal coefficients of sensitivity of less than  $\pm 0.015\%$  FS/ $^{\circ}\text{F}$  and  $\pm 0.02\%$  FS/ $^{\circ}\text{F}$  respectively. The transducer and sensor systems in the DPG are slightly more or less sensitive than the factory specifications because of their fluid back-fill. As the DPG environment changes temperature the back-filling gin expands or contracts. Moreover, a temperature change induces a slight differential pressure across the differential transducers because of the greater volume of fluid in the (longer) arm sensors. Since the volumetric expansion of a fluid is linearly proportional to the change in temperature and initial volume of fluid, the expanded volume in the arm sensors will be four times that of the center sensors, (since the arm tubing is four times the length of the center tubing.) But since temperature changes under twenty feet of ocean water are typically small and of low frequency, it is assumed that any thermal transducer drift during a sampling interval will be interpreted as a very long period wave or as a mean which changes

from record to record. Such thermal effects accordingly affect the mean of a pressure record. This could be mistakenly interpreted as instrument tilt if two differential records taken at different ambient temperatures are compared (Section III.C.4). It could also affect the tide calculation by altering the back-fill pressure term,  $P_{bf}$ , of the absolute sensor in Equation 4.35. Future development of the DPG should more thoroughly investigate the effects of temperature on the transducers and sensors.

#### 7. Absolute Sensor Back-Fill Pressure

The absolute pressure sensor back-fill pressure,  $P_{bf}$ , is obtained in the laboratory by either of two ways. (1) The instrument is positioned such that there is no fluid head above the transducer and the absolute pressure reported above the atmospheric is recorded. (2) The instrument is oriented upright and the absolute pressure that is reported beyond the atmospheric and sensor fluid head is recorded.

#### D. CERC Wave Tank Tests

##### 1. Introduction

The first DPG prototype was laboratory tested at the large outdoor wave tank at the Coastal Engineering Research Center, Fort Belvoir, Va. The instrument and cradle proved themselves easily maneuverable -- both above and below water. Although three of the

four differential pressure channels failed and/or were disturbed by the wave tank, the analysis of measurements from the absolute and one differential pressure channel suggest satisfactory performance of the DPG.

## 2. Installation

The cradle was secured to a small flatbed trailer and the instrument mounted upon it. The trailer was easily pulled and delivered to the CERC wave tank by a light vehicle. The outdoor wave tank is a long, 15 foot wide, 20 foot deep facility with a large piston-type wavemaker. The cradle was lowered on its side over the

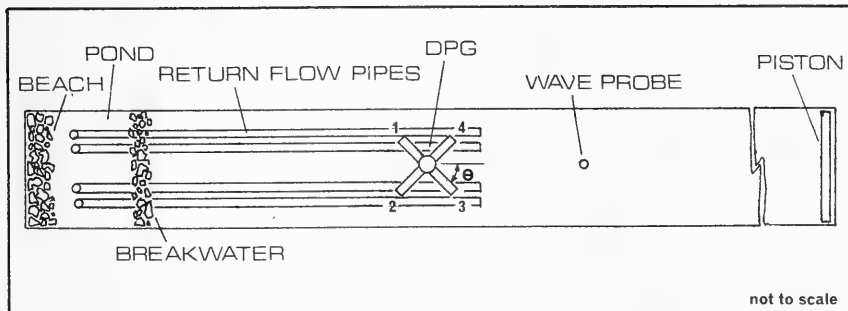


FIGURE V-6: Orientation of the DPG during CERC wave tank tests.  
Configuration I:  $\theta=55^\circ$ ; Configuration II:  $\theta=35^\circ$ .

tank wall by ropes and dropped slowly into the water. It was positioned by two divers under 10.2 feet of water at approximately

mid-length of the tank. The cradle, in the center of the tank, was then secured by ropes to large U-bolts on return-flow pipes that terminated at this location, (Figure V-6). It was not clear whether the outflow of the pipes during testing would influence the DPG.

The instrument, carried upon the shoulder of one deck-hand, was then positioned on a trestle over the tank and lowered into the water by another rope slung through an arm on the trestle. Care was taken to keep the instrument arms away from the trestle and tank walls using two lateral control lines that were held on each side of the tank. The instrument was received by a diver, guided and positioned into the cradle, and secured with cable ties. The orientation of the instrument was checked by measuring the distance from the wall to each of the cradle legs with a tape secured along a wooden "T." The top of the "T" was held against the wall to ensure that the measurement was taken perpendicular to the wall. A 100 foot length of unarmored cable, earlier mated to the instrument above water, was interfaced with a power supply and strip chart recorder in a trailer alongside the tank. Despite the poor underwater visibility, (less than six inches), the entire installation took less than two hours and required only two divers and one deck-hand.

To remove the equipment, the procedure was reversed. The cradle was lifted from the water by securing a rope between it and a van, then the van was driven away and the cradle hoisted up along the wall.

Diver entry and exit was made using a long flat aluminum ladder tied to the top of one of the tank walls.

### 3. Tests and Results

The facility was, at the time, in the final week of testing rubble mound breakwater structures. So the DPG tests conveniently "piggy-backed" with the regularly scheduled tests. Sets of eleven waves of 1 meter nominal height (3.28 feet) and 5 second period were run every 4 to 5 minutes. Wave height and period were monitored by resistance probes and recorded on a strip chart located inside the trailer.

Initially, the three differential channels monitored appeared ill-behaved (Figure V-7). The fourth, dP2, had already been confirmed inoperative due to a broken arm tubing connector. It was then discovered that the end-cap on the dP3 arm had accidentally been left on. The instrument was assembled for the CERC tests with the arm isolation diaphragms flush with the end of the PVC arms. With the arm plugged, the diaphragm could communicate with the ambient water only through a thin crescent part-way around the diaphragm housing. It is assumed that such a small gap damped the dynamic pressure field of the passing waves.

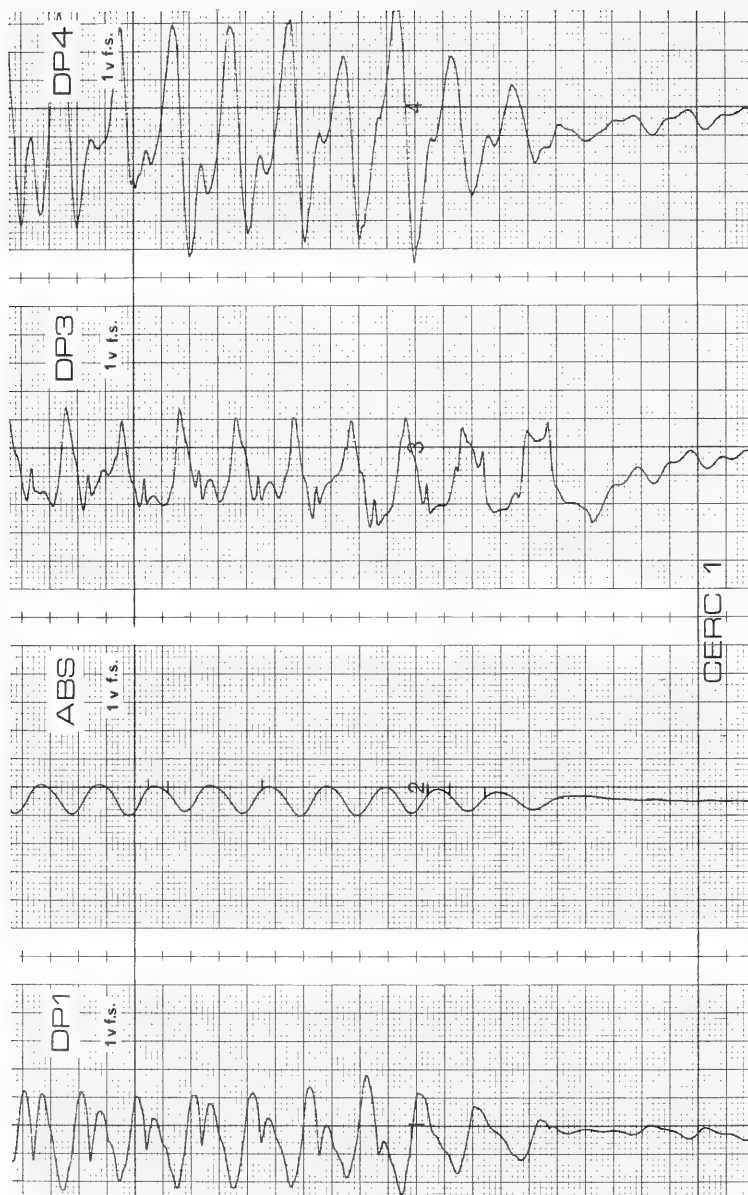


FIGURE V-7: Sample strip chart recording; CERC test. Configuration 1. DP3 arm end-cap accidentally left on. Chart speed: 2 mm/sec. Calibration: 10 psia/V and 0.2 psid/V.

Once the end-cap was removed, the third channel demonstrated sinusoidal output with the expected  $\pi/2$  phase difference to the absolute signal as predicted by Equations 2.1 and 2.2. The unexpected characteristics of the first and fourth differential channels, however, remained unexplained. Both channels indicated the passage of a trough, as expected, but did not report the actual crest passage -- instead suggesting the passage of two crests  $\pi/4$  before and after the actual passage. This phenomenon was noted in both orientations of the DPG tested. It is thought that the unexpected characteristics of these differential channels could have been due to the poor positioning of the sensors at the unprotected ends of the PVC arms. It is also possible that the arm tubings were broken at the time of the tests or that the sensitive differential gauges were adversely influenced by the return flow pipes to which the cradle was attached.

The instrument was originally positioned such that the dP1 and dP3 arms were aligned approximately 55 degrees from the centerline of the tank, or wave ray. The cradle and instrument were next rotated about 20 degrees such that arms 1 and 3 were approximately 35 degrees from the wave ray. Figures V-8 and V-9 are strip chart recordings from each of the configurations, respectively. The rotation of the DPG was restricted between these two positions because of the pipes that surrounded either side of the cradle. These pipes, however, offered the only structure to which the cradle

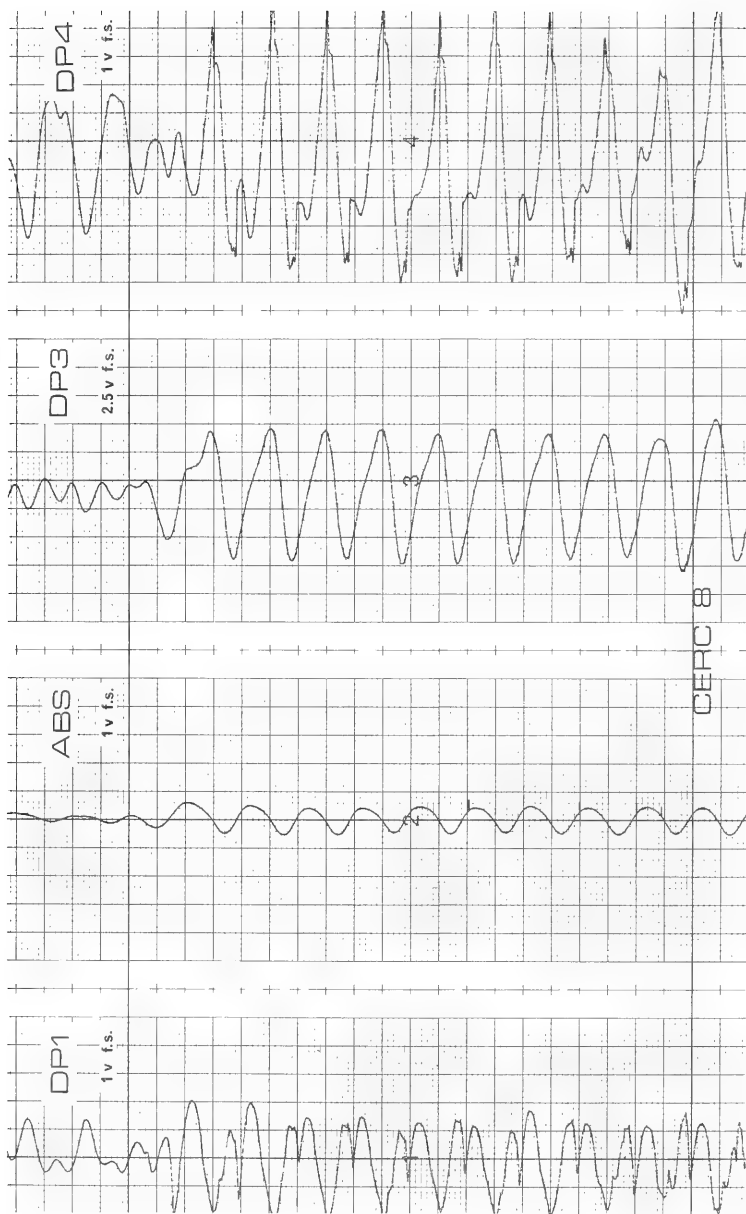


FIGURE V-8: Sample strip chart recording; CERC test. Configuration I. Chart speed: 2 mm/sec. Calibration: 10 psia/V and 0.2 psid/V.

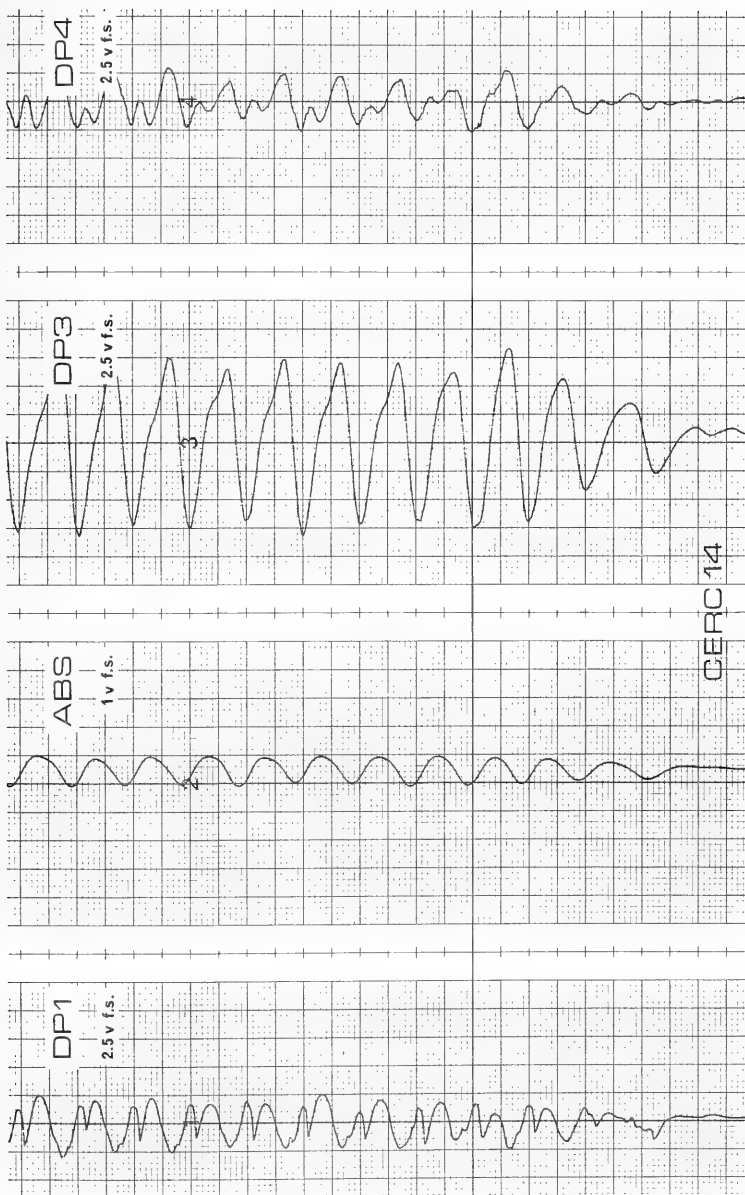


FIGURE V-9: Sample strip chart recording; CERC test. Configuration II. Chart speed: 2 mm/sec. Calibration: 10 psia/V and 0.2 psid/V.

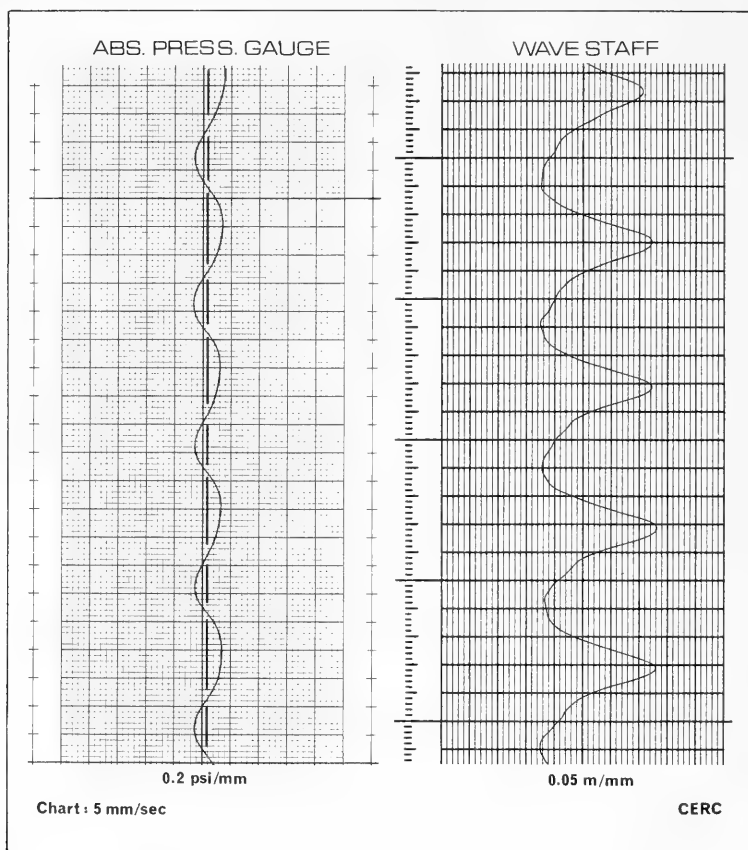


FIGURE V-10: Comparison of DPG absolute pressure gauge and CERC resistance wave probe.

could be secured.

Figure V-10 compares the absolute pressure transducer signal with that of the tank's resistance wave probe located about sixty feet upstream of the DPG site. The resistance probe describes the waves' non-linear profile featuring peaked crests and long shallow troughs. Wave period is 5.0 seconds and the height is between 3.0 feet (0.925 m) and 3.36 feet (1.025 m) from crest to trough. The absolute transducer also reports a period of 5.0 seconds and a wave height of about 3.2 feet as calculated using stream function theory (Dean, 1974). Stream function theory is used because of the great non-linear appearance of the wave form. The calculated wave height is only about 2.8 feet if linear theory is assumed. From Eq. 2.1,

$$\text{amplitude} \left[ \frac{\text{crest}}{\text{trough}} \right] = \frac{P_{\text{dyn}} \left[ \frac{\text{crest}}{\text{trough}} \right]}{\gamma K_p \left[ \frac{\text{crest}}{\text{trough}} \right]} \quad (5.15)$$

Here,  $\gamma = 62.23 \text{ lb/cu.ft.}$  (13 C), and  $K_p$  is approximately 0.874 and 1.068 for the wave crest and trough respectively from stream function theory (Dean, 1974). This was calculated for a wave of five second period in water depth 10.2 feet and absolute sensor height above the bottom of 4.25 feet. The intimation of static water level is also good. The no-wave tare value was steadily reported as 18.23 psia, which corresponds to a water height above the sensor, from Eq. 4.35 of 5.91 feet.

$$z_s = (P_{\text{mean}} - \gamma_{bf} l_{bf} - P_{\text{atm}} - P_{bf})/\gamma \quad (4.35)$$

where  $\gamma_{bf} = 55.6 \text{ lb/cu.ft.}$

$l_{bf} = 18.5 \text{ inches}$

$P_{\text{atm}} = 14.74 \text{ psi}$

$P_{bf} = 0.34 \text{ psi}$

$\gamma = 62.23 \text{ lb/cu.ft.}$

A value of 5.95 feet is expected from the difference of the tank water depth, 10.2 feet, and the sensor's height above bottom, 4.25 feet.

An estimate of the wave direction was attempted from the signal of dP3 using wave parameters as predicted by stream function theory. The average magnitude of the channel's signal was estimated and the maximum differential pressure expected along the wave ray calculated from stream function theory. The angle  $\Theta$  between the wave ray and the dP3 arm is then:

$$\Theta = \cos^{-1} \left[ \frac{[dP/dx]_{\text{measured}}}{[dP/dx]_{\text{max}}} \right] \quad (5.16)$$

The wavenumber  $k$  was calculated using stream function theory for a 5 second wave in the water depths stipulated earlier. The pressure response function  $K_p$  was similarly estimated for a depth equal to the

mean of the center and arm sensor vertical positions above the bottom. The gage length  $dx$  was 3.5 feet. For configuration I, the estimated angle,  $51.3^\circ$ , compares well with the  $55^\circ$  angle expected. For configuration II, the estimated angle is  $35.4^\circ$  compared to an expected value of  $35^\circ$ .

The experiment at CERC, although plagued with arm sensor failures and highly non-linear waves, demonstrated the capability of the instrument to measure wave direction. The tests also served the purpose of defining several important modifications required to improve the performance of the DPG system.

#### E. The Second DPG Prototype

The DPG was returned to the University of Delaware laboratory and partially disassembled to install the new hardware modifications. The fracture of the arm lines of dP1, dP2, and dP4 were confirmed. All of the stainless steel tubing exterior to the water-tight instrument cylinder was replaced with flexible tubing and back-filled, and the system was calibrated as described in Section C of this chapter. New PVC arms were machined to house the flexible tubing and isolation diaphragms and the instrument was reassembled as described in Appendix D. Care was taken to ensure that the sensors' elastomer diaphragms were well back from the ends of the PVC arms and exposed to the holes in the sides of each arm. Some dimensions of

the instrument, reassembled for the field evaluation, are specified in Appendix C.

CHAPTER VI  
FIELD INSTALLATION AND EVALUATION

A. Installation at the FRF

The newly re-assembled instrument and cradle were towed on a trailer to the Coastal Engineering Research Center Field Research Facility at Duck, North Carolina, in early May of 1982. An installation site was chosen approximately 735 feet directly south of the seaward end of the 1800 feet long research pier. This site fell safely between the FRF's regular bathymetric profile lines, allowed a reasonable safety margin of length for cable deployment (18%), exhibited a relatively stable 20 foot depth contour over time, and was considered to be sufficiently far from the large scour hole at the end of the pier to avoid any related refraction effects. The geographic location and typical nearshore bathymetry of the site are illustrated in Figures VI-1 and VI-2.

It was decided to install the DPG using the facility's Coastal Research Amphibious Buggy (CRAB) marine vehicle. The CRAB is a three-wheeled tripod vehicle capable of driving across the beach

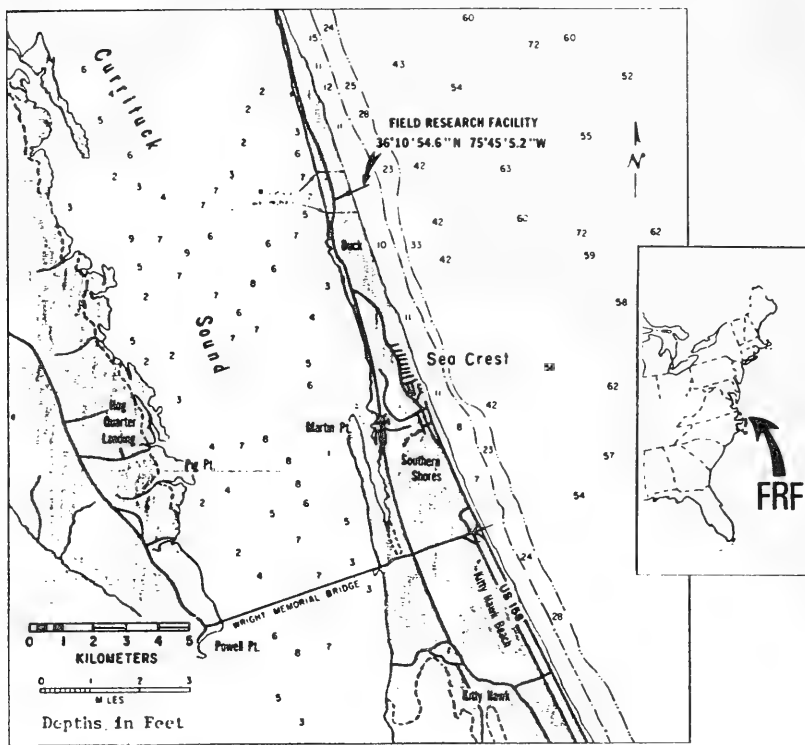


FIGURE VI-1: Site of the DPG field evaluation; (from Birkemeier, et.al., 1981).

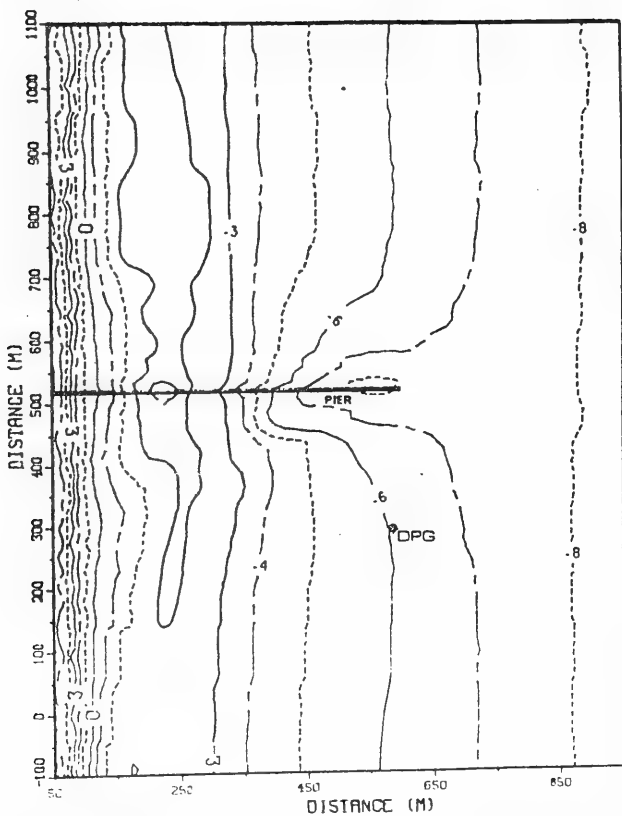


FIGURE VI-2  
FRF BATHYMETRY 3 NOV 81  
CONTOURS IN METERS

FIGURE VI-2: Nearshore bathymetry of installation site.



FIGURE VI-3: Preparing for field installation: the DPG suspended underneath the operator's platform of the CRAB.

face and through the surf zone. The instrument was secured to the cradle and hoisted underneath the top (operator's) platform, (Figure VI-3). The cable and service box were then brought to the end of the pier.

On May 14, 1982, the wave activity settled sufficiently to attempt the installation. The CRAB was driven offshore with the instrument and positioned about 200 feet south of the end of the pier. Three divers and a boat operator entered the surf in a Zodiac and motored underneath the pier. The service box, with its 80 feet of unarmored cable secured inside, was lowered into the Zodiac and then motored towards the CRAB -- pulling the cable behind it. The service box was carried by a diver below the rear of the CRAB and brought underneath the center of the vehicle. In what became the only difficult phase of the operation, the service box was pushed up into the cradle and the cable mated to the instrument. Large, long period swell made this maneuver both frustrating and often dangerous -- as the sharp corners of the cradle feet posed a hazard to the divers. The cable was secured to the bottom of the CRAB using a prussick knot and the vehicle was driven towards the installation site -- pulling out the cable. Floats were placed every 80 feet along the cable from the end of the pier.

Once at the site, originally marked by a buoy, the instrument was lowered into the water. Divers maneuvered the instrument between the two rear legs of the CRAB to the seafloor, detached the lines from the CRAB to the cradle and cable, and the CRAB drove away a short distance. A four-foot screw anchor was turned into the sandy bottom approximately three and a half feet from the end of each arm and chain was attached from each arm to its respective screw anchor. The chains were secured taut by a chain binder and each rested at about a 45 degree angle to the seafloor. A fifth screw anchor and buoy was next installed twenty feet away from the DPG and a heavy line secured between this anchor and the cradle. Satisfied with the instrument installation, the buoys were released from the cable and work commenced at the pier.

The cable had to be secured under the pier and prevented from chafing on the cement piling jackets. The cable descended from the pier deck inside a stainless steel case along the northeastern-most piling. A steel cable was looped around the base of this piling and attached to a wire jacket that cinched the cable under tension. To prevent chafing about the south pilings among which the cable passed, a long pipe was jetted between the two southeastern-most pilings and a similar steel line and wire jacket attached between the pipe and cable. The cable began to bury itself into the sand within hours of the deployment.

The cable leads were interfaced with FRF power and data-logging equipment and regular data recording commenced that evening.

#### B. Instrument Orientation

The orientation of the instrument with respect to magnetic north was determined using a submersible digital compass and conventional diving compasses. The digital compass was mounted at the end of a five-foot length of aluminum angle. One diver recorded the value indicated by the compass while another diver held two feet of the free end of the angle onto the top of each PVC arm of the instrument. In this way, the digital compass was at least six feet from the steel cradle. Compass headings were recorded for each arm twice -- once by each of the two divers -- and then averaged. The orientation of each arm was also measured by securing a diver's compass around the end of an arm using the compass wrist strap. Measurements were taken three times for each arm using two different compasses and then averaged. All of the values recorded for each technique along each arm agreed reasonably well within a technique. The wrist compass, strapped around an arm, indicated the heading perpendicular to the arm. Accordingly, ninety degrees was subtracted from each wrist compass reading to give the heading of the arm.

As an experiment, the divers' compasses were placed on an arm above the end of the steel channel that holds the arm. The compass was then slid towards the end of the arm. The heading changed as the compass was slid across the end of the steel channel and then remained relatively stable. It was therefore thought at the time that the readings taken at the ends of the PVC arms were sufficiently far from the steel cradle to avoid any bias of the divers' compasses. However, as can be seen from Table 6.1, this was not true. Since each arm is perpendicular to its neighboring arm, each of the compass readings are restrained to be 90 degrees apart. Although the digital compass measurements approximate 90 degree separation, those of the wrist compasses clearly do not.

TABLE 6-1: ORIENTATION HEADINGS OF THE DPG ARMS

ARM	WRIST COMPASS		DIGITAL COMPASS		RESOLVED average
	apparent	actual	apparent	actual	
1	228.33	241.75	238.80	241.89	241.82
2	155.33	151.75	153.90	151.89	151.82
3	78.00	61.75	61.20	61.89	61.82
4	325.33	331.75	333.65	331.89	331.82

\* Headings are with respect to magnetic north, 6/15/82.

This directional anomaly was resolved using a technique suggested by Dr. Robert Dean (personal conversation). The apparent (biased) direction,  $\beta'_n$ , indicated by the compass for each arm  $n$ , can

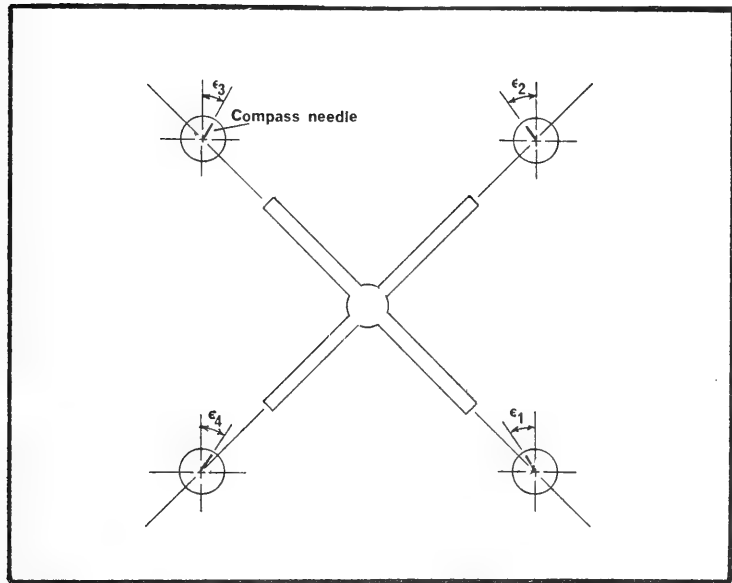


FIGURE VI-4: Typical influence of the steel cradle upon the magnetic compasses used for orientation measurements.

be expressed in terms of the actual orientation of that arm,  $\beta_n$ , and the error associated with that arm,  $\epsilon_n$ , that is introduced by the metal mass of the cradle:

$$\beta_n' = \beta_n + \epsilon_n \quad (6.1)$$

Since the compasses were placed upon each arm at about the same distance from the center of the instrument, and if one assumes that the effect of the metal mass upon the compass readings is the same for each arm (i.e., radially inward), then the errors associated with each of two collinear arms should be equal and opposite in sense. (See Figure VI-4). Accordingly, the sum of the errors associated with the reading for each arm should equal zero;

$$\sum_{n=1}^4 \epsilon_n = 0 \quad (6.2)$$

If one expresses the actual orientation of each arm in terms of the orientation of the arm with the smallest value of apparent direction, Equation 6.1 may be written as:

$$\beta_3' = \beta_3 + \epsilon_3 \quad (6.3a)$$

$$\beta_4' = \beta_3 + 90^\circ + \epsilon_4 \quad (6.3b)$$

$$\beta_1' = \beta_3 + 180^\circ + \epsilon_1 \quad (6.3c)$$

$$\beta_2' = \beta_3 + 270^\circ + \epsilon_2 \quad (6.3d)$$

The sum of Equations 6.3 a through d is:

$$\sum_{n=1}^4 \beta_n' = 4\beta_3 + \sum_{n=1}^4 \epsilon_n \quad (6.4)$$

From Equation 6.2,

$$\beta_3 = \frac{1}{4} \sum_{n=1}^4 \beta_n' \quad (6.5)$$

and the corresponding orientation for each of the other three arms may be found by subtracting Equations 6.3 from 6.1. The corrected orientation headings for each arm and for each type of compass used are listed in Table 6.1. Somewhat surprisingly, the agreement between the corrected averages of the arm headings as found using the expensive digital compass and the simple wrist compasses is very good -- within 0.14 degrees of one another. The final orientation of each

DPG arm was taken as the average of the corrected values found from the digital and wrist compass measurements. The values of each correspond to the heading towards which the end of each arm points with respect to magnetic north. The values were corrected to true north using the 1982 value of the variation for Cape Hatteras, N.C.

This investigation indicates the importance of careful redundant checks of instrument orientation when working near a steel structure. The analysis technique outlined here requires at least one pair of compass measurements made on opposite sides and equidistant from the approximate center of the metal structure. The investigation suggests that simple wrist compasses may be adequate for determining instrument orientation if special care is taken during the measurement and interpretation of the results.

#### C. First Month's Inspection

The instrument was re-inspected on June 15, 1982 -- one month after installation. The cradle and instrument had settled into the seafloor only four or five inches with minimal disturbance to the bed around the gauge. The cable had buried itself deeply immediately outside of the service box. The system's anti-fouling agents had thus far worked excellently.

## D. Results of DPG Data Analysis

### 1. Introduction

Multiple sets of data were analyzed to determine the integrity of the gravity wave information obtained from the DPG. Although output was available from the facility's HF radar system, there were no other functioning in-situ directional wave monitors at the FRF during the weeks after the instrument installation. Hence, DPG directional information was compared with visual and radar estimates. Wave height and period could, however, be compared with CERC Baylor gauge data from near the end of the pier. The data were also inspected for irregularities in the time domain that could signal system malfunction.

### 2. Time Domain Signal Analysis

The five transducers' records corresponding to a single set of wave data were input to the DPG software package and scanned for signals beyond three standard deviations from the mean of the record. The means were then re-calculated and subtracted from the records which were then converted to pressure signals. (See Sections IV.D.1-3.)

In each data set analyzed, the number of points beyond the three standard deviation limit was satisfactorily small -- less than one percent of the record, as expected. The mean of channels dP2, dP3, and the absolute agreed well between data sets, (possibly indicating minimal instrument tilt over time due to settling -- see Section IV.D.4). The means of dP1 and dP4 often varied between sets, however. It was expected that the mean of dP4 might vary given the signal drift observed during bench calibration. Similarly, it was not surprising to encounter difficulty with dP1 after considering its irregularities on the bench.

The mean values of the absolute records predicted tide levels reasonably well as is shown in Table 6-2. DPG tidal calculation is compared with that determined by a stilling well located near the middle of the pier. Differences might be attributed to temperature effects upon the absolute sensor, (see Section V.C.6). Atmospheric pressure fluctuations were accounted for.

The mean values of dP2 and dP3 differ significantly from these two channels' tare values recorded on land. In-situ mean values are 2.31 V and 2.56 V for dP2 and dP3 respectively, and 0.60 V and 0.71 V on land. Both subaerial and subaqueous checks were made with the same 1100 foot long cable. The subaerial tare values were checked on a hot afternoon and the ocean was some 8°C cooler. But it was not likely that this rise in mean voltage was due to temperature changes since one expects a voltage drop with a decrease

TABLE 6-2: COMPARISON OF TIDE LEVEL

1982		TIDE		AMBIENT CONDITIONS	
DATE	TIME	DPG (m)	FRF (m)	T (°C)	P (mb)
5/18	0700	-0.26	-0.26	16.8	1018.0
	1300	+0.12	+0.18		
5/19	0700	-0.15	-0.15	16.3	1020.0
	1300	-0.07	-0.02		
5/20	0700	-0.05	-0.05	13.0	1018.3
	1300	-0.36	-0.30		
5/21	0700	+0.13	+0.12	13.3	1015.5
	1300	-0.53	-0.54		
5/22	0700	+0.46	+0.43	17.5	1013.2
	1300	-0.53	-0.57		
5/23	0700	+0.58	+0.57	16.8	1019.5
	1300	-0.64	-0.66		
5/24	0700	+0.56	+0.56	16.5	1018.0
	1300	-0.56	-0.62		

NOTES:

FRF data is from stilling well at pier.

Tide elevations are referenced to NGVD.

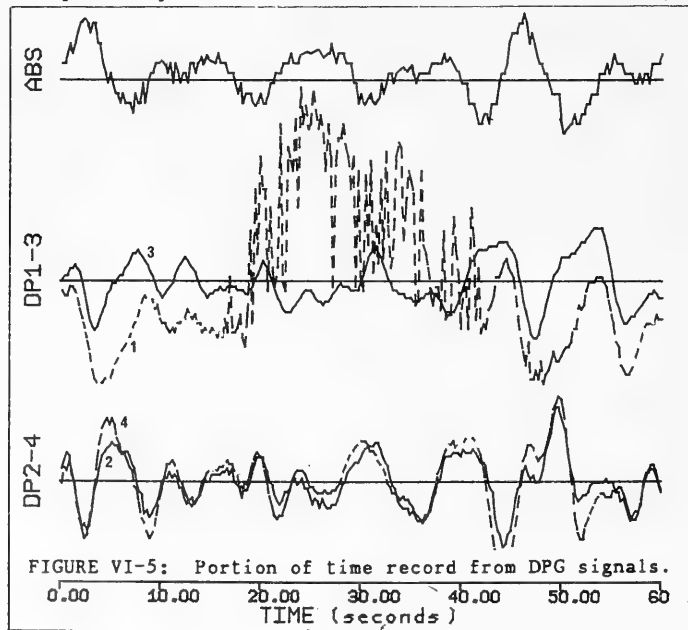
DPG P<sub>bf</sub>(abs) = 1.32 psi.

TIME is Eastern Standard.

Temperature is for sea-water.

in temperature in the present DPG configuration, (Section V.C.6). The difference could indicate slanted installation of the instrument. The changes in mean voltages suggest that arms 2 and 3 could be tilted  $9.7^\circ$  and  $11.8^\circ$  above the horizontal, respectively; (from Equation 4.34). This could be confirmed by comparison with dP1 and dP4; however, neither of these channels show a clear trend in the change of mean value between land and sea.

A portion of the time record of one data set is shown in Figure VI-5. The mean value has been removed from each record and the signs of dP1 and dP2 have been reversed. The dP1 signals have been multiplied by the channel 1 calibration factor of 1.65. The



absolute record corresponds to pounds per square inch and the signals of the differential records to pounds per square inch differential per inch of gage length. It is immediately obvious that the signal of dP1 is extremely erratic with high frequency energy that would alias into the energy spectrum. At other times, it agrees in form with dP3 satisfactorily although it is shifted downwards because of the large mean value subtracted from the record. This large mean is apparently the result of the large positive-valued high frequency oscillations. This disturbance is intermittent and does not appear in all of the records from dP1. These high frequency oscillations have never been observed on the strip chart output at the FRF, and so it is possible that the problem lies within the digitization of the signal.

The records of dP2 and dP4 agree well as expected for two collinear gauges. There are slight phase and amplitude differences as would be expected since the two gauges are separated in space a finite amount.

There is reasonable phase agreement between the dP2, dP3, and dP4 signals with those of the absolute gauge -- as best as can be seen. Again, one expects a ninety degree phase difference between the absolute and differential signals.

The "graininess" of the absolute gauge signal is due to resolution limitations of the transducer and digitizer.

It is reasonable to conclude from inspection of the raw data, then, that the dP1 records should not be included in the spectral analyses, and that less faith should be placed in dP4 because of its tendency to drift (as is exhibited by its changing mean). If these two channels do not provide valid data, it is not possible to generate the water surface curvature terms as described in Chapter IV with any confidence.

### 3. Record Length

In beginning the conversion of the data to the frequency domain, it was discovered that the DEC-10 computer system could not handle the 17 minute long four-samples-per-second data records, (4096 points). So the data size was halved by averaging two adjacent points in the time series. The Fast Fourier Transform, then, operated upon a 17 minute record with an effective sampling rate of two Hertz. (The corresponding Nyquist frequency was still safely above the two rad/sec cut-off frequency used in the analysis program.) The number of data points in the time series was halved after the initial scan for bad points and calculation of the record mean.

It was discovered that this modification was very important. The results of the analysis of DPG data varied considerably between a 17 minute long record with an effective sampling interval of 0.5 seconds compared to the analysis of an 8.5 minute long record with 0.25 second sampling. Further, there are considerable differences between the analysis results of the first 8.5 minutes of a record compared to the last 8.5 minutes. This variability may be due to sampling and the confidence limits on the spectrum. Figures VI-6 through VI-8 are copies of the analysis output for one data set analyzed with a 17 minute record, the first 8.5 minutes of the record, and the last 8.5 minutes, respectively. The 17 minute record with 0.5 second sampling interval block-averages 8 adjacent frequency bands compared to 4 bands for the 0.25 second sampled records. The spectra developed from the 17 minute long record, then, is more stable than for the 8.5 minute long record, yet retains the same frequency resolution. Figure VI-9 and Figure VI-10 illustrate the energy and non-smoothed peak-energy directional spectra for each case. The analysis results most closely match other observations made at the FRF when the full 17 minute long record with effective 2-Hertz sampling is utilized. Table 6.3 lists the results of each type of analysis and compares the results with independent FRF observations over a period of four days.

UNIVERSITY OF DELAWARE  
DEPARTMENT OF CIVIL ENGINEERING  
DPG DIRECTIONAL WAVE MONITOR / FRF, DUCK, N.C.

DEV	YR	MO	DAY	TIME
111	82	6	11	7 0
121	82	6	11	7 0
141	82	6	11	7 0

4096 POINTS ANALYZED AT .50 SECOND SAMPLING  
8 BANDS BLOCK AVERAGED

GAGE NUMBER 2  
8 LOW truncations; 6 HIGH truncations  
Mean= 2.299 S.Dev= 0.09652 Lower Limit= 2.010 Upper Limit= 2.589

GAGE NUMBER 3  
0 LOW truncations; 8 HIGH truncations  
Mean= 2.039 S.Dev= 0.19138 Lower Limit= 1.465 Upper Limit= 2.613

GAGE NUMBER 5  
0 LOW truncations; 1 HIGH truncations  
Mean= 2.364 S.Dev= 0.03900 Lower Limit= 2.247 Upper Limit= 2.481

TIDE LEVEL IS 0.824 FEET.

POSSIBLE INSTRUMENT TILT (deg)  
OP2 DP3  
-0.061 -3.365

Significant Wave Height (ABS gage) = 4.32 feet.

Effective period = 7.817 seconds.

Maximum Energy located at bands:

11.070	exceeds average energy by	715.00 %
10.189	exceeds average energy by	266.13 %
12.118	exceeds average energy by	194.16 %
13.386	exceeds average energy by	159.03 %
8.790	exceeds average energy by	115.97 %
8.225	exceeds average energy by	108.46 %

Compass heading from which waves propagate

Band 11.070 secs:	Greatest Energy at	73. deg
Band 10.189 secs:	Greatest Energy at	71. deg
Band 12.118 secs:	Greatest Energy at	67. deg
Band 13.385 secs:	Greatest Energy at	69. deg
Band 8.790 secs:	Greatest Energy at	69. deg
Band 8.225 secs:	Greatest Energy at	75. deg

FIGURE VI-6: DPG analysis results using the full record length of 17 minutes with effective 2 hertz sampling.

UNIVERSITY OF DELAWARE  
DEPARTMENT OF CIVIL ENGINEERING  
DPG DIRECTIONAL WAVE MONITOR / FRF, DUCK, N.C.

DEV	YR	MO	DAY	TIME
111	82	6	11	7 0
121	82	6	11	7 0
141	82	6	11	7 0

2048 POINTS ANALYZED AT .25 SECOND SAMPLING  
4 BANDS BLOCK AVERAGED

GAGE NUMBER 2  
7 LOW truncations; 2 HIGH truncations  
Mean= 2.299 S.Dev= 0.10032 Lower Limit= 1.998 Upper Limit= 2.600

GAGE NUMBER 3  
0 LOW truncations; 4 HIGH truncations  
Mean= 2.037 S.Dev= 0.18856 Lower Limit= 1.471 Upper Limit= 2.603

GAGE NUMBER 5  
0 LOW truncations; 4 HIGH truncations  
Mean= 2.360 S.Dev= 0.03693 Lower Limit= 2.250 Upper Limit= 2.471

TIDE LEVEL IS 0.743 FEET.

POSSIBLE INSTRUMENT TILT (deg)  
DP2 DP3  
-0.065 -3.377

Significant Wave Height (ABS gage) = 4.24 feet.

Effective period = 7.206 seconds.

Maximum Energy located at bands:

11.011	exceeds average energy by	435.16 %
12.047	exceeds average energy by	343.94 %
8.192	exceeds average energy by	233.40 %
10.139	exceeds average energy by	138.87 %
9.394	exceeds average energy by	136.97 %
6.872	exceeds average energy by	127.69 %

Compass heading from which waves propagate

Band 11.011	secs: Greatest Energy at	77. deg
Band 12.047	secs: Greatest Energy at	77. deg
Band 8.192	secs: Greatest Energy at	71. deg
Band 10.138	secs: Greatest Energy at	81. deg
Band 9.394	secs: Greatest Energy at	61. deg
Band 6.872	secs: Greatest Energy at	61. deg

FIGURE VI-7: DPG analysis results using the first 8.5 minutes of the record, (4 hertz sampling).

UNIVERSITY OF DELAWARE  
DEPARTMENT OF CIVIL ENGINEERING  
DPG DIRECTIONAL WAVE MONITOR / FRF, DUCK, N.C.

DEV	YR	MO	DAY	TIME
111	82	6	11	7 0
121	82	6	11	7 0
141	82	6	11	7 0

2048 POINTS ANALYZED AT .25 SECOND SAMPLING  
4 BANDS BLOCK AVERAGED

GAGE NUMBER 2  
0 LOW truncations; 4 HIGH truncations  
Mean= 2.300 S.Dev= 0.09259 Lower Limit= 2.022 Upper Limit= 2.578

GAGE NUMBER 3  
0 LOW truncations; 4 HIGH truncations  
Mean= 2.041 S.Dev= 0.19418 Lower Limit= 1.458 Upper Limit= 2.623

GAGE NUMBER 5  
0 LOW truncations; 0 HIGH truncations  
Mean= 2.367 S.Dev= 0.04066 Lower Limit= 2.246 Upper Limit= 2.489

TIDE LEVEL IS 0.904 FEET.

POSSIBLE INSTRUMENT TILT (deg)  
DP2 DP3  
-0.058 -3.351

Significant Wave Height (ABS gage) = 4.43 feet.

Effective period = 8.245 seconds.

Maximum Energy located at bands:

11.011	exceeds average energy by	931.01 %
10.139	exceeds average energy by	301.30 %
13.299	exceeds average energy by	291.62 %
8.752	exceeds average energy by	199.04 %
7.699	exceeds average energy by	185.02 %
12.047	exceeds average energy by	118.44 %

Compass heading from which waves propagate

Band 11.011 secs:	Greatest Energy at	73. deg
Band 10.138 secs:	Greatest Energy at	63. deg
Band 13.299 secs:	Greatest Energy at	67. deg
Band 8.752 secs:	Greatest Energy at	75. deg
Band 7.699 secs:	Greatest Energy at	71. deg
Band 12.047 secs:	Greatest Energy at	65. deg

FIGURE VI-8: DPG analysis results using the last 8.5 minutes of the record, (4 hertz sampling).

6/11/82 0700 EST

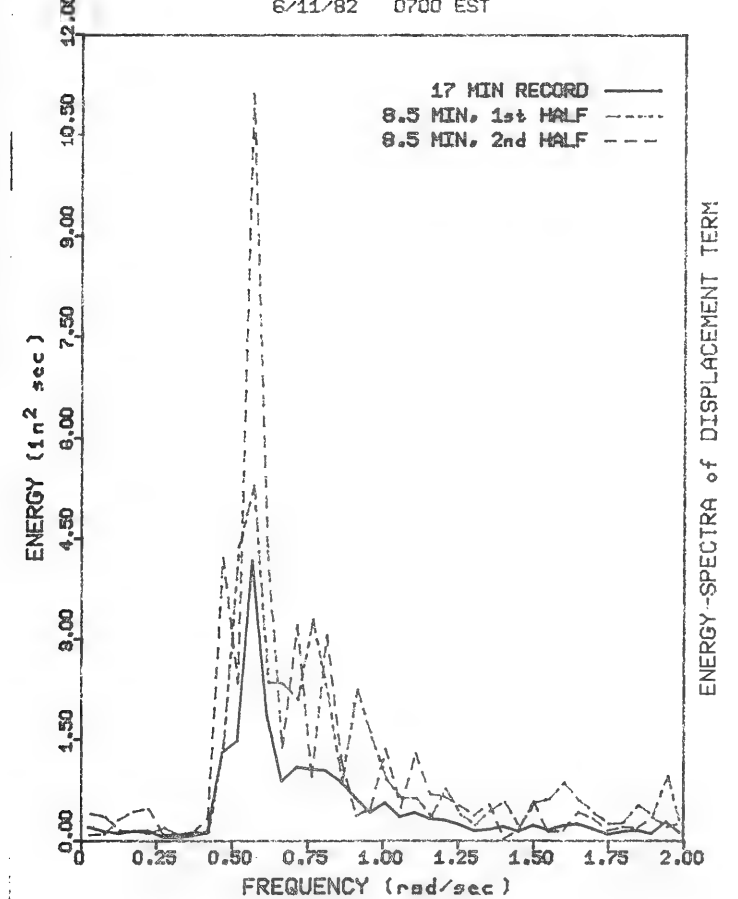


FIGURE VI-9: Block-averaged energy spectra of water surface displacement for a 17 minute long record and 8.5 minute long records.

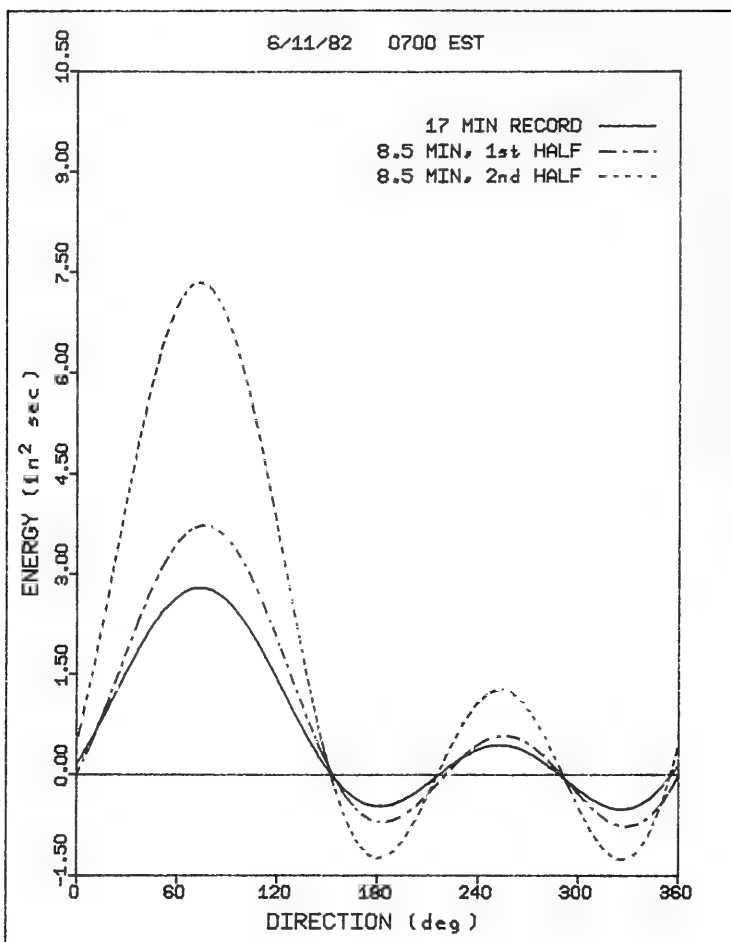


FIGURE VI-10: Non-weighted directional spectra of peak energy band (11.0 seconds) for a 17 minute long record and 8.5 minute long records.

TABLE 6-3: COMPARISON OF DPG RESULTS WITH FRF OBSERVATIONS

8 June - 11 June, 1982

DATE	TIME	DPG			FRF OBSERVATIONS
		first half of record	second half of record	FULL RECORD	
6/8	0700	dirxn	59°	59°	58° <sub>a</sub> (50°) <sub>b</sub>
		Hsig	1.48	1.30	1.41 <sub>c</sub>
		period	8.75	8.19	8.00 <sub>c</sub>
	1300	dirxn	59°	59°	- - -
		Hsig	1.31	1.26	1.33 <sub>c</sub>
		period	8.75	6.39	9.57 <sub>c</sub>
6/9	0700	dirxn	69°	65°	68° <sub>a</sub> ? (50°) <sub>b</sub>
		Hsig	1.37	1.32	1.33 <sub>c</sub>
		period	9.39	10.14	9.66 <sub>c</sub>
6/10	0700	dirxn	63°	69°	66° <sub>a</sub> (55°) <sub>b</sub>
		Hsig	1.31	1.16	1.56 <sub>c</sub>
		period	10.14	11.01	10.56 <sub>c</sub>
	1300	dirxn	69°	91°	- - -
		Hsig	1.69	1.74	1.82 <sub>c</sub>
		period	11.01	12.05	10.34 <sub>c</sub>
6/11	0700	dirxn	77°	73°	69° <sub>a</sub> (60°) <sub>b</sub>
		Hsig	1.29	1.35	1.53 <sub>c</sub>
		period	11.01	11.01	10.89 <sub>c</sub>

## NOTES:

"dirxn" listed is the principal direction (peak energy), TN.

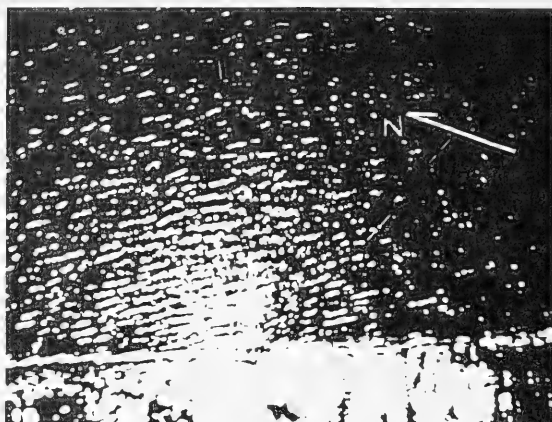
"Hsig" is the significant wave height in meters.

"period" corresponds to the frequency band of greatest energy.

<sup>a</sup> CERC Radar (+ 2°)<sup>b</sup> Visual estimate from the end of the pier<sup>c</sup> CERC Baylor Gauge near the end of the pier

8 June '82

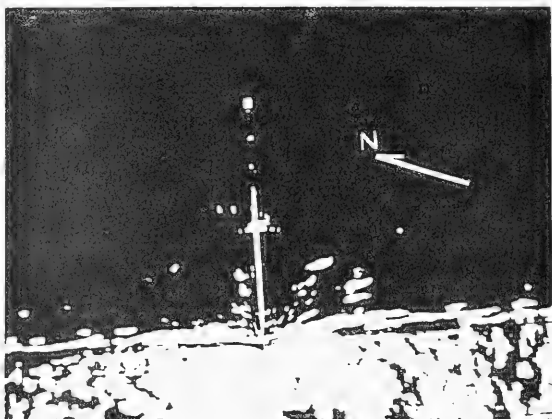
0730 EST



.75 mile

9 June '82

0800 EST

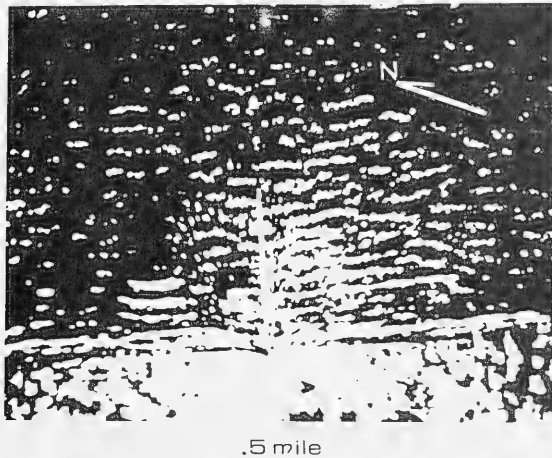


.5 mile

FIGURE VI-11: Photographs of CERC radar screen illustrating wave activity from June 8 - June 11, 1982. Distances indicate offshore range of radar.

10 June '82

0740 EST



11 June '82

0610 EST

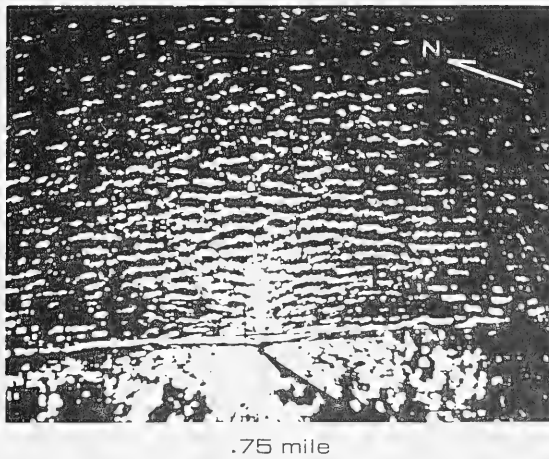


FIGURE VI-11 (Continued).

#### 4. Capability of the DPG System

The DPG results shown in Table 6.3 were generated using differential channels 2 and 3 and the absolute channel. These results lend encouraging evidence that the DPG is capable of accurately detecting wave direction. The radar pictures to which the DPG results were compared are shown in Figure VI-11. One can appreciate that it is often difficult to accurately resolve an approximate direction from the radar images; in fact, it is impossible during low wave activity or in the absence of capillary waves of appropriate frequency. Hence, the small differences between the reported wave direction from the DPG and the estimate from radar is likely attributable to the poor resolution of the radar images. It is instructive to note the accuracy of the visual estimates of wave direction. Anyone who has tried to visually resolve the direction of a wave train, especially that of short-crested waves, appreciates the difficulty in making visual directional estimates.

The significant height and period of greatest energy reported by the DPG and the Baylor gauge near the end of the pier agree well. Slight differences may be attributed to the different locations, measurement techniques, and analysis details of each of the two instruments. Analysis of the Baylor gauge data is carried out upon a 17 minute long record of one-quarter second sampling.

## 5. Directional Spectra Smoothing

The analysis results of six data sets from the DPG over a four day period are presented in Appendix A. The analysis was carried out using the absolute pressure gauge and differential gauges dP2 and dP3.

The smoothed directional spectra of the six peak energy bands are illustrated for each data set. In the development of these results, the directional spectra is expressed as the partial Fourier series in terms of the wave direction  $\Theta$  as in Equation 4.14:

$$S(\sigma, \theta) = w_0 a_0(\sigma) + \sum_{n=1}^N w_n a_n \cos n\theta + \sum_{n=1}^N w_n b_n \sin n\theta$$

where  $N=2$ . This is smoothed by the weighting function

$$\frac{8}{3} \cos^4 \frac{1}{2}(\theta' - \theta) \quad (6.6)$$

such that  $w_0 = 1$ ,  $w_1 = 2/3$ , and  $w_2 = 1/6$ . Such smoothing eliminates negative energy side-lobes in the directional spectra by imposing an always-positive function of the same angular frequency upon the directional distribution (Longuet-Higgins, Cartwright and Smith, 1963). The function

$$B \cos^4 b\theta \quad (6.7)$$

is first considered, and then expressed in complex form:

$$= \operatorname{Re} \left[ B \left( \frac{e^{ib\theta} + e^{-ib\theta}}{2} \right)^4 \right] \quad (6.8)$$

Expanding,

$$= R_e \left[ \frac{B}{16} (e^{4ib\theta} + 4e^{2ib\theta} + 4e^{-2ib\theta} + e^{4ib\theta} + 6) \right]$$

Equation 6.7 can be written as:

$$= \frac{B}{8} (\cos 4b\theta + 4\cos 2b\theta + 3)$$

Letting  $b=1/2$ , and factoring 3, the function becomes:

$$= \frac{3}{8} B (1 + \frac{4}{3} \cos \theta + \frac{1}{3} \cos 2\theta) \quad (6.9)$$

The weighted angular distribution must satisfy the requirement

$$S(\sigma) = \int_0^{2\pi} S(\sigma, \theta) d\theta \quad (6.10)$$

to retain the original energy calculated in the spectra. Hence,  $B$  must equal  $8/3$ . The coefficients  $w_0$ ,  $w_1$ , and  $w_2$  are taken as  $1$ ,  $2/3$ , and  $1/6$  in accordance with the definition of the Fourier coefficients

described in Equations 4-18 through 4-24. If the first seven directional Fourier coefficients, (i.e.,  $N=3$ ), were developed, then the directional spectra might be smoothed by a weighting function

$$\frac{16}{5} \cos^6 \frac{1}{2}(\theta' - \theta) \quad (6.11)$$

such that  $w_0 = 1$ ,  $w_1 = 66/77$ ,  $w_2 = 15/28$ , and  $w_3 = 5/21$ .

## 6. Redundancy of dP2 and dP4 Measurements

If differential pressure gauges dP2 and dP4 work correctly, then the results of directional analysis of wave data using either of these two collinear gauges should be nearly identical. To check this, a number of wave records were analyzed using the signals from the absolute pressure channel, dP3, and dP2, and then the signals from the absolute, dP3, and dP4 channels. Two of the results are shown in Figures VI-12 and VI-13. Figure VI-12 illustrates the energy spectrum and the non-smoothed directional spectra of the first two peak energy bands for one data set using both combinations of gauges. The energy spectrum, taken from the signals of the absolute gauge, is the same for either gauge combination. There is good directional agreement in this case of well-defined swell. Figure VI-13 illustrates the energy spectrum and non-smoothed directional spectra of the first two peak energy bands for another data set. The

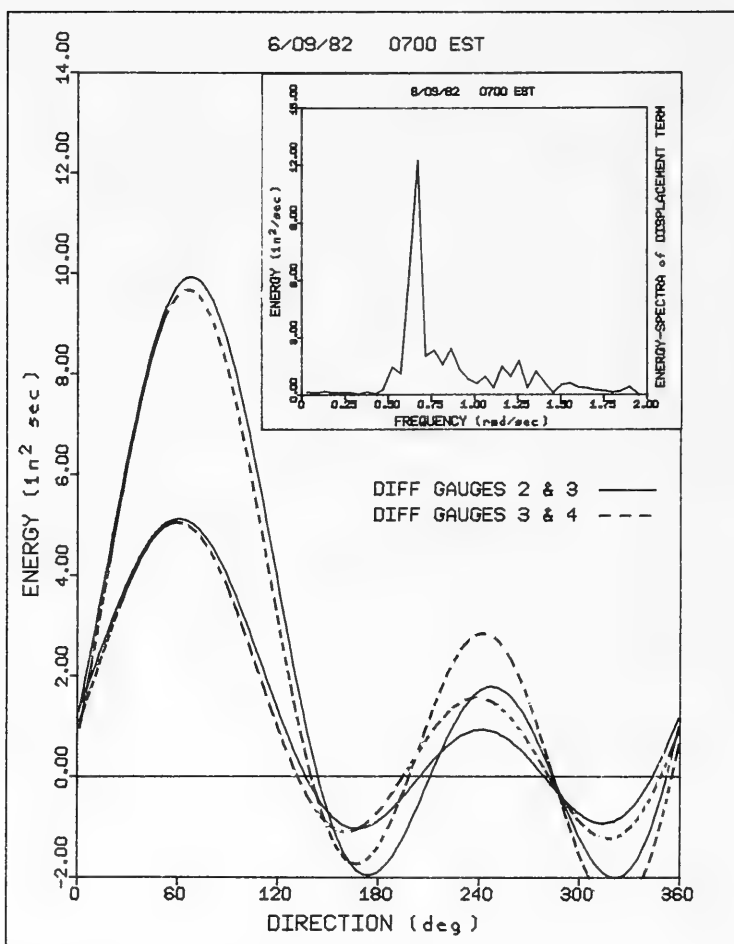


FIGURE VI-12: Non-weighted directional spectra of the first two peak energy bands using ABS, dP2, dP3 gauge combination and ABS, dP4, dP3 gauge combination. Case 1: Well-defined swell. Block-averaged water surface displacement energy spectrum shown in inset.

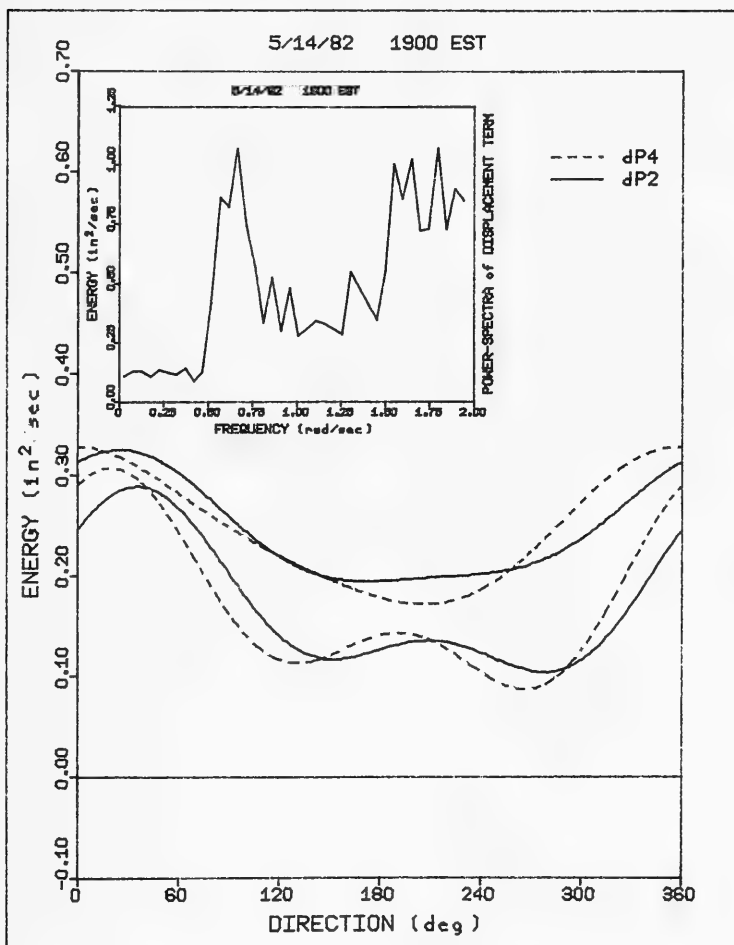


FIGURE VI-13: Non-weighted directional spectra for the first two peak energy bands using ABS, dP2, dP3 gauge combination and ABS, dP4, dP3 gauge combination. Case 2: Omnidirectional sea. Block-averaged water surface displacement spectrum shown in inset.

agreement between different combinations of gauges is not as good for this set that represents a "ragged" sea state. This is most probably because each of the two gauges, separated a finite distance, independently measure more slightly different wave activity than in the first data set shown. For such a confused sea state of relatively short period waves, it was not possible to verify which channel, dP2 or dP4, gave the more accurate estimate of wave direction (if indeed there was any one principal direction). Accurate radar and visual observations are practically impossible during such conditions. As expected, the omnidirectional energy spectra generated from the DPG data for this confused sea state agrees in form with that of the computer-simulated case of one wave frequency with two directions as shown in Figures IV-10 and IV-11.

#### 7. Energy Spectra from Differential Pressure Gauges

Figure VI-14 illustrates one record's wave energy spectra generated from the absolute pressure gauge and the water surface slope energy spectrum from each of the two perpendicular differential pressure gauges dP2 and dP3. The record was taken during wave activity from the northwest -- the direction in which DPG arm 3 is oriented towards. Accordingly, one observes that there is considerably more energy contained in the slope spectrum from dP3 than from dP2. This is because there are relatively small slope (and pressure) differences along the wave crests and troughs which are

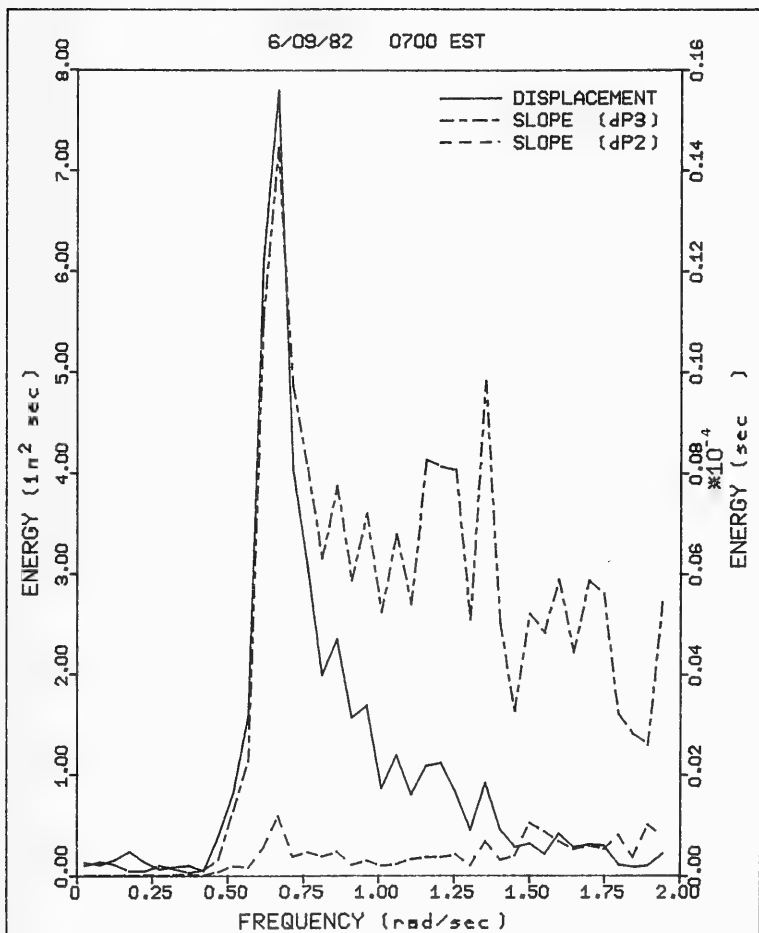


FIGURE VI-14: Block-averaged power spectra of water surface displacement (developed from the absolute pressure gauges) and water surface slope (developed from differential pressure gauges dP2 and dP3).

aligned with arm 2 whereas there are relatively large slope (and pressure) differences along the wave ray -- aligned with arm 3. (See Figure VI-15.)

As is illustrated in Figure VI-14, one expects that the wave frequencies of greatest energy should be the same for both the water surface displacement and slope terms. It is instructive to note, however, that greater energy appears in the higher frequency bands of the slope spectra than in those of the wave spectrum. This too is an expected result since the energy spectrum of slope (developed from a differential pressure signal) differs from that of water surface displacement (generated from the absolute pressure signal) by a factor of wavenumber-squared. The energy spectrum of the water surface displacement is developed through the frequency-by-frequency division of the dynamic pressure energy spectrum by the specific gravity of seawater (squared) and the square of the pressure response function,  $K_p$ . The water surface slope energy spectrum is similarly developed through the division of the differential pressure energy spectrum by the squares of the specific gravity of seawater and the pressure response function. The energy

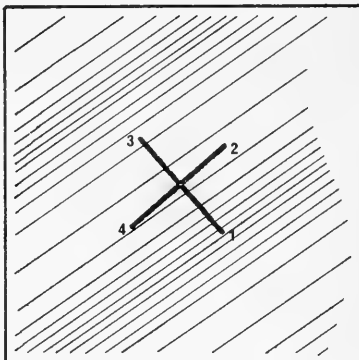


FIGURE VI-15: Wave crest approximately aligned with  $dP2$  arm.

spectrum of the water surface displacement is then as Equation 4.46:

$$S_{\eta\eta}(\sigma) = \frac{H^2}{8} \quad (4.46)$$

and the energy spectra of the water surface slopes are as Equations 4.47 and 4.48:

$$S_{\eta_x\eta_x}(\sigma) = \frac{H^2}{8} k^2 \cos^2\theta \quad (4.47)$$

$$S_{\eta_y\eta_y}(\sigma) = \frac{H^2}{8} k^2 \sin^2\theta \quad (4.48)$$

Since wavenumber increases with wave frequency, energy leaked into the higher frequency differential pressure bands is enhanced in the generation of the water surface slope spectrum relative to the displacement spectrum. It is for this reason that the frequency bands of greatest energy are selected for directional analysis from the water surface displacement spectrum. (Spectral leakage is the "spilling" of energy from the frequencies that are actually present in the record to other frequencies. It occurs naturally in the analysis of a finite length of record due to the inability of the FFT to exactly resolve the spectral content of a time record on the frequency axis.)

From Eqns. 4.46, 4.47, and 4.48, one might expect that the sum of the orthogonal slope energy spectra divided by the square of the wavenumber would be equivalent to the water surface displacement spectra for some frequency of frequencies, (Section IV.D.9). However, this would be true only for an idealized narrow wave spectra with no frequency or directional leakage.

#### 8. Directional Estimates without the Absolute Pressure Gauge

Estimates made of the wave direction without the absolute pressure gauge are generally unreliable. Typical results calculated using Equation 4.52 and the dP2 and dP3 signals for the data sets illustrated in Appendix A are listed at the end of the appendix. Equations 4.52 and 4.54 are valid if there exists only one wave direction per frequency. When waves of one frequency arrive at slightly different directions and spectral frequency bands are contaminated by leakage, the validity of Equations 4.52 and 4.54 fails. As a general statement, it can be said that these equations do not usually provide reliable estimates of the principal wave direction in typical ocean wave analysis. The estimates might be improved by some sort of data conditioning.

## 9. Arithmetic Development of the Curvature Terms

For investigative purposes, it was attempted to create the water surface curvature terms as described earlier. Typically, this was only done along the y-axis using the dP2 and dP4 signals since

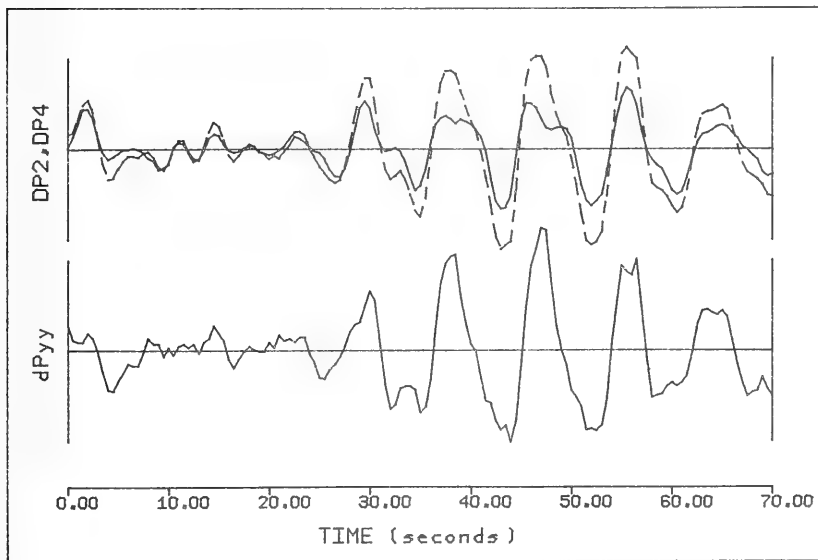


FIGURE VI-16: Typical portion of time series of dP2 and dP4 "slope" signals with the associated dP4-dP2 "curvature" signals. Signal of dP4 is dashed line.

the digitized x-axis signal of dP1 was erratic. The terms were arithmetically created in the time domain through the difference of the dP2 and dP4 signals after adjacent values in each channel's record were averaged and the number of points in the 17 minute long

record halved. A portion of the resulting y-axis curvature term in the time domain is shown in Figure VI-16. The time series was processed by the FFT and the energy spectra developed. Figure VI-17 illustrates the energy spectrum of the curvature term compared to that of the displacement term. The wave frequencies corresponding to peak energy levels of the data set correspond well between the spectra. The curvature spectrum contains greater energy in the high frequency bands than the displacement spectrum. This is expected since the curvature spectrum differs from the displacement spectrum by a factor of the fourth power of the wavenumber.

Despite the reasonable appearance of the curvature spectra, the directional Fourier coefficient  $b_3$ , developed using the water surface curvature along the y-axis, was at least an order of magnitude larger than the other directional coefficients for each case tested. The dominance of this term would create three high energy peaks in the directional spectra and invalidate directional estimates.

The curvature terms were also developed in the time domain before adjacent values in the record were averaged. The results were similar.

The inability to generate higher order directional Fourier coefficients through the arithmetic creation of the water surface curvature terms is not surprising. The DPG was developed upon the

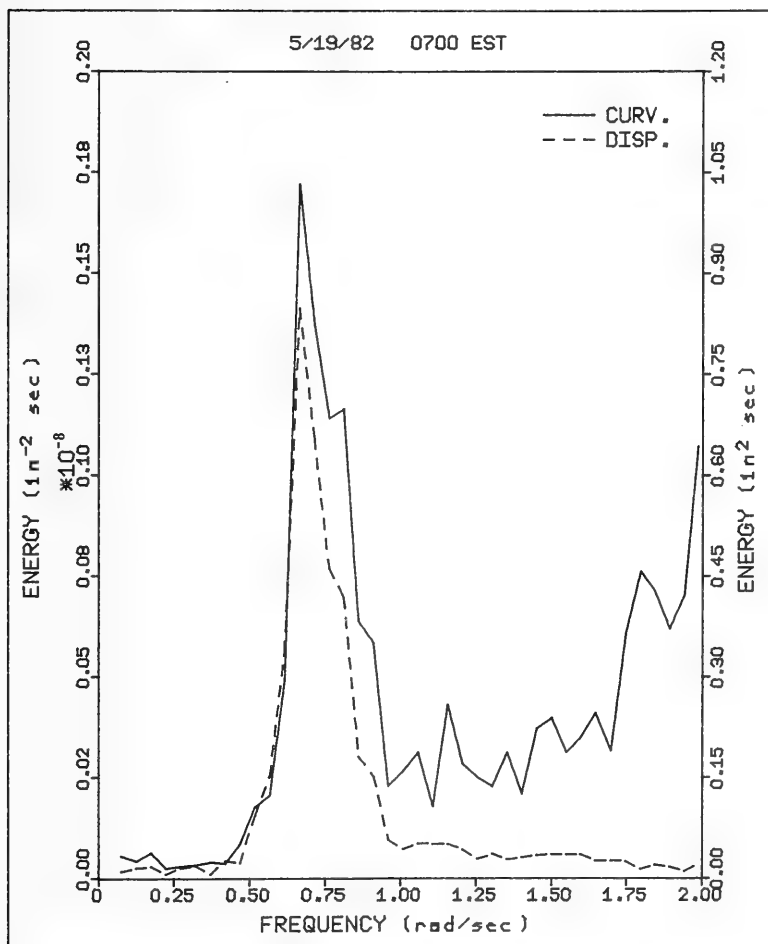


FIGURE VI-17: Block-averaged power spectra of water surface displacement and water surface curvature terms.

premise that there is inherent error in the creation of small-valued water surface slope terms through the subtraction of two large pressure values. Similarly, the attempt was made in this case to create the very small-valued water surface curvature terms through the subtraction of two small differential pressure values.

CHAPTER VII  
RECOMMENDATIONS

During the design, development, testing, installation, and evaluation of the DPG directional wave monitor system, some problem areas and phenomena of interest were cited for further investigation and/or development. Foremost, thorough comparisons should be made of the DPG analysis results with those of other in-situ directional wave monitors at the Field Research Facility -- particularly those instruments that typically generate water surface slope terms through the subtraction of signals from adjacent pressure sensors. Also, the digitization of the dP1 signals from the DPG should be checked and/or differential transducers 1 and 4 should be repaired or replaced.

There are certain design characteristics of the first DPG prototype that might be investigated and improved. One might re-design the fuselage to align the differential pressure sensors exactly upon the x- and y- axes. In the first prototype, as installed at the FRF, the dP2, dP3, and dP4 sensors are misaligned by one to two degrees as discussed in Section III.C.1. The instrument

might be re-designed such that the arm and center sensors are also at the same elevation above the seafloor. However, for the first DPG prototype, the nine inch difference in height between the sensors leads to very small error in the calculation of an average pressure response function used in the development of the water surface slope terms. (See Section III.C.2.) In water depths as shallow as 10 feet (3.1 m), the error is still small -- less than three percent for waves of three second period.

The instrument might be re-designed such that the lengths of each tubing used in the sensor systems are identical. This would help ensure that the response time of each channel is identical and that there is no difference in response time for the loading of an arm sensor compared to a center sensor. This would eliminate differential pressure drift induced by changes in ambient temperature, thus disabling the instrument to measure ambient water temperature.

The arrangement of the transducers inside the water-tight cylinder might be re-designed to allow servicing of individual pressure transducers without the need to bring the entire instrument to the surface. Such a design change could, however, add additional problems to the dependability of the transducers since this would most probably require the addition of underwater-pluggable connectors for each transducer. The present instrument utilizes one such connector that is mated only above water in routine maintenance.

For DPG operation in water depths of 20 feet, the absolute pressure transducer should be changed from 50 psia rated capacity to 30 or 35 psia to improve resolution.

Different designs of the isolation sensor diaphragms could be considered in order to create a sensor that is easier to back-fill and less difficult to machine. When calibrating the sensors, an oscillating pressure pump used in conjunction with the calibration system described in Section V.C.1 might better estimate the system's dynamic loading characteristics. Temperature effects upon the transducers and their respective sensors should be investigated more thoroughly during instrument calibration.

The effects of vortex shedding about the sensor diaphragms might be investigated. The sensors could be re-configured within the PVC arms and fuselage to minimize vortex shedding effects if they are found to be of sufficient magnitude for some application of the DPG. Tests in the large wave tank at the Coastal Engineering Research Center suggest that the configuration of the sensors within the arms is important for accurate directional estimates, (Section V.D.3).

Although a tripod was at one time considered for the instrument cradle, the four-legged cradle used for the DPG at the Field Research Facility proved stable and easy to maneuver in the installation and first weeks of operation in the field. Future DPG systems may retain this four-legged cradle or experiment with a

tripod. Any sharp corners on the cradle should be rounded and smoothed for safety.

The DPG might be better protected against high voltage transients, (i.e., lightning), by bonding the steel armor of the cable to the water-tight instrumentation cylinder at the seaward end and to the ground system of the FRF at the landward end of the cable, (J. Anderson Plumer, Lightning Technologies, Inc., personal conversation).

Various configurations of the DPG arms used for differential pressure measurements might be considered for investigative purposes. Intuitively, one might expect that the most effective directional measurements made by the DPG would be for the case of a maximum signal reported by each differential pressure transducer. This requires that the differential transducers be oriented 45 degrees to the wave ray or crest. In this way, the peak signals from each transducer would be of the same amplitude, and for sufficiently large wave activity, above the noise level of each transducer channel. If the incident wave direction at a site was normally distributed about the shore normal, then one might expect the most effective directional measurements to be made by a DPG with its arms oriented 45 degrees to the shore normal. The DPG prototype was placed at the FRF (with little consideration for orientation) such that the x-axis (dP1 and dP3) arms and the y-axis (dP2 and dP4) arms are 17 and 73 degrees from the shore normal, respectively. Various configurations

of the arms with respect to one another might be considered. The angle between arms might be varied to "tune" the DPG to the incident wave field -- much the same as a directional antenna. Changes in arm orientation could also permit the estimation of higher order directional Fourier coefficients, (see Appendix E).

In future versions of the DPG system, wave data could be transmitted to ship or shore by telemetry -- eliminating difficult cable installations. Data might also be integrated in-situ and reported in concise segments by telemetry or on tape. Present coastal field measurements are often made over long periods of time, where the results of such measurements represent coastal processes that are essentially integrated over time. In such cases, specific hour-by-hour wave data may not be necessary or even desirable. Concise, integrated wave information is just as useful. Software capability on site with the DPG could be developed to integrate large amounts of wave data and report one or two numbers (say, measures of  $P_{1s}$  or  $S_{xy}$ ) to characterize the wave climate over time, (Robert Dean, personal conversation).

A technique has also been considered to directly measure water surface curvature using differential pressure gauges. This measurement technique could be developed and evaluated in the hope of accurately developing higher orders of directional Fourier coefficients from directly measured data.

Various types of directional data analysis schemes should be investigated. Among them are the Maximum Likelihood Method, (Clarke and Gedling, 1981; Jefferys, et.al., 1981; Goda, 1981; LaCoss, 1971). and the estimate of higher order directional Fourier coefficients as alluded to in Section II.B.1 and discussed in Appendix E. Proper conditioning of DPG data might also allow directional estimates made without the signal of the absolute pressure gauge.

In all future developments of the DPG, as with any well-designed ocean instrument, careful consideration must be given to the problems of corrosion, biological fouling, scour and instrument settlement into the seabed, installation and maintenance, electronics failure and noise, and interference from local marine activity. The limitations of directional wave spectra analyses should always be recognized when dealing with the data obtained from the instrument.

## CHAPTER VIII

### CONCLUSIONS

This thesis has presented a description of the design, development, and evaluation of a new type of directional wave monitor. The work undertaken in the preparation of this thesis indicates that differential pressure transducers used with an absolute pressure transducer, as employed in the DPG directional wave monitor, appear capable of generating accurate estimates of wave direction using the first five directional Fourier coefficients as determined from direct measurements of water surface displacement and slope. This conclusion is based upon the comparison of analyzed data from the DPG with estimates from the CERC radar located at the CERC Field Research Facility, Duck, N.C. The relatively small dimensions and light weight of the DPG system, (two-fifths the size and less than one-seventh the weight of conventional pressure sensor arrays), allowed a smooth, relatively simple field installation. The DPG, as designed, should similarly allow for easy retrieval and re-deployment of the instrument for maintenance purposes.

It has been demonstrated that the differential pressure transducer can be considered to be an inherently more effective instrument for determining wave direction. The design is well suited to the measurement of water surface slope and the response of surface slope with depth is a maximum over frequencies that are more representative of typical ocean gravity waves than the response of conventional absolute pressure transducers.

In the development of the DPG system, it was discovered that careful attention must be given to the diameter of the tubing and to the nature of the back-filling fluid used in the transducers' sensors. This is to ensure a small response time for each transducer. The DPG prototype, as installed at the CERC Field Research Facility, utilizes gin and 1/8 inch I.D. flexible tubing in its sensor systems. Ambient temperature changes induce differential pressure changes as measured by the transducers since the tubing used in the arm sensors is four times the length of that of the center sensors.

A simple bench-calibration device was developed to monitor the response of the transducers and sensor systems to applied loads. It is important that the load be distributed uniformly across the sensor diaphragm.

Experiments conducted with the first DPG model in the large wave tank at the Coastal Engineering Research Center were plagued by highly non-linear waves and the failure of three differential pressure channels. However, results from the absolute pressure gauge and one differential pressure gauge indicated the ability of the DPG to estimate wave height, period, and direction. The tests were also valuable in defining several important modifications required to improve the performance of the DPG system.

Measurements of the orientation of the instrument were discussed and the importance of careful consideration of compass readings in the vicinity of steel structure was stressed. Although it initially appeared that diving compasses were placed upon the instrument sufficiently far from the steel cradle to avoid its magnetic effects, redundant measurements of the instrument orientation indicated that the compass readings were biased. The error was resolved using a simple technique outlined in the thesis. It was suggested that measurements from simple wrist compasses, when taken and interpreted carefully, may be adequate in determining instrument orientation.

The DPG utilizes four differential pressure gauges placed to the bow, port, stern, and starboard of an absolute pressure gauge such that there are two adjacent differential gauges along each of two perpendicular axes. The DPG system develops the first five directional Fourier coefficients using signals from the absolute

pressure gauge and one differential pressure gauge along each axis. The other differential transducers on each axis were installed for redundancy and for the generation of higher order directional Fourier coefficients. The absolute pressure transducer and one differential pressure transducer along each axis (dP2 and dP3) appear to work satisfactorily. The redundant differential pressure gauges dP4 and dP1 intermittently exhibit drift and high frequency oscillation, respectively. The failure of either gauge invalidates reliable generation of higher order directional Fourier coefficients by conventional techniques as discussed in this paper. Accurate, reliable generation of the higher order (N=3) directional Fourier coefficients through the subtraction of collinear differential pressure signals -- similar to the generation of lower order directional coefficients through the subtraction of adjacent absolute pressure signals -- remains questionable.

For well-defined swell, directional spectra generated from the signals of dP2, dP3, and the absolute gauge correspond well with the directional spectra generated from the signals of dP4, dP3, and the absolute gauge. There is less agreement for poorly-defined sea. Directional estimates made without the absolute pressure gauge signals are generally unreliable using techniques discussed in this paper.

Estimates of wave direction developed from DPG data agree best with those of the CERC radar for a 17 minute long DPG record with 2 Hertz effective sampling and 16 degrees of freedom. Analysis results for an 8.5 minute record with 4 Hertz sampling and 8 degrees of freedom differ from the results of a 17 minute record depending upon which half of the record is analyzed.

Possible modifications to the instrument design and recommendations for future DPG development have been outlined. The configuration of the DPG arms and the manner in which the data is processed, transmitted, and analyzed might be altered to obtain more accurate or effective directional wave data.

The DPG directional wave monitor prototype has thus far provided reliable, accurate directional wave data through the use of a smaller and lighter instrument than conventional pressure sensor arrays. It generates directional wave spectra using data that is directly measured instead of arithmetically created and could potentially develop higher order directional Fourier coefficients than conventional arrays. Overall, the DPG appears to be a promising advancement in the technology of directional wave measurement.

REFERENCES

1. Aubrey, D.G., "Field Evaluation of Sea Water Directional Wave Gauges (Model 635-9)," Woods Hole Oceanographic Institution No. 81-28; May 1981.
2. Birkemeier, W.A., DeWall, A.E., Gorbics, C.S., and Miller, H.C., "A Users Guide to CERC's Field Research Facility," Misc. Report No. 81-7, p. 10,40; October 1981.
3. Borgman, L.E., "Confidence Limits for Ocean Wave Spectra," Geology Dept. Research Report 72-1, University of Wyoming; September; 1972.
4. Borgman, L.E., "Directional Spectra Models for Design Use," Proc., Ocean Technology Conference, Houston, Texas; 1969.
5. Bowden, K.F. and White, R.A., "Measurements of the Orbital Velocities Of Sea Waves and their Use in Determining the Directional Spectrum," Geophys. Journal Royal Astro. Soc., 12, pp.33-54; 1966.
6. Cartwright, D.E. and Smith, N.D., "Buoy Techniques for Obtaining Directional wave Spectra," Buoy Technology, Marine Tech. Society; Washington, D.C., pp. 112-121; 1964.
7. Chakrabarti, S.K., "Wave Train Directional Analysis," Jour. Waterways, Harbors, and Coastal Eng. Div., ASCE, 97, pp. 787-792; 1971.
8. Chakrabarti, S.K. and Snider, R.H., "Two Dimensional Wave Energy Spectra," Underwater Technology, 2, pp. 80-85; 1973.
9. Clarke, D. and Gedling, P., "MLM Estimation of Directional Wave Spectra," Proc., Directional Wave Spectra Applications, Berkeley, Calif.; 1981.

10. Dean, R.G., "Evaluation and Development of Water Wave Theories for Engineering Application, Volumes I and II," Coastal Engineering Research Center Special Report No. 1; November, 1974.
11. Dean, R.G., "The NRC Workshop on Wave Measurement Technology: A Summary," Proc., Directional Wave Spectra Applications, Berkeley, Calif., pp. 220-232; 1982.
12. Dexter, S.C., Handbook of Oceanographic Engineering Materials, John Wiley and Sons, N.Y., p. 83, p. 178; 1979.
13. Forristal, G.Z., "Subsurface Wave Measuring Systems," Proc., National Research Council Workshop on Wave Measurement Technology; 1982
14. Goda, Y., "Simulation in Examination..." Directional Wave Spectra Applications, Berkeley, Calif.; 1981.
15. Jefferys, E.R., Wareham, G.T., Ramsden, N.A., and Platts, M.J., "Measuring Directional Spectra with the MLM," Proc., Directional Wave Spectra Applications, Berkeley, Calif.; 1981.
16. LaCoss, R.T., "Data Adaptive Spectral Analysis Methods," Geophysics 36, pp. 661-675; 1971.
17. Longuet-Higgins, M.S., Cartwright, D.E., and Smith, N.D., "Observations of the Directional Spectrum of Sea Waves Using the Motions of a Floating Buoy," Ocean Wave Spectra, Proceedings of a Conference, Prentice-Hall, Inc., Englewood Cliffs, N.J.; 1963.
18. Mitsayasu, H., et. al., "Studies on Techniques for Ocean Wave Measurements (1)," Bulletin Res. Inst. Appl. Mech., Kyushu Univ., No. 39; pp. 105-181; 1973.
19. Mobarek, I.E., "Directional Spectra of Laboratory Wind Waves," Jour. Waterways and Harbors Div., 91, ASCE; pp. 91-116; 1965.
20. Nagata, Y., "The Statistical Properties of Orbital Wave Motions and Their Applications for the Measurement of Directional Wave Wave Spectra," Journal of the Oceanographical Society of Japan, 19, pp. 169-181; 1964.
21. O'Brien, M.E., "An Urgent Need," Shore and Beach, Vol. 42, No. 2, p. 2; October 1974.
22. Panicker, N.N., "Review of Techniques for Directional Wave Spectra," Proc., International Symposium on Ocean Wave Measurement and Analysis, New Orleans, pp. 669-688; 1974.

23. Panicker, N.N., and Borgman, L.E., "Directional Spectra from Wave-Gauge Arrays," Proc., Twelfth Coastal Engineering Conference, Washington, D.C., pp. 117-136; 1970.
24. Peacock, H.G., "CERC Field Wave Guaging Program," Proceedings of the International Symposium on Ocean Wave Measurement and Analysis, New Orleans, La.; September 1974.
25. Peerless, S.J., Basic Fluid Mechanics, Pergamon Press, Oxford, p. 278; 1967.
26. Ploeg, J., "Some Results of a Directional Wave Recording Station," Proc., Thirteenth Coastal Engineering Conference; Vancouver, B.C., pp. 131-144; 1972.
27. \_\_\_\_\_, Proceedings of the National Research Council Workshop on Wave Measurement Technology; 1982.
28. Rickiishi, K., "A Study on the Measurement of the Directional Spectrum and Phase Velocity of Laboratory Waves," Res. Inst. for Applied Mechanics, Kyushu Univ., Fukuoka, Japan; 1977.
29. Seymour, R.J., and Higgins, A.L., "A Slope Array for Estimating Wave Direction," Proc. of a Workshop on Coastal Processes Instrumentation, June 16, 1977; LaJolla, Calif., Univ. of Calif., San Diego. Sea Grant Publ. No. 62; Institute of Marine Resources Ref. No. 78-102; 1978.
30. \_\_\_\_\_, Shore Protection Manual, I, Coastal Engineering Research Center, figure 4-11; 1977.
31. Simpson, J.H., "Observations of the Directional Characteristics of Sea Waves," Geophysical Journal of Royal Astronomical Soc., 17, pp. 93-120; 1969.
32. Suzuki, Y., "Determination of Approximate Directional Spectra for Coastal Waves," Rep. of the Port and Harbor Res. Inst., 8, pp. 43-101; 1969
33. van Heteren, J., and Keyser, H., "Directional Spectra: Comparison of Three Methods," Proc., Directional Wave Spectra Applications, Berkeley, Calif., ASCE; 1981.

APPENDIX A

SAMPLE DPG ANALYSIS RESULTS

June 8 - 11, 1982

UNIVERSITY OF DELAWARE  
DEPARTMENT OF CIVIL ENGINEERING  
DPG DIRECTIONAL WAVE MONITOR / FRF, DUCK, N.C.

DEV	YR	MO	DAY	TIME
111	82	6	8	7 0
121	82	6	8	7 0
141	82	6	8	7 0

4096 POINTS ANALYZED AT .50 SECOND SAMPLING  
8 BANDS BLOCK AVERAGED

GAGE NUMBER 2  
9 LOW truncations; 10 HIGH truncations  
Mean= 2.301 S.Dev= 0.06192 Lower Limit= 2.115 Upper Limit= 2.486

GAGE NUMBER 3  
5 LOW truncations; 5 HIGH truncations  
Mean= 2.211 S.Dev= 0.22893 Lower Limit= 1.524 Upper Limit= 2.898

GAGE NUMBER 5  
1 LOW truncations; 0 HIGH truncations  
Mean= 2.423 S.Dev= 0.03973 Lower Limit= 2.304 Upper Limit= 2.542

TIDE LEVEL IS 2.156 FEET.

POSSIBLE INSTRUMENT TILT (deg)  
DP2 DP3  
-0.057 -2.252

Significant Wave Height (ABS gage) = 4.55 feet.

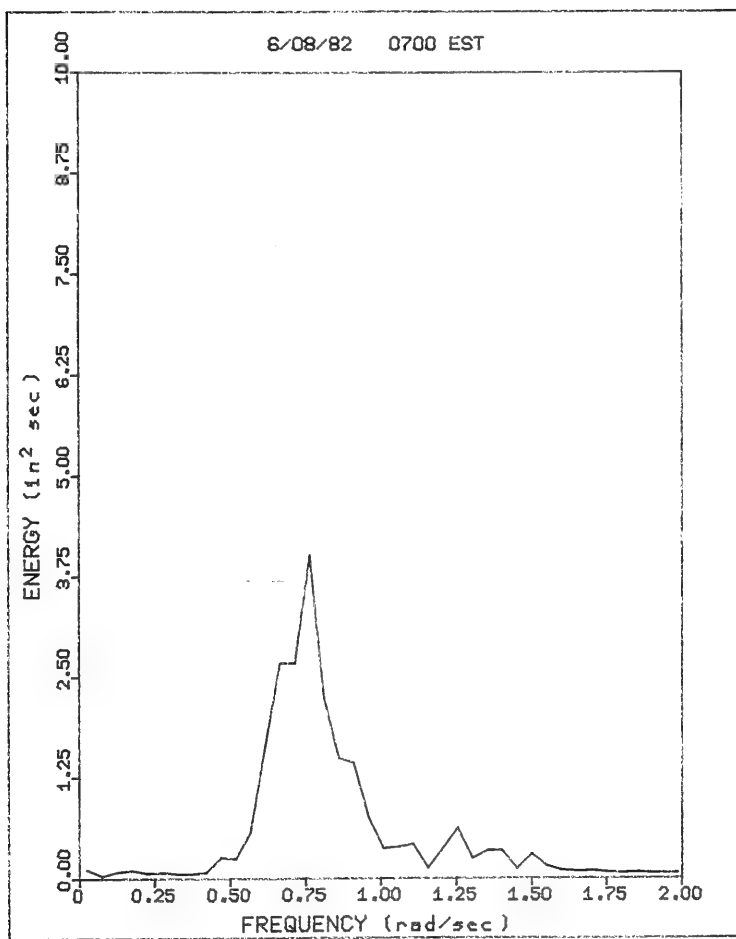
Effective period = 7.425 seconds.

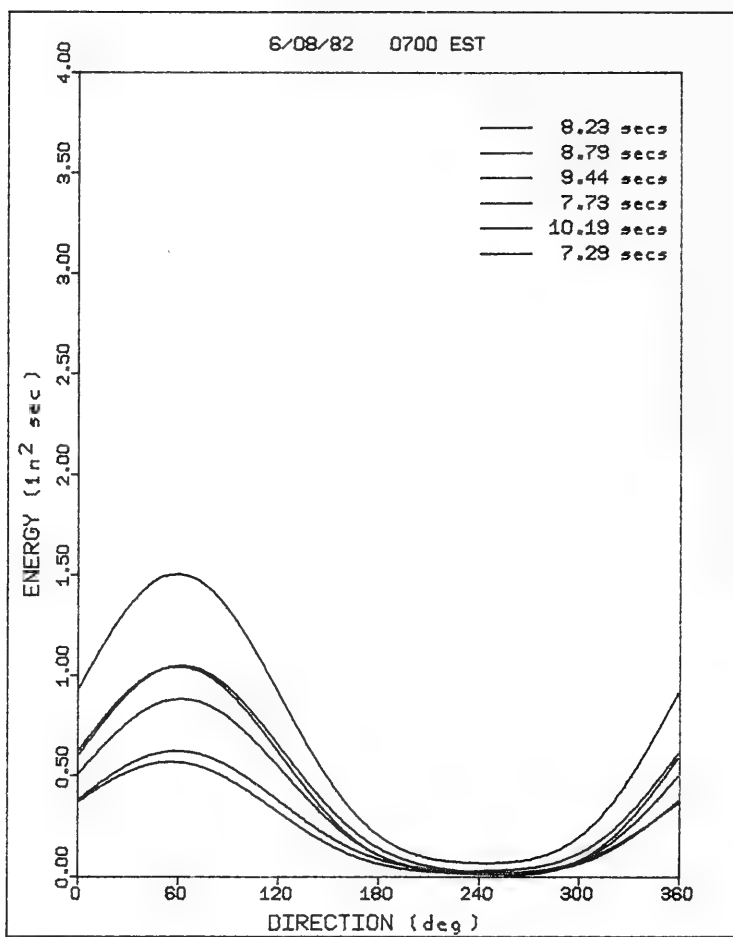
Maximum Energy located at bands:

8.225	exceeds average energy by	606.14 %
8.790	exceeds average energy by	371.26 %
9.438	exceeds average energy by	371.10 %
7.728	exceeds average energy by	297.40 %
10.189	exceeds average energy by	190.45 %
7.288	exceeds average energy by	164.24 %

Compass heading from which waves propagate

Band 8.225	secs: Greatest Energy at	59. deg
Band 8.790	secs: Greatest Energy at	61. deg
Band 9.438	secs: Greatest Energy at	61. deg
Band 7.728	secs: Greatest Energy at	61. deg
Band 10.189	secs: Greatest Energy at	59. deg
Band 7.288	secs: Greatest Energy at	55. deg





UNIVERSITY OF DELAWARE  
DEPARTMENT OF CIVIL ENGINEERING  
DPG DIRECTIONAL WAVE MONITOR / FRF, DUCK, N.C.

DEV	YR	MO	DAY	TIME
111	82	6	8	13 2
121	82	6	8	13 2
141	82	6	8	13 2

4096 POINTS ANALYZED AT .50 SECOND SAMPLING  
8 BANDS BLOCK AVERAGED

GAGE NUMBER 2

11 LOW truncations; 9 HIGH truncations  
Mean= 2.306 S.Dev= 0.05554 Lower Limit= 2.139 Upper Limit= 2.473

GAGE NUMBER 3

7 LOW truncations; 26 HIGH truncations  
Mean= 2.191 S.Dev= 0.23225 Lower Limit= 1.495 Upper Limit= 2.888

GAGE NUMBER 5

7 LOW truncations; 5 HIGH truncations  
Mean= 2.344 S.Dev= 0.03559 Lower Limit= 2.237 Upper Limit= 2.450

TIDE LEVEL IS 0.369 FEET.

POSSIBLE INSTRUMENT TILT (deg)  
DP2 DP3  
-0.023 -2.383

Significant Wave Height (ABS gage) = 4.19 feet.

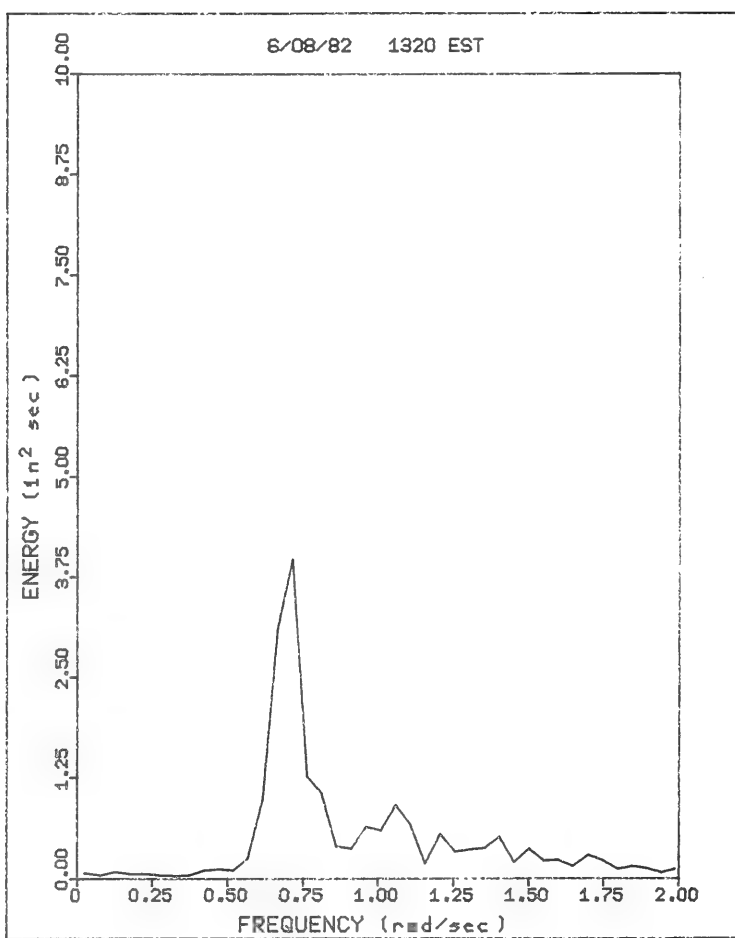
Effective period = 6.784 seconds.

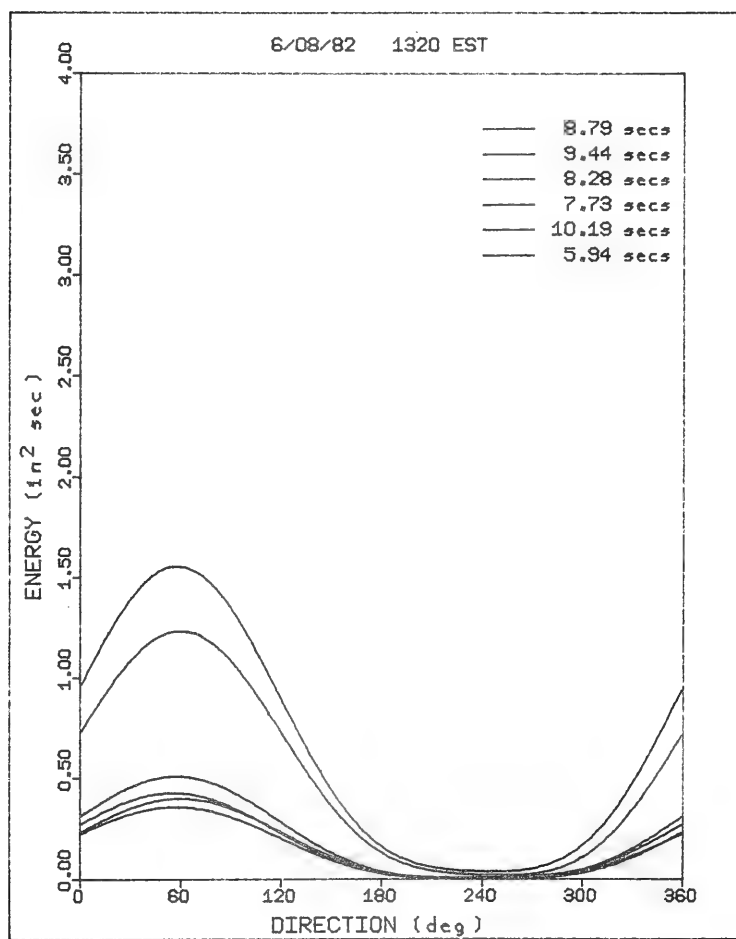
Maximum Energy located at bands:

8.790	exceeds average energy by	722.92 %
9.438	exceeds average energy by	545.18 %
8.225	exceeds average energy by	163.39 %
7.728	exceeds average energy by	122.59 %
10.189	exceeds average energy by	106.14 %
5.936	exceeds average energy by	91.64 %

Compass heading from which waves propagate

Band 8.790	secs: Greatest Energy at	59. deg
Band 9.438	secs: Greatest Energy at	61. deg
Band 8.225	secs: Greatest Energy at	57. deg
Band 7.728	secs: Greatest Energy at	55. deg
Band 10.189	secs: Greatest Energy at	61. deg
Band 5.936	secs: Greatest Energy at	57. deg





UNIVERSITY OF DELAWARE  
DEPARTMENT OF CIVIL ENGINEERING  
DPG DIRECTIONAL WAVE MONITOR / FRF, DUCK, N.C.

DEV	YR	MO	DAY	TIME
111	82	6	9	7 0
121	82	6	9	7 0
141	82	6	9	7 0

4096 POINTS ANALYZED AT .50 SECOND SAMPLING  
8 BANDS BLOCK AVERAGED

GAGE NUMBER 2  
6 LOW truncations; 11 HIGH truncations  
Mean= 2.300 S.Dev= 0.06456 Lower Limit= 2.106 Upper Limit= 2.494

GAGE NUMBER 3  
0 LOW truncations; 5 HIGH truncations  
Mean= 2.146 S.Dev= 0.22337 Lower Limit= 1.476 Upper Limit= 2.816

GAGE NUMBER 5  
0 LOW truncations; 1 HIGH truncations  
Mean= 2.397 S.Dev= 0.03837 Lower Limit= 2.282 Upper Limit= 2.512

TIDE LEVEL IS 1.578 FEET.

POSSIBLE INSTRUMENT TILT (deg)  
DP2 DP3  
-0.058 -2.676

Significant Wave Height (ABS gage) = 4.38 feet.

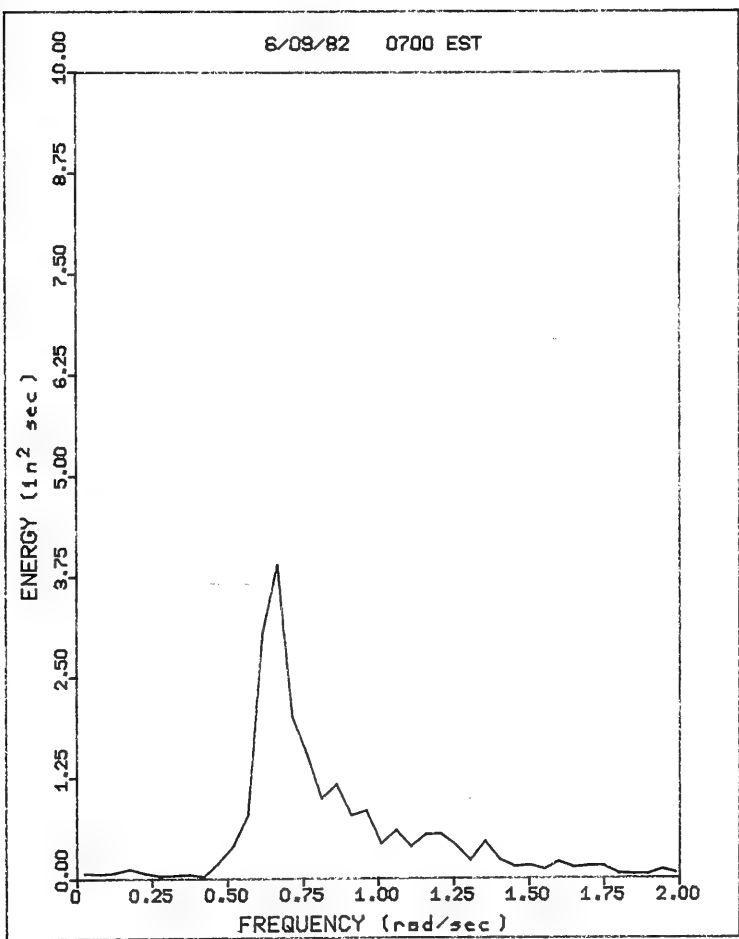
Effective period = 7.418 seconds.

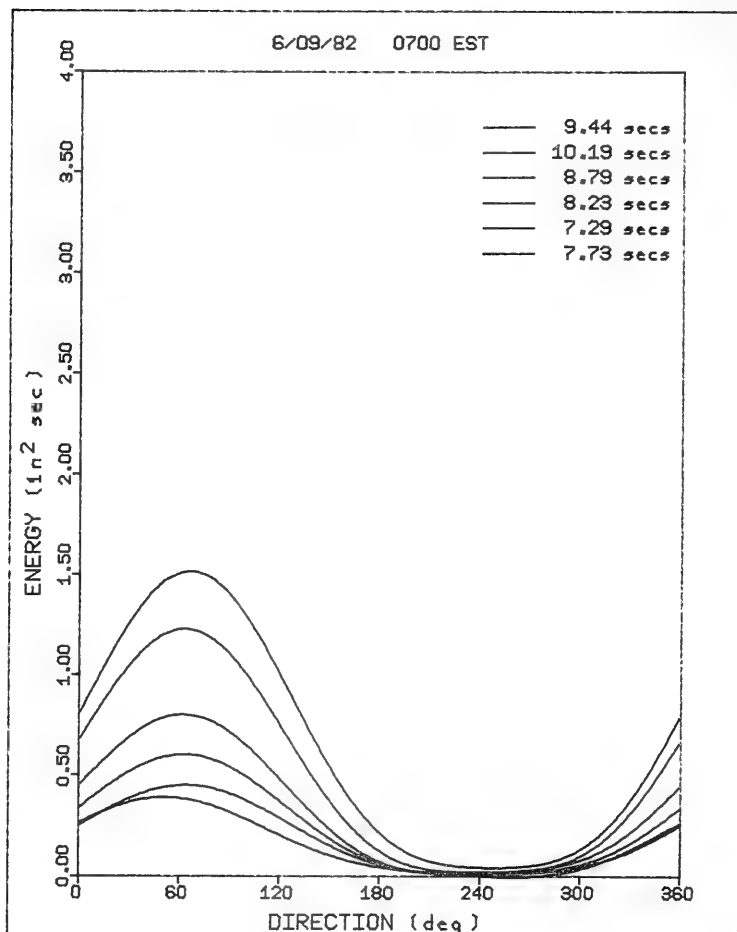
Maximum Energy located at bands:

9.438	exceeds average energy by	641.68 %
10.189	exceeds average energy by	481.35 %
8.790	exceeds average energy by	282.71 %
8.225	exceeds average energy by	191.30 %
7.288	exceeds average energy by	123.66 %
7.728	exceeds average energy by	89.83 %

Compass heading from which waves propagate

Band 9.438	secs: Greatest Energy at	67. deg
Band 10.189	secs: Greatest Energy at	63. deg
Band 8.790	secs: Greatest Energy at	63. deg
Band 8.225	secs: Greatest Energy at	63. deg
Band 7.288	secs: Greatest Energy at	65. deg
Band 7.728	secs: Greatest Energy at	51. deg





UNIVERSITY OF DELAWARE  
DEPARTMENT OF CIVIL ENGINEERING  
DPG DIRECTIONAL WAVE MONITOR / FRF, DUCK, N.C.

DEV	YR	MO	DAY	TIME
111	82	6	10	7 0
121	82	6	10	7 0
141	82	6	10	7 0

4096 POINTS ANALYZED AT .50 SECOND SAMPLING  
8 BANDS BLOCK AVERAGED

GAGE NUMBER 2  
14 LOW truncations; 9 HIGH truncations  
Mean= 2.302 S.Dev= 0.06642 Lower Limit= 2.103 Upper Limit= 2.501

GAGE NUMBER 3  
3 LOW truncations; 18 HIGH truncations  
Mean= 2.104 S.Dev= 0.19050 Lower Limit= 1.532 Upper Limit= 2.675

GAGE NUMBER 5  
0 LOW truncations; 5 HIGH truncations  
Mean= 2.381 S.Dev= 0.03698 Lower Limit= 2.270 Upper Limit= 2.492

TIDE LEVEL IS 1.245 FEET.

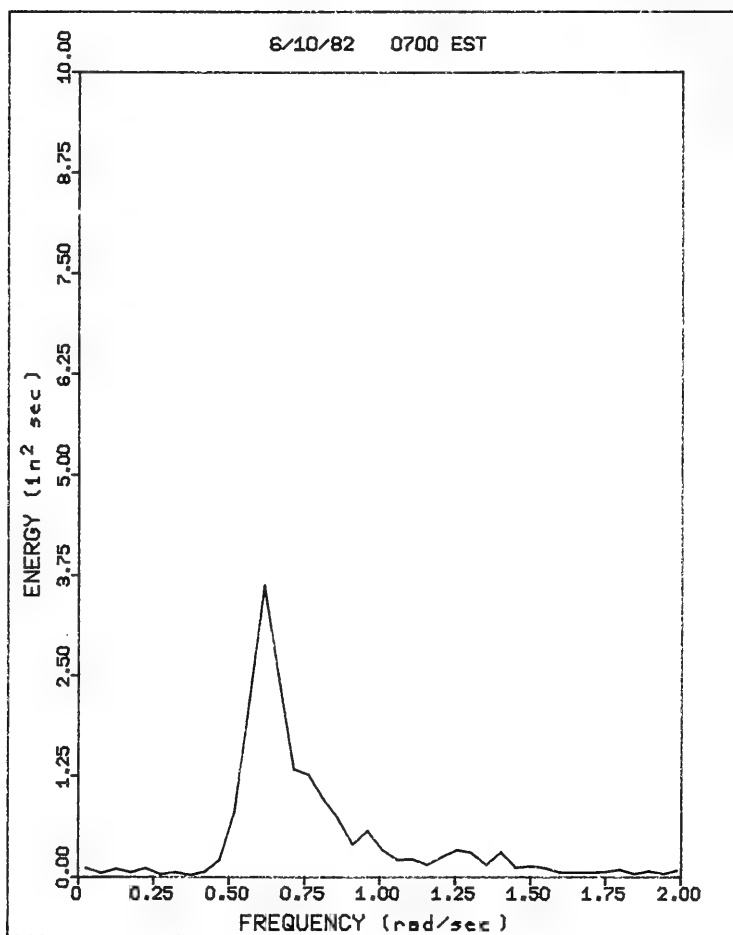
POSSIBLE INSTRUMENT TILT (deg)  
DP2 DP3  
-0.048 -2.962

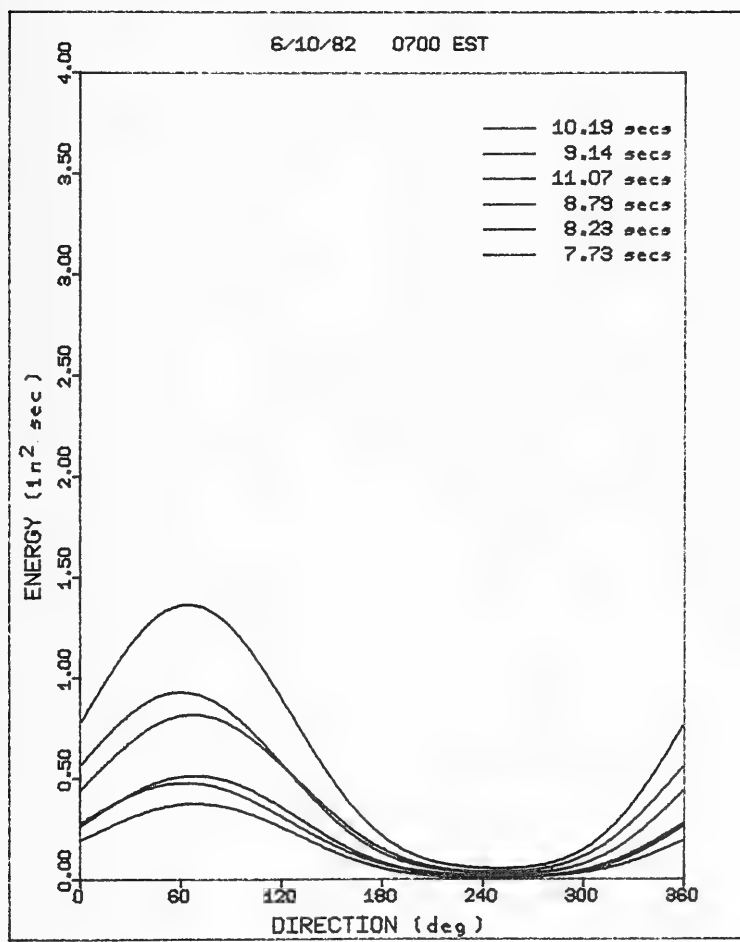
Significant Wave Height (ABS gage) = 4.05 feet.

Effective period = 8.073 seconds.

Maximum Energy located at bands:  
10.189 exceeds average energy by 704.75 %  
9.438 exceeds average energy by 448.02 %  
11.070 exceeds average energy by 385.94 %  
8.790 exceeds average energy by 196.96 %  
8.225 exceeds average energy by 182.72 %  
7.728 exceeds average energy by 117.25 %

Compass heading from which waves propagate  
Band 10.189 secs: Greatest Energy at 65. deg  
Band 9.438 secs: Greatest Energy at 61. deg  
Band 11.070 secs: Greatest Energy at 67. deg  
Band 8.790 secs: Greatest Energy at 69. deg  
Band 8.225 secs: Greatest Energy at 63. deg  
Band 7.728 secs: Greatest Energy at 69. deg





UNIVERSITY OF DELAWARE  
DEPARTMENT OF CIVIL ENGINEERING  
DPG DIRECTIONAL WAVE MONITOR / FRF, DUCK, N.C.

DEV	YR	MO	DAY	TIME
111	82	6	10	13 0
121	82	6	10	13 0
141	82	6	10	13 0

4096 POINTS ANALYZED AT .50 SECOND SAMPLING  
8 BANDS BLOCK AVERAGED

GAGE NUMBER 2  
6 LOW truncations; 55 HIGH truncations  
Mean= 2.272 S.Dev= 0.21523 Lower Limit= 1.626 Upper Limit= 2.917

GAGE NUMBER 3  
3 LOW truncations; 41 HIGH truncations  
Mean= 2.116 S.Dev= 0.26262 Lower Limit= 1.329 Upper Limit= 2.904

GAGE NUMBER 5  
0 LOW truncations; 2 HIGH truncations  
Mean= 2.368 S.Dev= 0.05197 Lower Limit= 2.212 Upper Limit= 2.524

TIDE LEVEL IS 0.893 FEET.

POSSIBLE INSTRUMENT TILT (deg)  
DP2 DP3  
-0.285 -2.871

Significant Wave Height (ABS gage) = 5.60 feet.

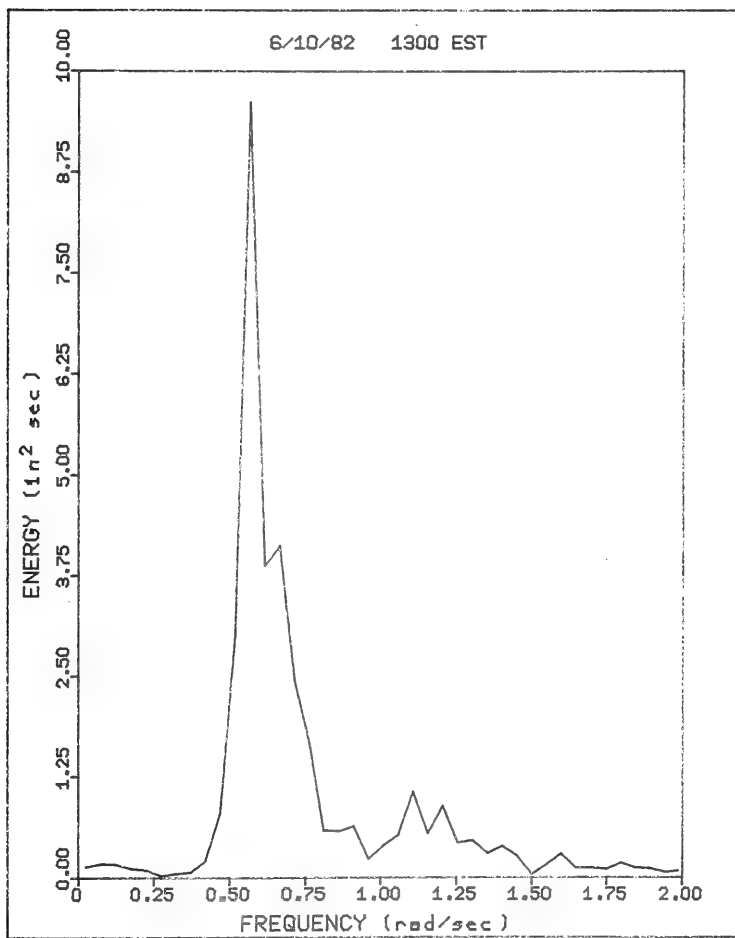
Effective period = 8.412 seconds.

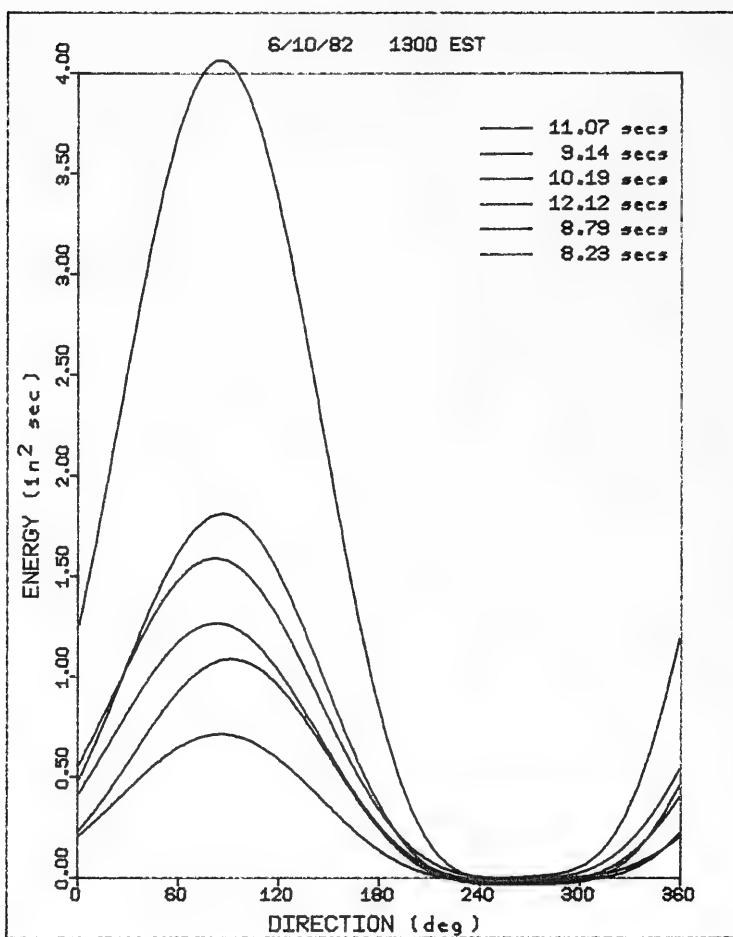
Maximum Energy located at bands:

11.070	exceeds average energy by	1016.50 %
9.438	exceeds average energy by	377.97 %
10.189	exceeds average energy by	349.36 %
12.118	exceeds average energy by	248.42 %
8.790	exceeds average energy by	184.15 %
8.225	exceeds average energy by	93.46 %

Compass heading from which waves propagate

Band 11.070	secs: Greatest Energy at	85. deg
Band 9.438	secs: Greatest Energy at	87. deg
Band 10.189	secs: Greatest Energy at	83. deg
Band 12.118	secs: Greatest Energy at	83. deg
Band 8.790	secs: Greatest Energy at	91. deg
Band 8.225	secs: Greatest Energy at	85. deg





UNIVERSITY OF DELAWARE  
DEPARTMENT OF CIVIL ENGINEERING  
DPG DIRECTIONAL WAVE MONITOR / FRF, DUCK, N.C.

DEV	YR	MO	DAY	TIME
111	82	6	11	7 0
121	82	6	11	7 0
141	82	6	11	7 0

4096 POINTS ANALYZED AT .50 SECOND SAMPLING  
8 BANDS BLOCK AVERAGED

GAGE NUMBER 2  
8 LOW truncations; 6 HIGH truncations  
Mean= 2.299 S.Dev= 0.09652 Lower Limit= 2.010 Upper Limit= 2.589

GAGE NUMBER 3  
0 LOW truncations; 8 HIGH truncations  
Mean= 2.039 S.Dev= 0.19138 Lower Limit= 1.465 Upper Limit= 2.613

GAGE NUMBER 5  
0 LOW truncations; 1 HIGH truncations  
Mean= 2.364 S.Dev= 0.09900 Lower Limit= 2.247 Upper Limit= 2.481

TIDE LEVEL IS 0.824 FEET.

POSSIBLE INSTRUMENT TILT (deg)  
DP2 DP3  
-0.061 -3.365

Significant Wave Height (ABS gage) = 4.32 feet.

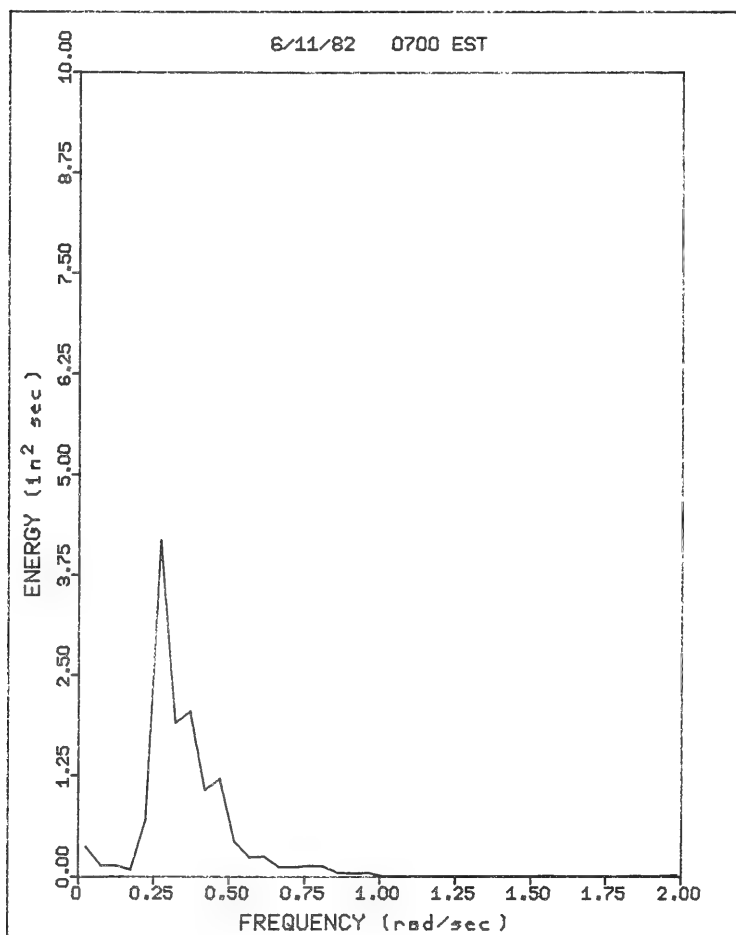
Effective period = 7.817 seconds.

Maximum Energy located at bands:

11.070	exceeds average energy by	715.00 %
10.189	exceeds average energy by	266.13 %
12.118	exceeds average energy by	194.16 %
13.386	exceeds average energy by	159.03 %
8.790	exceeds average energy by	115.97 %
8.225	exceeds average energy by	108.46 %

Compass heading from which waves propagate

Band 11.070	secs: Greatest Energy at	73. deg
Band 10.189	secs: Greatest Energy at	71. deg
Band 12.118	secs: Greatest Energy at	67. deg
Band 13.385	secs: Greatest Energy at	69. deg
Band 8.790	secs: Greatest Energy at	69. deg
Band 8.225	secs: Greatest Energy at	75. deg



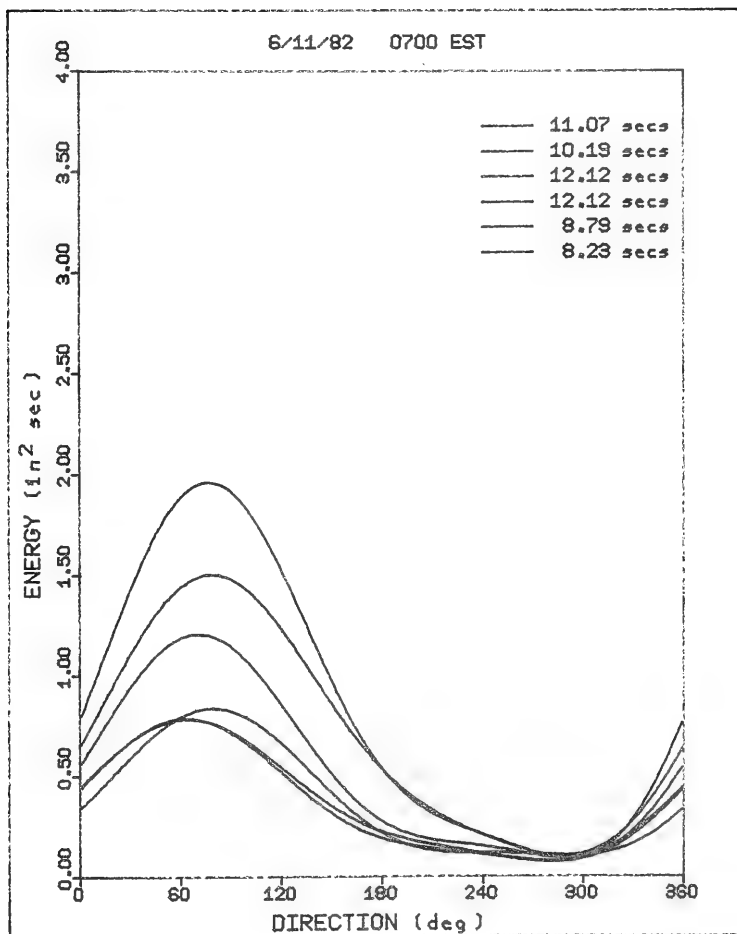


TABLE A-1: COMPARISON OF OTHER DIRECTIONAL ESTIMATES

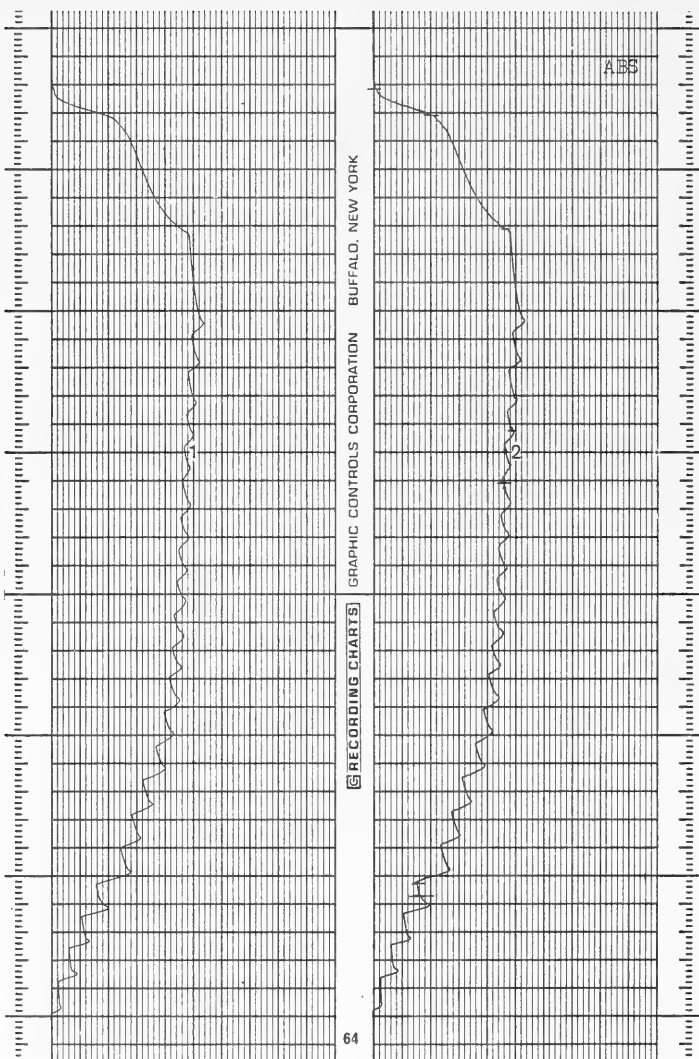
June 8 - 11, 1982

DATE	TIME	PERIOD (secs)	SPECTRAL PEAK (deg)	ESTIMATE $dP2/dP3$ (deg)	MEAN DIRECTION	
					$\tan^{-1} \frac{b_1}{a_1}$ (deg)	$\tan^{-1} \frac{b_2}{a_2}$ (deg)
6/8	0700	8.22	59	144	60.1	65.3
		8.79	61	148	64.1	65.7
		9.44	61	194	60.0	68.3
	1320	8.79	59	238	58.8	62.1
		9.44	61	104	61.0	65.0
		8.23	57	188	57.9	62.1
6/9	0700	9.44	67	109	66.7	79.9
		10.19	63	144	63.2	73.8
		8.79	63	113	61.5	74.8
6/10	0700	10.19	65	119	65.1	74.5
		9.44	61	194	61.1	65.9
		11.07	67	276	68.6	78.4
	1300	11.07	85	85	84.6	117.7
		9.44	87	85	86.6	120.5
		10.19	83	200	82.4	110.9
6/11	0700	11.07	73	76	74.8	94.2
		10.19	71	204	68.2	88.0
		12.12	67	227	73.0	76.8

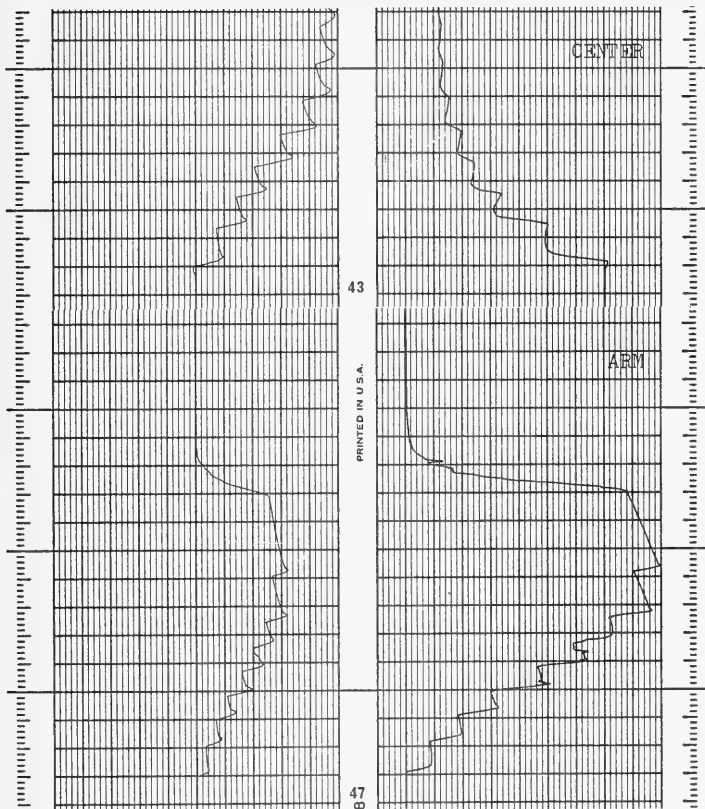
APPENDIX B

TYPICAL STRIP CHART RECORDINGS FROM  
BENCH CALIBRATION

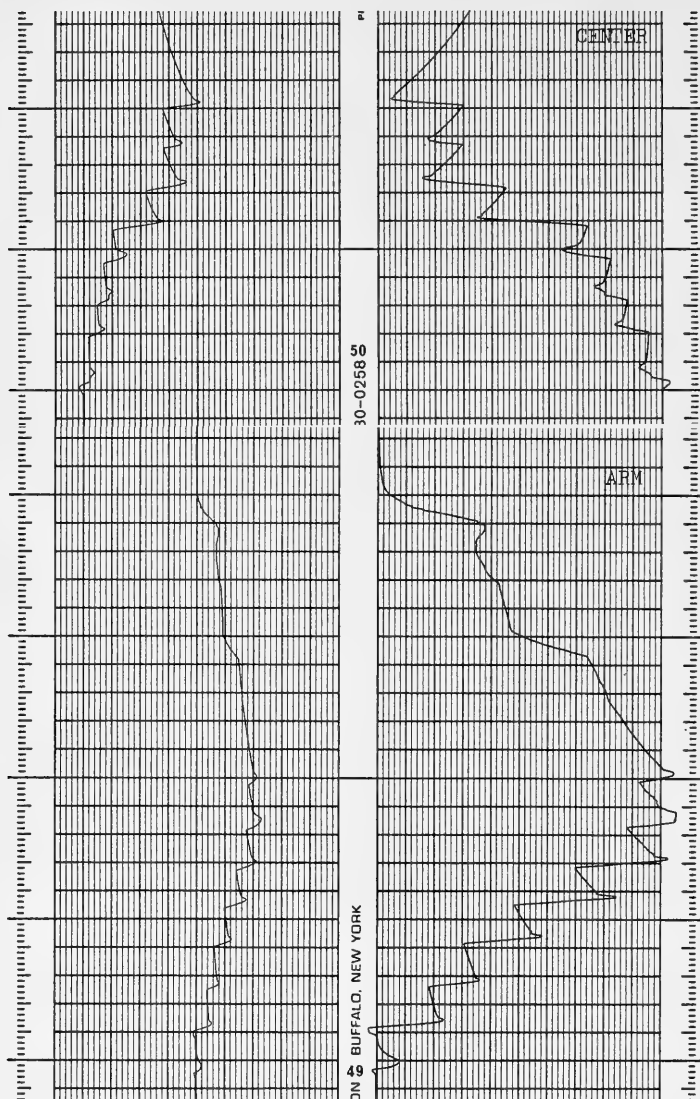
Results from Calibration Test  
Performed 1 Week before Field Installation.



Chamber Pressure Xdcr. ABS.  
Calib. Factor: 0.1 psi/mm Calib. Factor: 0.1 psi/mm  
Chart Speed: 5 mm/sec



Chamber Pressure Xdcr. dP1  
Calib. Factor: 0.1 psi/mm Calib. Factor: .02 psid/mm  
Chart Speed: 5 mm/sec



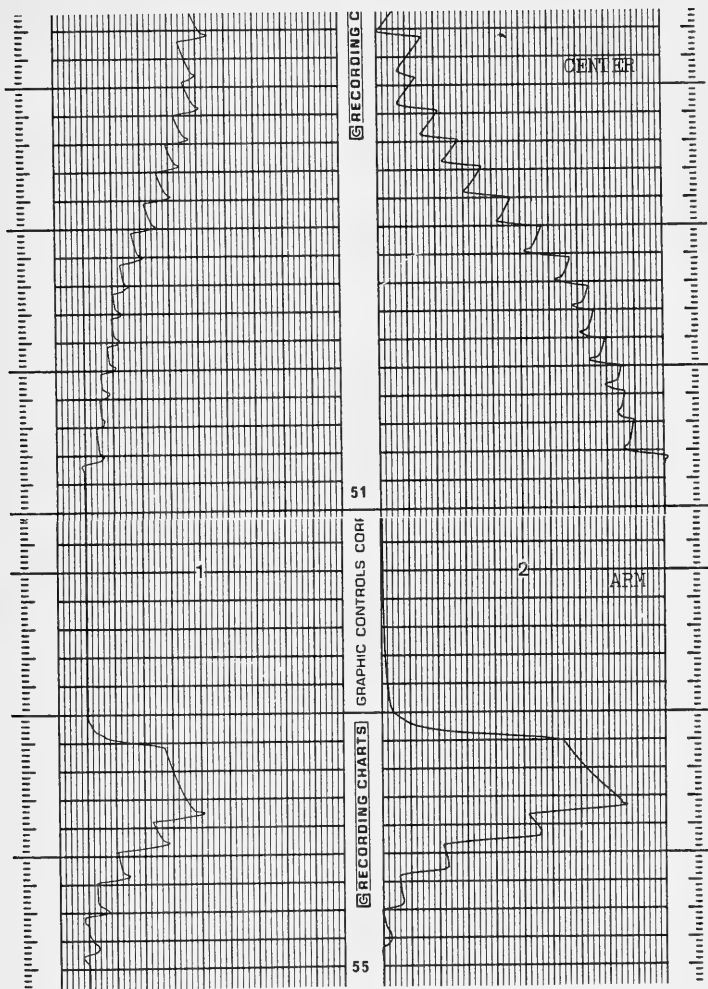
Chamber Pressure Xdcr.

Cal. Factor (top): .05 psi/mm  
Cal. Factor (bottom): 0.1 psi/mm

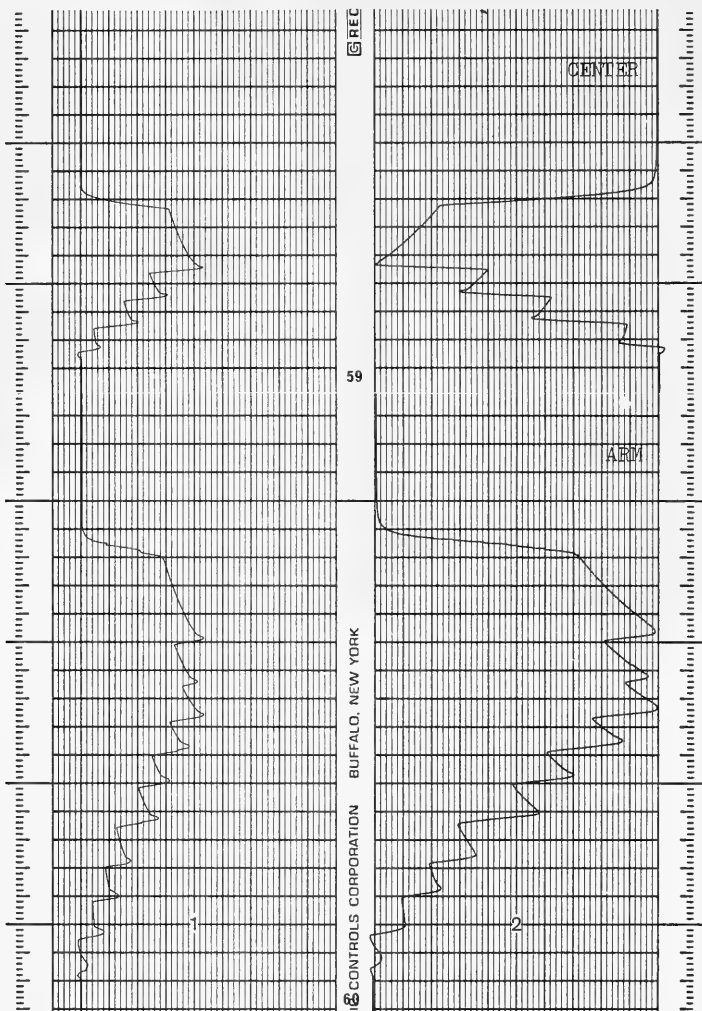
dP2

Calib. Factor: .02 psid/mm

Chart Speed: 5 mm/sec



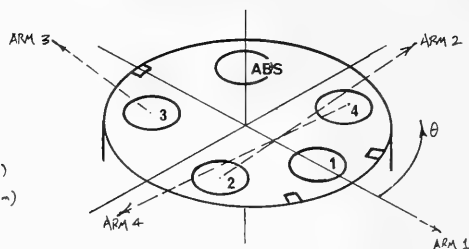
Chamber Pressure Xdcr.  $dP_3$   
Calib. Factor: .05 psi/mm Calib. Factor: .02 psid/mm  
Chart Speed: 5 mm/sec



Chamber Pressure Xdr. dP4  
Calib. Factor: .05 psi/mm Calib. Factor: .02 psid/mm  
Chart Speed: 5 mm/sec

APPENDIX C

A PARTIAL LIST OF DPG DIMENSIONS



LENGTH, ARM TO ARM : 9'-9" (2.97 m)

HEIGHT OF INSTRUMENT : 40.5" (1.03 m)

IN CRADLE : 51.5" (1.31 m)

APPROX. WEIGHT IN AIR

INSTRUMENT : 80 LBS (36 kg)

CRADLE : 200 LBS (91 kg)

DIFF. PRESSURE GAGE LENGTH

dP1 : 17.25"

dP2 : 53.75"

dP3 : 47.75"

dP4 : 53.875"

CONFIGURATION OF CENTER  
SENSORS

ELASTOMER DEPTH BENEATH FUSELAGE COVER PLATE = 0.4375"

HOLE DIAMETER IN FUSELAGE COVER PLATE = 0.625"

ELASTOMER DISTANCE BEHIND ARM HOLES = 1.5625"

ARM HOLE DIAMETER = 0.6875"

PRECISE ORIENTATION OF DIFF. PRESSURE GAUGE MEASUREMENTS

dP1: 0.000°

dP2: 91.013°

dP3: 182.100°

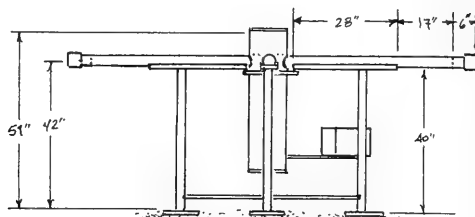
dP4: 269.00°

FUSELAGE CLEARANCE FROM LEVEL EARTH = 19"

BACK-FILL PRESSURE (ABS. GAGE) = 1.32 psi

(LENGTH OF ABS. GAGE TUBING = 18.5 inches)

INSTRUMENT SECURED INTO CRADLE



APPENDIX D

ASSEMBLY AND MAINTENANCE OF THE DPG

## INSTRUMENT ASSEMBLY AND MAINTENANCE

### A. Initial Assembly

1. The transducer stack is created by placing the transducers within the plexiglass wafers and attaching the acrylic stand-off rods between the wafers.
2. The stack is attached to the bottom of the water-tight cylinder (can) end-cap.
3. Nylon tubing is connected between the the bottom of the end-cap and the transducer pressure ports.
4. The wiring is then completed terminating to a 16-pin connector positioned just below the can end-cap.
5. The exterior stainless steel tubing and acrylic diaphragm housings are attached to the top of the end-cap.
6. The center housings are larger in diameter and should connect to the slightly "elevated" Swage-Locks on the transducers.

## B. Fluid Back-Filling

6. The center differential lines are filled first. The transducer stack is laid on its side with the bottom slightly elevated. Two center bleed ports face up. The line to be filled is flexed up so that the housing is above the stack. Fluid is poured in to the housing until a steady flow streams from the bleed port. The port is then closed. (Figure D-1.)

7. Enough fluid must be poured into the housing so that it forms an inverted meniscus about the o-ring. The elastomer diaphragm is slid horizontally over the fluid until its holes line up with the threaded holes in the housing. The copper-nickel ring is then lowered carefully onto the elastomer and secured to the housing with Monel screws. Each housing, elastomer, and ring is labelled as a set. The labels should fall in line so that the holes in each of the three match.

8. The process is repeated for each of the center differential lines.

9. The arm sensors are filled next.

10. A large plate is attached to the bottom of the stack using the threaded ( 6-32) holes in the stand-offs.

11. The stack is inverted (end-cap down) on top of a stand or

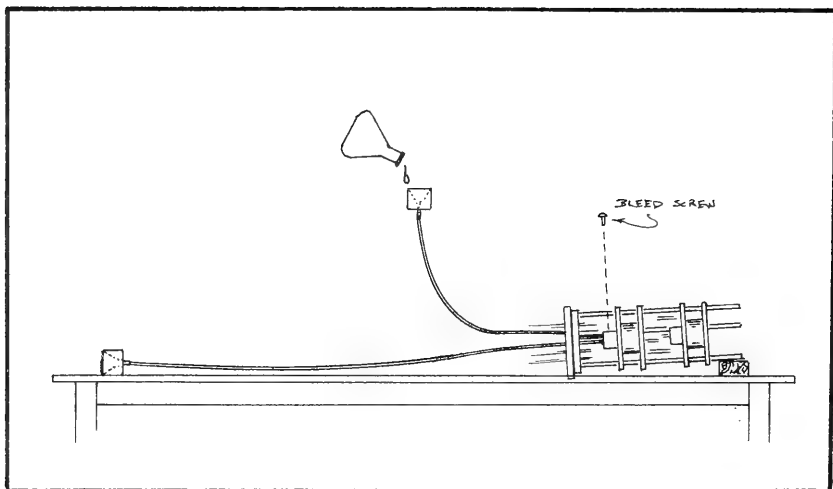


FIGURE D-1: Back-filling the center sensors.



FIGURE D-2: Back-filling the arm sensors. (Brian Jacobs shown with instrument.)

platform.

12. The arm line to be filled is lifted above its transducer and the filling process is repeated. (Figure D-2.)

13. After each arm line is filled, the stack is positioned upright to fill the absolute transducer.

14. The absolute transducer has no bleed port, so the nylon tubing is removed from the transducer and the port filled to overflowing. Fluid is then poured into the absolute line's sensor housing until it streams out of the bottom of the nylon line. While it is still flowing, the line is inserted into the pressure port and secured. The housing is then sealed with the elastomer diaphragm and ring as usual.

15. The exterior tubing should be flexed and the assembly re-positioned and inspected several times to ensure that no air has been trapped in the lines. It should then be placed in sunlight or a warm temperature -- with the isolation diaphragms above the transducers -- to allow any small bubbles in the fluid to appear.

16. Air bubbles that appear can be eliminated by removing the copper-nickel ring and elastomer, adding more fluid to the housing and then re-sealing.

17. Once the system is air-free, the instrument is ready for

calibration.

C. Assembly of the Housing

18. After calibration, the can is slid over the stack -- guiding the cable from the bottom of the can into a large cut-out on the outer edge of the wafers.

19. When the can's cable reaches the transducer stack's electrical connector, the two are mated and the can is secured to the end-cap.

20. The can is then slid into the bottom of the fuselage, sensors first. The arm sensors are guided out the four large fuselage holes and the can pushed upwards until it hits the stops inside the fuselage.

21. The bottom stops are then screwed into the fuselage walls to secure the can.

22. This assembly is then stood up on blocks (to protect the titanium bolts on the underside of the fuselage).

23. The PVC spider is pushed in through the top of the fuselage until it lines up with the arm-holes. The PVC arms are pushed through the fuselage walls and into the spider. They are secured by bolts that thread through the top of the spider.

24. The sensors are secured to the inside of the PVC arms by two brass screws that pass through the arms and thread into the acrylic housings.

25. The center plate is next placed into the top of the fuselage and the center sensors positioned within it.

26. The plexiglass end-cap is then attached to the top of the fuselage.

#### D. Field Preparation and Installation

27. Copper scour pads are placed into the ends of the arms and the arm end-caps screwed on.

28. The cable is retrieved and mated to the instrument on the underside of the can and a plexiglass plate attached to the bottom of the fuselage.

29. With the cradle already on the seafloor, the instrument is brought underwater and positioned onto it. The plate breaching the gap about the center of the cradle must be removed to allow passage of the cable, then replaced after installation.

30. Free cable may then be stored in the service box; the top of which is removed by unthreading a titanium nut on each top corner of the box.

#### E. Maintenance

The DPG system should receive standard marine maintenance as due for an instrument of its type. Diver inspection should be made at least semi-annually with copper scour pad change-out at the beginning and end of the heavy fouling season. Special attention should be given to the chain binders to ensure that they are securing the anchor chains tautly. It is recommended that the instrument be removed from the water and thoroughly inspected after a period of four years at which time it should be re-coated with anti-fouling paints. The buoy line should be replaced annually before the heavy seas of winter.

**Note:** To ensure satisfactory DPG operation with the software as written, it is essential that the instrument be re-assembled in precisely the same configuration as its original state of deployment.

APPENDIX E

THE ESTIMATION OF HIGHER ORDER  
DIRECTIONAL FOURIER COEFFICIENTS

Borgman (1969) has developed a technique to estimate higher order directional Fourier coefficients which does not require the subtraction of signals from adjacent pressure gauges. If the distance and angle between a pair of pressure gauges in an array is  $D$  and  $\beta$ , respectively, then the cross-spectral density, normalized by the unidirectional spectral density  $S(\phi)$  can be expressed as:

$$c' + iq' = J_0(kD) + 2 \sum_{n=1}^{\infty} (a_n \cos n\beta + b_n \sin n\beta) \pi(i)^n J_n(kD) \quad (F.1)$$

for some frequency  $\phi$ .  $J_n(\text{argument})$  and  $J_n(\text{argument})$  are Bessel functions. In terms of real and imaginary parts, Eq. F.1 can be written:

$$c' = J_0(kD)$$

$$\begin{aligned} & - 2\pi J_2(kD) (a_2 \cos 2\beta + b_2 \sin 2\beta) \\ & + 2\pi J_4(kD) (a_4 \cos 4\beta + b_4 \sin 4\beta) \\ & - 2\pi J_6(kD) (a_6 \cos 6\beta + b_6 \sin 6\beta) \\ & + \dots \end{aligned}$$

$$\begin{aligned} q' = & 2\pi J_1(kD) (a_1 \cos \beta + b_1 \sin \beta) \\ & - 2\pi J_3(kD) (a_3 \cos 3\beta + b_3 \sin 3\beta) \\ & + 2\pi J_5(kD) (a_5 \cos 5\beta + b_5 \sin 5\beta) \\ & - \dots \end{aligned}$$

The Fourier series can be accurately truncated to  $N$  if  $J(kD)$  is negligible for  $n > N$  or if  $a_n$  and  $b_n$  are negligible for  $n > N$ . There is a set, then, of  $2N$  equations;  $N$  equations from each of the real and imaginary parts of Equation F.1, and each with the unknowns  $a_n$  and  $b_n$ . The maximum possible value of  $N$  is determined by the number of different non-ambiguous cross-correlations possible from the gauges in the array. If there are no ambiguous cross-correlations between the gauges, the number of possible combinations for  $M$  gauges is

$M(M-1)/2$ . This is the number of coefficient pairs  $N$  that one can develop. It is suggested that one does not develop all  $N$  pairs, but stops at least two pairs sooner so that there are more equations than unknowns. The coefficients may then be fitted by least squares analysis.

As an example, four pressure gauges positioned at the axes of an irregular three-faced pyramid could potentially develop six coefficient pairs (or the first thirteen directional Fourier coefficients). It could more effectively develop four coefficient pairs (or the first nine coefficients) using least squares analysis to fit the coefficients. Signals from four pressure gauges positioned at the corners of a square, such as in the Scripps Sxy gauge (Seymour, 1978), develop only four non-ambiguous cross-correlations and thusly could generate the first four coefficient pairs (or the first nine coefficients). There are two other possible (ambiguous) correlations that can be utilized to fit the first nine coefficients by least squares analysis -- just as the pyramid-shaped array does by excluding the development of the last two coefficient pairs.

Since the DPG utilizes differential pressure gauges, the relations for the cross-spectral densities differ from Equation F.1. The cross-spectral density for two colinear differential pressure signals can be shown to be:

$$(c' + i\eta_x') \begin{bmatrix} \eta_{x_1} & \eta_{x_3} \\ \eta_{y_2} & \eta_{y_4} \end{bmatrix} = \frac{k^2}{2} [J_0(kD) + 2 \sum_{n=1}^N (a_n \cos n\beta + b_n \sin n\beta) \pi i^n J_n(kD)]$$

$$\mp J_2(kD) \pi \cos 2\beta$$

$$\pm \sum_{n=1}^N (a_n \cos(n+2)\beta + b_n \sin(n+2)\beta) \pi i^{n+2} J_{n+2}(kD) \pm \sum_{n=1}^N (a_n \cos(n-2)\beta + b_n \sin(n-2)\beta) \pi i^{n-2} J_{n-2}(kD)$$

for some frequency  $\Omega$ . The cross-spectral density of the absolute pressure signal and x-axis and y-axis differential pressure signals are respectively:

$$(c' + i\eta_x')_{\eta\eta_x} = k [J_0(kD) \cos \beta + \sum_{n=1}^N (a_n \cos(n+1)\beta + b_n \sin(n+1)\beta) \pi i^{n+1} J_{n+1}(kD) + \sum_{n=1}^N (a_n \cos(n-1)\beta + b_n \sin(n-1)\beta) \pi i^{n-1} J_{n-1}(kD)]$$

[F.4]

$$\begin{aligned} (c' + iq') \eta \eta_y &= k [J_0(kD) \sin \beta \\ &+ \sum_{n=1}^N (a_n \sin(n+1)\beta - b_n \cos(n+1)\beta) \pi i^{n+1} J_{n+1}(kD) \\ &+ \sum_{n=1}^N (b_n \cos(n-1)\beta - a_n \sin(n-1)\beta) \pi i^{n-1} J_{n-1}(kD)] \end{aligned}$$

for some frequency  $\omega$ . The cross-spectral density for the signals of two perpendicular differential pressure gauges is:

[F.5]

$$\begin{aligned} (c' + iq') \eta_x \eta_y &= \frac{k^2}{2} [- J_2(kD) \sin 2\beta \\ &+ \sum_{n=1}^N (a_n \sin(n+2)\beta - b_n \cos(n+2)\beta) \pi i^{n+2} J_{n+2}(kD) \\ &- \sum_{n=1}^N (a_n \sin(n-2)\beta - b_n \cos(n-2)\beta) \pi i^{n-2} J_{n-2}(kD)] \end{aligned}$$

For the configuration of the DPG prototype, five non-ambiguous cross-correlations are possible. This suggests that the first five directional Fourier coefficient pairs (first eleven coefficients) could be developed from Equations F.2 through F.5. Five additional ambiguous cross-correlations are possible so that these eleven coefficients might be better fit by least squares analysis. If the configuration of the DPG arms was altered such that the angle between each of the arms was unique, it is theoretically

possible to develop the first twenty-one directional Fourier coefficients with no least squares fit; or more practically, the first fifteen or seventeen coefficients.

APPENDIX F

FORTRAN ANALYSIS PROGRAM FOR DPG DATA

```
00050 C
00100 C
00150 C
00200 C
00250 C
00300 C
00350 C
00400 C
00450 C
00500 C
00550 C
00600 C
00650 C
00700 C
00750 C
00800 C
00850 C
00900 C
00950
01000
01050
01100
01150
01200
01250
01300
01350
01400
01450
01500
01550
01600
01650
01700
01750
01800
01850
01900
01950
02000
02050
02100
02150
02200
02250
02300 C
02350 C
02400 C
02450 C
02500 C
02550 C
02600 C
02650 C
02700 C
02750 C
02800 C
02850 C
02900 C
02950 C
03000 C

-----  
This program is designed for use with the University  
of Delaware DPG Directional Wave Monitor as installed  
at the FRF on 14 May, 1982. The instrument and software  
were designed by Kevin R. Dodge under the direction of  
Dr. Robert G. Dean.  
The program, as utilized by the FRF, uses only  
differential pressure channels dp2 and dp3 with the  
absolute gauge. It generates the directional spectra  
using the first 5 directional Fourier coefficients.  
The program as listed utilizes all four differ-  
ential gauges with the absolute gauge and is capable  
of generating the directional spectra using  
the first seven directional Fourier coefficients.  
English units are used throughout.  
-----  
DIMENSION dp1(4100),dp2(4100),dp3(4100),dp4(4100),  
1      abs(4100),dpxx(4100),dpyy(4100)  
1      DIMENSION d11(2050),d21(2050),d31(2050),d41(2050),  
1      ab1(2050),dxx1(2050),dyy1(2050)  
1      DIMENSION d1(2050),d2(2050),d3(2050),d4(2050),  
1      ab(2050),dxx(2050),dyy(2050)  
1      DIMENSION prsp(2050),wvnr(2050),freq(2050),maxfrq(20)  
DIMENSION thta1(400),thta2(400),thta3(400),pd(20)  
DIMENSION ao(400),a1(400),a2(400),a3(400),  
1      b1(400),b2(400),b3(400)  
1      DIMENSION dir1(400),dir2(400),dir3(400),dir4(400),  
1      ang1(400),ang2(400),ang3(400),ang4(400)  
1      INTEGER     blk  
OPEN(unit=18,device='dsk',file='DP1.dat')  
OPEN(unit=19,device='dsk',file='DP2.dat')  
OPEN(unit=20,device='dsk',file='DP3.dat')  
OPEN(unit=21,device='dsk',file='DP4.dat')  
OPEN(unit=22,device='dsk',file='DP5.dat')  
OPEN(unit=17,device='dsk',file='PWR.DAT')  
OPEN(unit=14,device='dsk',file='RAW.dat')  
OPEN(unit= 3,device='dsk',file='DIR.dat')  
OPEN(unit= 4,device='dsk',file='FRF.dat')  
-----  
INPUT ANALYSIS DETAILS:  
ATM = Atmospheric Pressure (mb)  
GAMMA = Seawater Specific Gravity (1b/cu.ft.)  
N = # of sampled points to analyze (power of 2)  
K = such that 2**K=N  
dT = sampling interval (secs)  
BLK = # of freq. bands to block-average  
NUFF = # of peak energy bands to identify  
Icut = # of non-block-averaged cut-off freq.  
-----  
ATM = 1013.0  
ATM = ATM*0.0145038
```

```
03050      GAMMA = 64.18
03100      GAMMA = GAMMA/1728.
03150      N = 4096
03200      K=11
03250      N2 = N/2
03300      DT = 0.5
03350      MOST = N+4
03400      BLK = 8
03450      NUFF = 6
03500      Icut = 327
03550
03600      C
03650      C
03700      C      DPG PHYSICAL DETAILS:
03750      C      ORIENT = compass heading of arm 3 w.r.t. true north
03800      C      SGAGE = mean depth of sensors below mean water (ft)
03850      C      DXin1 = length of arm 1 diff. measurement (in)
03900      C      DXin2 = length of arm 2 diff. measurement (in)
03950      C      DXin3 = length of arm 3 diff. measurement (in)
04000      C      DXin4 = length of arm 4 diff. measurement (in)
04050      C      ARM13 = distance between DP1 & DP3 measurement (in)
04100      C      ARM24 = distance between DP2 & DP4 measurement (in)
04150      C      Pbf = fluid back-fill pressure on absolute (psi)
04200      C
04250      C
04300      ORIENT = 53.
04350      SGAGE = 16.49
04400      DXin1 = 47.25
04450      DXin2 = 53.75
04500      DXin3 = 47.75
04550      DXin4 = 53.875
04600      ARM13 = 53.25
04650      ARM24 = 50.94
04700      Pbf = 1.23
04750
04800
04850      pi = 3.14159265
04900      twopi = 2.0 * pi
04950
05000      6008  Format(i4)
05050      WRITE(4,819)
05100      819  Format(//,40X,'UNIVERSITY OF DELAWARE',//,
05150      1     36X,'DEPARTMENT OF CIVIL ENGINEERING',//,
05200      2     29X,'DPG DIRECTIONAL WAVE MONITOR / ',
05250      3     'FRF, DUCK, N.C.',//)
05300
05350
05400
05450      C      Load data arrays with zeroes for cleanliness.
05500      DO 115 I=1,mst
05550      DP1(i) = 0.00
05600      DP2(i) = 0.00
05650      DP3(i) = 0.00
05700      DP4(i) = 0.00
05750      115  ABS(i) = 0.00
05800
05850      CALL INPUT (dp1,dp2,dp3,dp4,abs)
05900
05950      WRITE(4,3055) N,dt
06000      3055  Format(/,35x,i5,' POINTS ANALYZED AT ',f4.2,' SECOND',
```

```
18050      READ(19,900) dev,yr,mo,day,hr,min
18100      WRITE(4,901) dev,yr,mo,day,hr,min
18150      n=1
18200      DO 202 j=1,410
18250      READ(19,905) (A(i),i=1,10),LAST
18300      DO 102 i=1,10
18350      DPV2(n) = A(i)/200.0
18400      102      n=n+1
18450      202      Continue
18500
18550      READ(20,900) dev,yr,mo,day,hr,min
18600      WRITE(4,901) dev,yr,mo,day,hr,min
18650      n=1
18700      DO 203 j=1,410
18750      READ(20,905) (A(i),i=1,10),LAST
18800      DO 103 i=1,10
18850      DPV3(n) = A(i)/200.0
18900      103      n=n+1
18950      203      Continue
19000
19050      READ(21,900) dev,yr,mo,day,hr,min
19100      WRITE(4,901) dev,yr,mo,day,hr,min
19150      n=1
19200      DO 204 j=1,410
19250      READ(21,905) (A(i),i=1,10),LAST
19300      DO 104 i=1,10
19350      DPV4(n) = A(i)/200.0
19400      104      n=n+1
19450      204      Continue
19500
19550      READ(22,900) dev,yr,mo,day,hr,min
19600      WRITE(4,901) dev,yr,mo,day,hr,min
19650      n=1
19700      DO 205 j=1,410
19750      READ(22,905) (A(i),i=1,10),LAST
19800      DO 105 i=1,10
19850      ABSV(n) = A(i)/200.0
19900      105      n=n+1
19950      205      Continue
20000
20050
20100      890      Format(//,15X,' DEV  YR  MO DAY    TIME')
20150      900      Format(6i4)
20200      901      Format(15x,6i4)
20250      905      Format(10i5,11)
20300
20350      Return
20400      End
20450
20500
20550
20600      C      _____
20650      C      SUBROUTINE PERIOD (ab,d1,d2,d3,d4,n,icut,dT,prsp,wvnr,
20700      C      freq)
20750      C      Computes the centroid of the power spectra
20800      C      and reports the corresponding frequency
20850      C      as the "effective period".
20900      DIMENSION ab(2050),d1(2050),d2(2050),d3(2050),d4(2050),
20950      1      prsp(2050),wvnr(2050),freq(2050)
21000
```

```
21050      twopi = 6.283185
21100      N2 = N/2
21150
21200      DATA sumabk,sum1k,sum2k,sum3k,sum4k,sabsk,s1k,s2k,
21250      1      s3k,s4k/0.,0.,0.,0.,0.,0.,0.,0./
21300
21350      DO 420 J=2,icut
21400      SUMABK = sumabk + ab(j)
21450      SUM1K = sum1k + d1(j)
21500      SUM2K = sum2k + d2(j)
21550      SUM3K = sum3k + d3(j)
21600      SUM4K = sum4k + d4(j)
21650      SABSK = SABSK + AB(j) * freq(j)
21700      S1K = s1k + d1(j) * freq(j)
21750      S2K = s2k + d2(j) * freq(j)
21800      S3K = s3k + d3(j) * freq(j)
21850      S4K = s4k + d4(j) * freq(j)
21900 420  Continue
21950
22000
22050      Tabsk = twopi * sumabk/sabsk
22100      T1k = twopi * sum1k/s1k
22150      T2k = twopi * sum2k/s2k
22200      T3k = twopi * sum3k/s3k
22250      T4k = twopi * sum4k/s4k
22300
22350      C  Report the effective period from the absolute gage.
22400      WRITE(4,929) Tabsk
22450      929  Format(' Effective period =',f7.3,' seconds.')
22500
22550      Return
22600      End
22650
22700  C
22750
22800      SUBROUTINE SURF (icut,d1,d2,d3,d4,dp1,dp2,dp3,dp4,
22850      1      d1i,d2i,d3i,d4i,dir1,dir2,dir3,dir4,b1k,
22900      2      orient)
22950
23000      DIMENSION d1(2050),d2(2050),d3(2050),
23050      1      d4(2050)
23100      1      DIMENSION dp1(4100),dp2(4100),dp3(4100),dp4(4100),
23150      1      d1i(2050),d2i(2050),d3i(2050),d4i(2050)
23200      DIMENSION dir1(400),dir2(400),dir3(400),dir4(400)
23250      INTEGER    b1k
23300
23350
23400  C  Generates directional estimate without absolute gage.
23450  C  DIR1 uses gages DP1 and DP2;
23500  C  DIR2 uses gages DP3 and DP4;
23550  C  DIR3 uses gages DP2 and DP3;
23600  C  DIR4 uses gages DP1 and DP4.
23650
23700      DO 435 J=2,icut
23750      if(dp1(j).ne.0.0)tan1=atan2(d1i(j),dp1(j))
23800      if(dp1(j).eq.0.)tan1 = 0.0
23850      if(dp2(j).ne.0.0)tan2=atan2(d2i(j),dp2(j))
23900      if(dp2(j).eq.0.)tan2 = 0.0
23950      if(dp3(j).ne.0.0)tan3=atan2(d3i(j),dp3(j))
24000      if(dp3(j).eq.0.)tan3 = 0.0
```

```
12050      DYY(i) = 2.0*(dpyy(i)**2 + dyyi(i)**2)
12100      67      Continue
12150
12200      C   Store the raw power spectra, if desired
12250          GO TO 4003
12300          WRITE(17,4007)
12350          WRITE(17,3098)
12400          DO 4003 i=2,icut
12450              WRITE(17,914)freq(i),ab(i),d1(i),d2(i),d3(i),
12500              1                   d4(i),dxx(i),dyy(i)
12550      4003  Continue
12600      4007  Format(' RAW POWER SPECTRA')
12650
12700
12750      C   Calculate significant wave height from absolute gage.
12800          E=0.0
12850          DO 405 j=2,icut
12900              E = ab(j) + E
12950          Hsig = (4.*sqrt(E))/12.0
13000          WRITE(4,914) Hsig
13050          921  Format(/, ' Significant Wave Height (ABS gage) =',f6.2,
13100              1                   ' feet.',//)
13150
13200
13250
13300      C   Determine effective period from all gauges.
13350
13400          CALL PERIOD (ab,d1,d2,d3,d4,n,icut,dT,prsp,wvnr,freq)
13450
13500
13550      C   Estimate direction without absolute gage.
13600
13650          GO TO 6002
13700          CALL SURF (icut,d1,d2,d3,d4,dp1,dp2,dp3,dp4,
13750              1                   dti,d2i,d3i,d4i,dir1,dir2,dir3,dir4,blk,
13800              2                   orient)
13850
13900
13950          CALL SURF2(ab,d1,d2,d3,d4,ang1,ang2,ang3,ang4,icut,
14000              1                   wvnr,blk,orient)
14050
14100      6002  Continue
14150
14200
14250      C   Generate the directional Fourier coefficients
14300
14350          CALL FCOEFS(ab,abs,abi,d1,dp1,d1i,d2,dp2,d2i,d3,
14400              1                   dp3,d3i,d4,dp4,d4i,dxx,dpxx,dxxi,dyy,dpyy,dyyi,
14450              2                   wvnr,freq,thta1,thta2,thta3,
14500              3                   a0,a1,a2,a3,b1,b2,b3,blk,icut)
14550
14600
14650      C   Store the block-averaged power spectra
14700          WRITE(17,3097) blk
14750          WRITE(17,3098)
14800          3097  Format(/, ' BLOCK AVERAGED BY',i3,
14850              1                   ' BANDS')
14900          3098  Format(' freq . ab . d1 . d2 . d3 . d4',
14950              1                   ' . dxx . dyy',/),
15000          DO 77 i=2,icut
```

```
15050      WRITE(17,914) freq(i), ab(i),d1(i),d2(i),d3(i),
15100      1      d4(i),dxx(i),dy(i)
15150      77  Continue
15200      914  Format(f11.3,f11.5,4F14.9,2F20.18)
15250
15300
15350  C  Identify bands of highest energy
15400      Call MAXSIG(ab,icut,maxfrq,n,dT,nuff,freq)
15500
15550
15600  C  Generate directional spectra for highest energy bands
15650
15700      Call DIRXSP (AO,A1,A2,A3,B1,B2,B3, freq,n,dT,nuff,
15750      1      maxfrq,orient)
15800
15850
15900  C      GO TO 9999
15950
16000      WRITE(4,910)
16050      DO 666 nn=1,nuff
16100      LKM = maxfrq(nn)
16150      PD(nn) = twopi/freq(1km)
16200      IF(thta1(1km).lt.0.)thta1(1km)=360.+thta1(1km)
16250      IF(thta2(1km).lt.0.)thta2(1km)=360.+thta2(1km)
16300      IF(thta3(1km).lt.0.)thta3(1km)=360.+thta3(1km)
16350      WRITE(4,913) PD(nn),thta1(1km),thta2(1km),
16400      1      thta3(1km),dir1(1km),dir2(1km),dir3(1km),dir4(1km),
16450      2      ang1(1km),ang2(1km),ang3(1km),ang4(1km)
16500  666 Continue
16550  910  Format(/,5x,' MEAN DIRECTION OF PROPOGATION',6x,'ESTIM',
16600      1      'ATE W/OUT ABSOLUTE GAGE',12x,'WITH 1 CHANNEL',
16650      2      ' AND ABSOLUTE',/, ' Period',5x,'n=1',7x,'n=2',
16700      3      7x,'n=3',6x,'1-2',6x,'3-4',6x,'2-3',6x,'1-4',
16750      4      11x,'dp1',6x,'dp2',6x,'dp3',6x,'dp4')
16800  913  Format(f6.2,3f10.2,4f9.1,5x,4f9.1)
16850
16900
16950  9999  END
17000
17050  C
17100
17150      SUBROUTINE INPUT(dpv1,dpv2,dpv3,dpv4,absv)
17200
17250      DIMENSION dpv1(4100),dpv2(4100),dpv3(4100),
17300      1      dpv4(4100),absv(4100),M(4100)
17350      INTEGER dev,yr,day,hr,A(10)
17400
17450      WRITE(4,890)
17500
17550      READ(18,900) dev,yr,mo,day,hr,min
17600      WRITE(4,901) dev,yr,mo,day,hr,min
17650      n=1
17700      DO 200 j=1,410
17750      READ(18,905) (A(i),i=1,10),LAST
17800      DO 100 i=1,10
17850      DPV1(n) = A(i)/265.0 * 1.65
17900  100      n=n+1
17950  200  Continue
18000
```

```
06050      1      ' SAMPLING')
06100      WRIT(4,3056) blk
06150 3056 Format(57x,12,' BANDS BLOCK AVERAGED')
06200
06250
06300 C   Scan each record, calculate std.deviation, truncate
06350 C   unreasonable points, report them, calculate and subtract
06400 C   mean from record, convert to psi.
06450
06500      NGAGE = 1
06550      Call SCAN(dp1,n,ngage,avg1,dxin1)
06600      NGAGE = 2
06650      Call SCAN(dp2,n,ngage,avg2,dxin2)
06700      NGAGE = 3
06750      Call SCAN(dp3,n,ngage,avg3,dxin3)
06800      NGAGE = 4
06850      Call SCAN(dp4,n,ngage,avg4,dxin4)
06900      NGAGE = 5
06950      Call SCAN(abs,n,ngage,avgabs,dxin4)
07000
07050      N = N/2
07100      N2 = N2/2
07150
07200 C   Reverse signs on DP1 & DP2 for sign convention.
07250      DO 1057 JJ=1,N
07300      DP1(jj) = -DP1(jj)
07350      DP2(jj) = -DP2(jj)
07400 1057 Continue
07450
07500
07550 C   Record portion of pressure signals in scratch file
07600 C   if desired.
07650 C   GO TO 1056
07700      DO 1056 I=1,600
07750      WRITE(14,4096)i, dp1(i),dp2(i),dp3(i),dp4(i),abs(i)
07800 1056 Continue
07850 4096 Format(16,5f14.7)
07900
07950
08000 C   Calculate tide and water depth. Neglect
08050 C   temperature changes on back-filling fluid.
08100      DEPTH = ((AVGABS*10.-Pbf-atm)/gamma )/12.
08150      TIDE = (DEPTH - SGAGE)
08200 717 Format(./,' TIDE LEVEL IS',F7.3,' FEET.')
08250      WRITE(4,717) TIDE
08300
08350 C   Compare record mean and no-wave condition tare
08400 C   to approximate instrument tilt.
08450
08500      TARE1 = 7.5
08550      TARE2 = 2.31
08600      TARE3 = 2.56
08650      TARE4 = 3.825
08700
08750      t1 = (avg1 - tare1)/5.
08800      t2 = (avg2 - tare2)/5.
08850      t3 = (avg3 - tare3)/5.
08900      t4 = (avg4 - tare4)/5.
08950      g1 = gamma * dxin1
09000      g2 = gamma * dxin2
```

```
09050      g3 = gamma * dx1n3
09100      g4 = gamma * dx1n4
09150
09200      TILT1 = atan2(t1,g1) * 360./twopi
09250      TILT2 = atan2(t2,g2) * 360./twopi
09300      TILT3 = atan2(t3,g3) * 360./twopi
09350      TILT4 = atan2(t4,g4) * 360./twopi
09400
09450      WRITE(4,119) tilt1,tilt2,tilt3,tilt4
09500      119  Format(/, ' POSSIBLE INSTRUMENT TILT (deg)',/
09550      1      5x,'DP1',6x,'DP2',6x,'DP3',6x,'DP4',/,4f9.3,/)
09600
09650      C  Create acceleration terms
09700      DO 56 I=1,N
09750      DPXX(i) = (DP3(i) - DP1(i))/arm13
09800      DPYY(i) = (DP4(i) - DP2(i))/arm24
09850      56  Continue
09900
09950      DO 7034 I=1,600
10000      WRITE(14,7033) dpxx(i),dpyy(i)
10050      7034 Continue
10100      7033 Format(2f16.9)
10150
10200      CALL FFT(dp1,d1i,k,0)
10250      CALL FFT(dp2,d2i,k,0)
10300      CALL FFT(dp3,d3i,k,0)
10350      CALL FFT(dp4,d4i,k,0)
10400      CALL FFT(dpxx,dxxi,k,0)
10450      CALL FFT(dpyy,dyyi,k,0)
10500      CALL FFT(abs,abi,k,0)
10550
10600
10650      C  Generate Pressure Response Function and Wavenumber
10700      C  using the calculated water depth. Sensors are average
10750      C  height of 3.79 feet above bottom.
10800
10850      botcm = depth + 3.79
10900      DO 762 i=2,icut
10950      sigma = twopi/(N*dt) * (i-1)
11000      freq(i) = sigma
11050      call WVLEN (bottom,sigma,www)
11100      wvnr(i) = www/bottom
11150      762  PRSP(i)=cosh(wvnr(i)*(bottom-sgage))
11200      1      /cosh(wvnr(i)*bottom)
11250
11300
11350      C  Divide Fourier coefficients by pressure response
11400      C  function and seawater specific gravity.
11450
11500      CALL HYDRO(icut,prsp,wvnr,abs,abi,dp1,d1i,dp2,d2i,
11550      1      dp3,d3i,dp4,d4i,dpxx,dxxi,dpyy,dyyi,gamma)
11600
11650      C  Create power spectra
11700      DO 67 I=2,icut
11750      AB(i) = 2.0*(abs(i)**2 + abi(i)**2)
11800      D1(i) = 2.0*(dp1(i)**2 + d1i(i)**2)
11850      D2(i) = 2.0*(dp2(i)**2 + d2i(i)**2)
11900      D3(i) = 2.0*(dp3(i)**2 + d3i(i)**2)
11950      D4(i) = 2.0*(dp4(i)**2 + d4i(i)**2)
12000      DXX(i) = 2.0*(dpxx(i)**2 + dxxi(i)**2)
```

```
24050      if(dp4(j).ne.0.0)tan4=atan2(d4(j),dp4(j))
24100      if(dp4(j).eq.0.)tan4 = 0.0
24150      tanu = tan2 - tan1
24200      tanv = tan4 - tan3
24250      tanw = tan2 - tan3
24300      tanz = tan4 - tan1
24350      D12 = sqrt(d1(j))*sqrt(d2(j)) * (cos(tanu)+sin(tanu))
24400      D34 = sqrt(d3(j))*sqrt(d4(j)) * (cos(tanv)+sin(tanv))
24450      D23 = sqrt(d3(j))*sqrt(d2(j)) * (cos(tanw)+sin(tanw))
24500      D14 = sqrt(d1(j))*sqrt(d4(j)) * (cos(tanz)+sin(tanz))
24550      znum = 2*D12
24600      denom = d1(j) - d2(j)
24650      DIR1(j) =ORIENT- (180./3.14159)*0.5*atan2(znum,denom)
24700      znum = 2*D34
24750      denom = d3(j) - d4(j)
24800      DIR2(j) =ORIENT- (180./3.14159)*0.5*atan2(znum,denom)
24850      znum = 2*D23
24900      denom = d3(j) - d2(j)
24950      DIR3(j) =ORIENT- (180./3.14159)*0.5*atan2(znum,denom)
25000      znum = 2*D14
25050      denom = d1(j) - d4(j)
25100      DIR4(j) =ORIENT- (180./3.14159)*0.5*atan2(znum,denom)
25150
25200
25250      IF(dir1(j).lt.0.)dir1(j)=dir1(j)+360.0
25300      IF(dir2(j).lt.0.)dir2(j)=dir2(j)+360.0
25350      IF(dir3(j).lt.0.)dir3(j)=dir3(j)+360.0
25400      IF(dir4(j).lt.0.)dir4(j)=dir4(j)+360.0
25450
25500      435  Continue
25550
25600      CALL BLOCK(icut,dir1,maxblk,blk)
25650      CALL BLOCK(icut,dir2,maxblk,blk)
25700      CALL BLOCK(icut,dir3,maxblk,blk)
25750      CALL BLOCK(icut,dir4,maxblk,blk)
25800
25850
25900      Return
25950      End
26000
26050      C
26100
26150      SUBROUTINE MAXSIG (R,icut,maxfrq,n,dT,nuff,freq)
26200      C Locates "nuff" number of peak energy bands
26250      C and reports their location and relative magnitude.
26300
26350      Dimension R(2050), maxfrq(20), freq(2050),PD(20),
26400      1          exceed(20),A(2050)
26450      NN = Icut - 1
26500      TOT = 0.0
26550
26600      C Identify average energy in spectra
26650      DO 440 1=1,icut
26700      A(1) = R(1)
26750      440      TOT = A(1) + tot
26800      AVRG = TOT/nn
26850
26900      C Identify "nuff" number of peak bands. Calculate each
26950      C peak band's magnitude beyond the average. Set band = 0
27000      C after identification as a maximum in the temporary array.
```

```
27050      DO 445 m=1,nuff
27100      maxfrq(m) = 1
27150      egymax = 0.0
27200      DO 450 j=1,nn
27250      if(A(j+1).lt.EGYMAX) GO TO 450
27300      EGYMAX = A(j+1)
27350      maxfrq(m) = j+1
27400      450 Continue
27450      k = maxfrq(m)
27500      EXCEED(m) = (A(k)-avrg) / avrg * 100.0
27550      PD(m) = 6.28318/freq(k)
27600      A(k) = 0.0
27650      445 Continue
27700
27750      WRITE(4,945)
27800      945 Format(//,' Maximum Energy located at bands: ')
27850      WRITE(4,946) (pd(m),exceed(m),m=1,nuff)
27900      946 Format(f15.3,' exceeds average energy by',
27950      1      f8.2,' %')
28000
28050      Return
28100      End
28150
28200      C
28250
28300      subroutine FCOEFS (ab,abs,abi,d1,dp1,d11,d2,dp2,
28350      1      d21,d3,dp3,d31,d4,dp4,d41,dxx,dpxx,dxx1,dyv,
28400      2      dpyy,dyv,wvnr,freq,thta1,thta2,thta3,
28450      3      a0,a1,a2,a3,b1,b2,b3,b1k,icut)
28500
28550      C      Finds the first nine directional fourier coeffs
28600      C      for a few selected frequencies.
28650      C      This uses only one possible equation for each coef,
28700      C      but calculates each coefficient with all possible
28750      C      combinations of gages for that equation.
28800
28850      DIMENSION ab(2050),abs(4100),abi(2050),
28900      1      d1(2050),dp1(4100),d11(2050),
28950      2      d2(2050),dp2(4100),d21(2050)
29000      DIMENSION d3(2050),dp3(4100),d31(2050),
29050      1      d4(2050),dp4(4100),d41(2050),
29100      2      dxx(2050),dpxx(4100),dxx1(2050),
29150      3      dpyy(2050),dyv(4100),dyv1(2050)
29200      DIMENSION wvnr(2050),freq(2050)
29250      DIMENSION thta1(400),thta2(400),thta3(400)
29300      DIMENSION a0(400),a1(400),a2(400),a3(400),
29350      1      b1(400),b2(400),b3(400)
29400      INTEGER b1k
29450      DIMENSION a1d1(400),a1d3(400),a2d1d2(400),
29500      1      a2d1d4(400),a2d3d2(400),a2d3d4(400),a3d1(400),
29550      2      a3d3(400),b1d2(400),b1d4(400),
29600      3      b2d2d1(400),b2d2d3(400),b2d4d1(400),b2d4d3(400),
29650      4      b3d2(400),b3d4(400)
29700
29750      pi = 3.14159
29800      twopi = 6.283185
29850
29900      DO 510 I=2,icut
29950
30000
```

```
42050      DO 58 i=2,icut
42100      PK = prsp(i) * gamma
42150      abs(i) = abs(i) / PK
42200      abi(i) = abi(i) / PK
42250      a(i) = a(i) / PK
42300      b(i) = b(i) / PK
42350      c(i) = c(i) / PK
42400      d(i) = d(i) / PK
42450      e(i) = e(i) / PK
42500      f(i) = f(i) / PK
42550      g(i) = g(i) / PK
42600      h(i) = h(i) / PK
42650      p(i) = p(i) / PK
42700      q(i) = q(i) / PK
42750      r(i) = r(i) / PK
42800      s(i) = s(i) / PK
42850      58  Continue
42900
42950      Return
43000      End
43050
43100      C _____
43150
43200
43250      Subroutine DIRXSP (a0,a1,a2,a3,
43300      1      b1,b2,b3,freq,n,dT,nuff,maxfrq,orient)
43350      C      We weight the fourier series directional coefs with
43400      C      cosine**2s factors.  Here, s=2.  Then we create a
43450      C      matrix of the frequencies of interest analyzed at
43500      C      incremental degrees.
43550
43600      DIMENSION a0(400),a1(400),a2(400),a3(400),b1(400),
43650      1      b2(400),b3(400),freq(2050),maxfrq(20),
43700      2      S(20,186),deg(186),pd(20)
43750
43800      C      DEGINC is the increment in degrees for which the
43850      C      directional spectra is calculated over.
43900      C      DEGINC = 2.0
43950
44000      C      Weighting factors to smooth directional spectra and
44050      C      eliminate negative side energy lobes:
44100      C      W1 = 66./77.
44150      C      W2 = 15./28.
44200      C      W3 = 5./21.
44250
44300      C      Weighting factors for non-smoothed directional spectra:
44350      C      W1 = 1.
44400      C      W2 = 1.
44450      C      W3 = 0.
44500
44550
44600      C      Print out the directional Fourier coefficients,
44650      C      if desired.  The header follows:
44700
44750      WRITE(4,438)
44800      438  Format(1,' PERIOD',16x,'AO',14x,'A1',14x,'A2',14x,
44850      1      'A3',14x,'B1',14x,'B2',14x,'B3',/,'      ',16x,
44900      2      '      ',14x,'      ',14x,'      ',14x,'      ',14x,
44950      3      '      ',14x,'      ',/),
45000      4005  Continue
```

```
45050      DO 601 NN=1,nuff
45100      save = 0.0
45150      I = maxfrq(nn)
45200      PD(nn) = 6.2831/freq(i)
45300
45350      WRITE(4,439) pd(nn),a0(i),a1(i),a2(i),a3(i),
45400      , b1(i),b2(i),b3(i)
45450      439  Format(f6.2,' secs',7f16.4)
45500
45550      DO 604 m=1,181
45600      deg(m) = save
45650      as = a0(i) + a1(i)*w1 * cosd(deg(m))
45700      1      + a2(i)*w2 * cosd(2.0*deg(m))
45750      2      + a3(i)*w3 * cosd(3.0*deg(m))
45800      bs = b1(i)*w1 * sind(deg(m))
45850      1      + b2(i)*w2 * sind(2.0*deg(m))
45900      2      + b3(i)*w3 * sind(3.0*deg(m))
45950
46000      S(nn,m) = as + bs
46050
46100      save = save + deginc
46150      604  Continue
46200      601  Continue
46250
46300
46350 C  Determine the direction of greatest energy for
46400 C  each band and convert to true north heading from
46450 C  which waves propagate.
46500
46550      WRITE(4,6002)
46600      DO 613 NN=1,NUFF
46650      mBIG = 0
46700      BIG = 0.0
46750      DO 612 m=1,181
46800      IF(S(nn,m).gt.BIG)mBIG = m
46850      612  IF(S(NN,M).gt.BIG)BIG=S(NN,M)
46900      BIGDEG = mBIG * deginc - deginc
46950      BIGDEG = ORIENT - BIGDEG
47000      IF(BIGDEG.lt.0.)BIGDEG=BIGDEG+360.0
47050      WRITE(4,976) nn,BIGDEG
47100      613  Continue
47150      976  Format(' Band',i2,: Greatest Energy at',f7.2,
47200      1      ' deg')
47250
47300 C  Record the directional spectra for each band.
47350 C  Directions correspond to angle from which waves
47400 C  propagate with respect to true north.
47450
47500      WRITE(3,969) (pd(i), i=1,nuff)
47550      DO 615 m=1,181
47600      DEG(m) = ORIENT - DEG(m)
47650      IF(DEG(m).lt.0.)DEG(m)=DEG(m)+360.0
47700      WRITE(3,970) DEG(m),(S(nn,m),nn=1,nuFF)
47750      615  Continue
47800
47850      969  Format (//,' DIRECTIONAL - FREQUENCY SPECTRUM',//,
47900      , ' dirxn',9x,6f17.3,'secs',/)
47950      970  Format ( f8.1, ' deg',3x,6f17.3)
48000      6002 Format(/)
```

```
36050
36100      CALL BLOCK(icut,ab,maxblk,blk)
36150      CALL BLOCK(icut,a0,maxblk,blk)
36200      CALL BLOCK(icut,a1,maxblk,blk)
36250      CALL BLOCK(icut,a2,maxblk,blk)
36300      CALL BLOCK(icut,a3,maxblk,blk)
36350      CALL BLOCK(icut,b1,maxblk,blk)
36400      CALL BLOCK(icut,b2,maxblk,blk)
36450      CALL BLOCK(icut,b3,maxblk,blk)
36500      CALL BLOCK(icut,thta1,maxblk,blk)
36550      CALL BLOCK(icut,thta2,maxblk,blk)
36600      CALL BLOCK(icut,thta3,maxblk,blk)
36650      CALL BLOCK(icut,freq,maxblk,blk)
36700      CALL BLOCK(icut,d1,maxblk,blk)
36750      CALL BLOCK(icut,d2,maxblk,blk)
36800      CALL BLOCK(icut,d3,maxblk,blk)
36850      CALL BLOCK(icut,d4,maxblk,blk)
36900      CALL BLOCK(icut,dxx,maxblk,blk)
36950      CALL BLOCK(icut,dyy,maxblk,blk)
37000
37050      ICUT = MAXblk
37100
37150
37200      Return
37250      End
37300
37350      C
37400
37450      SUBROUTINE FFT(FR,FI,K,ICO)
37500      DIMENSION FR(4100),FI(4100)
37550      N=2**K
37600      IF(ICO.EQ.0) GO TO 10
37650      DO 8 I=1,N
37700      8 FI(I)=-FI(I)
37750      10 Continue
37800      MR=0
37850      NN=N-1
37900      DO 2 M=1,NN
37950      L=N
38000      1 L=L/2
38050      IF(MR+L.GT.NN) GO TO 1
38100      MR=MOD(MR,L)+L
38150      IF(MR.LE.M) GO TO 2
38200      TR=FR(M+1)
38250      FR(M+1)=FR(MR+1)
38300      FR(MR+1)=TR
38350      TI=FI(M+1)
38400      FI(M+1)=FI(MR+1)
38450      FI(MR+1)=TI
38500      2 Continue
38550      L=1
38600      3 IF(L.LE.N) GO TO 7
38650      ISTEP=2*L
38700      EL=L
38750      DO 4 M=1,L
38800      A=3.1415926535*FLOAT(1-M)/EL
38850      WR=COS(A)
38900      WI=SIN(A)
38950      DO 4 I=M,N,ISTEP
39000      J=I+L
```

```
39050      IF(ICO.EQ.1) GO TO 11
39100      TR=WR*FR(J)-WI*FI(J)
39150      TI=WR*FI(J)+WI*FR(J)
39200      GO TO 12
39250 11  TR=WR*FR(J)+WI*FI(J)
39300      TI=WR*FI(J)-WI*FR(J)
39350 12  FR(J)=FR(I)-TR
39400      FI(J)=FI(I)-TI
39450      FR(I)=FR(I)+TR
39500 4  FI(I)=FI(I)+TI
39550      L=ISTEP
39600      GO TO 3
39650 7  Continue
39700      AN=N
39750      IF(ICO.EQ.1) GO TO 6
39800      DO 5 I=1,N
39850      FR(I)=FR(I)/AN
39900 5  FI(I)=-FI(I)/AN
39950 6  RETURN
40000      END
40050
40100
40150  C
40200
40250
40300
40350  C*      SUBROUTINE WVLEN(DPT,SIG,XKH)
40400      C*      THIS SUBROUTINE CALCULATES LINEAR WAVELENGTH BY NEWTONS
40450      C*      METHOD
40450      PI=3.14159265
40500      TWOPi=2.0*PI
40550      XKHO=SIG**2*DPT/32.2
40600      IF(XKHO-6.3) 2,1,1
40650 1  XKH=XKH
40700      GO TO 9
40750 2  XKH=SQRT(XKHO)
40800 3  SH=SINH(XKH)
40850  CH=COSH(XKH)
40900  EPS=XKHO-XKH*SH/CH
40950  SLOPE=-XKH/CH**2-SH/CH
41000  DXKH=-EPS/SLOPE
41050  IF(ABS(DXKH/XKH)-0.0001) 9,9,4
41100 4  XKH=XKH+DXKH
41150      GO TO 3
41200 9  XLENGTH=TWOPi*DPT/XKH
41250      RETURN
41300      end
41350
41400  C
41450
41500      subroutine HYDRO (icut,prsp,wvnr,abs,abi,a,b,c,d,e,
41550      1      f,g,h,p,q,r,s,gamma)
41600  C      Divides through by pressure response function
41650  C      and gamma.
41700  C      Operates on the a(n)' and b(n)' terms from
41750  C      each of the five gages' FFT results.
41800
41850
41900      DIMENSION prsp(2050),wvnr(2050)
41950      DIMENSION abs(2050), abi(2050), a(4100),b(2050),
42000  1      c(4100),d(2050),e(4100),f(2050),g(4100),h(2050),
2      p(4100),q(2050),r(4100),s(2050)
```

```
30050      wvnr(i) = wvnr(i)/12.0
30100      tanab = atan2(abi(i),abs(i))
30150      IF(DP1(I).NE.0.0)
30200      1      TAN1 = atan2(D1I(I),DP1(I))
30250      if(dp1(i).eq.0.0) tan1 = 0.0
30300      if(dp2(i).ne.0.0)
30350      1      tan2 = atan2(d2i(i),dp2(i))
30400      if(d2i(i).eq.0.0) tan2 = 0.0
30450      if(dp3(i).ne.0.0)
30500      1      tan3 = atan2(d3i(i),dp3(i))
30550      if(dp3(i).eq.0.0) tan3 = 0.0
30600      if(dp4(i).ne.0.0)
30650      1      tan4 = atan2(d4i(i),dp4(i))
30700      if(d4i(i).eq.0.00) tan4 = 0.00
30750      if(dpix(i).ne.0.0)
30800      1      tanxx = atan2(dxxi(i),dpix(i))
30850      if(dpix(i).eq.0.0) tanxx = 0.0
30900      if(dpuy(i).ne.0.0)
30950      1      tanyy = atan2(dyui(i),dpuy(i))
31000      if(dyui(i).eq.0.0) tanyy = 0.0
31050
31100      AO(i) = ab(i) / (2.0 * pi)
31150
31200      tanM = tan1 - tanAB
31250      tanN = tan3 - tanAB
31300      A1d1(i) = -1.0/(pi * wvnr(i)) * sqrt(ab(i)) *
31350      1      sqrt(d1(i)) * sin(tanM)
31400      A1d3(i) = -1.0/(pi * wvnr(i)) * sqrt(ab(i)) *
31450      1      sqrt(d3(i)) * sin(tanN)
31500
31550      A2d1d2(i) = -(d2(i) - d1(i))/(wvnr(i)**2*pi)
31600      A2d1d4(i) = -(d4(i) - d1(i))/(wvnr(i)**2*pi)
31650      A2d3d2(i) = -(d2(i) - d3(i))/(wvnr(i)**2*pi)
31700      A2d3d4(i) = -(d4(i) - d3(i))/(wvnr(i)**2*pi)
31750
31800      C      GO TO 4001
31850      tan0 = tanXX - tan1
31900      tanP = tanXX - tan3
31950      tanQ = tan1 - tanAB
32000      tanR = tan3 - tanAB
32050      A3d1(i) = 4.0/(pi * wvnr(i)**3)
32100      1      * (-sqrt(d1(i)) * sqrt(dxx(i)) * sin(tan0))
32150      2      + 0.75 * wvnr(i)**2 * sqrt(ab(i)) * sqrt(d1(i))
32200      3      * sin(tanQ))
32250      A3d3(i) = 4.0/(pi * wvnr(i)**3)
32300      1      * (-sqrt(d3(i)) * sqrt(dxx(i)) * sin(tanP))
32350      2      + 0.75 * wvnr(i)**2 * sqrt(ab(i)) * sqrt(d3(i))
32400      3      * sin(tanR))
32450      4001  Continue
32500
32550      tanS = tan2 - tanAB
32600      tanT = tan4 - tanAB
32650      B1d2(i) = -1.0/(pi * wvnr(i)) * sqrt(ab(i))
32700      1      * sqrt(d2(i)) * sin(tanS)
32750      B1d4(i) = -1.0/(pi * wvnr(i)) * sqrt(ab(i))
32800      1      * sqrt(d4(i)) * sin(tanT)
32850
32900      tanU = tan2 - tan1
32950      tanV = tan2 - tan3
33000      tanW = tan4 - tan1
```

```
33050      tanX = tan4 - tan3
33100      B2d2d1(i) = 2.0/(pi * wvnr(i)**2)
33150      1      * sqrt(d1(i)) * sqrt(d2(i)) * (cos(tanU)+sin(tanU))
33200      B2d2d3(i) = 2.0/(pi * wvnr(i)**2)
33250      1      * sqrt(d3(i)) * sqrt(d2(i)) * (cos(tanV)+sin(tanV))
33300      B2d4d1(i) = 2.0/(pi * wvnr(i)**2)
33350      1      * sqrt(d1(i)) * sqrt(d4(i)) * (cos(tanW)+sin(tanW))
33400      B2d4d3(i) = 2.0/(pi * wvnr(i)**2)
33450      1      * sqrt(d3(i)) * sqrt(d4(i)) * (cos(tanX)+sin(tanX))
33500
33550      C      GO TO 4002
33600      tany2 = tanyy - tan2
33650      tanz2 = tan2 - tanab
33700      tany4 = tanyy - tan4
33750      tanz4 = tan4 - tanab
33800      B3d2(i) = -4.0/(pi * wvnr(i)**3)
33850      1      * (-sqrt(d2(i)) * sqrt(dy(i)) * sin(tany2)
33900      2      + 0.75 * wvnr(i)**2 * sqrt(ab(i)) * sqrt(d2(i))
33950      3      * sin(tanz2))
34000      B3d4(i) = -4.0/(pi * wvnr(i)**3)
34050      1      * (-sqrt(d4(i)) * sqrt(dy(i)) * sin(tany4)
34100      2      + 0.75 * wvnr(i)**2 * sqrt(ab(i)) * sqrt(d4(i))
34150      3      * sin(tanz4))
34200      4002  Continue
34250
34300      510  CONTINUE
34350
34400
34450
34500
34550      DO 511 I=2,icut
34600      C  IF ALL GAGES ARE WORKING, USE THIS LOOP:
34650      GO TO 7
34700      A1(i) = (A1d1(i) + A1d3(i))/2.0
34750      A2(i) = (A2d1d2(i) + A2d1d4(i) + A2d3d2(i)
34800      1      + A2d3d4(i)) / 4.0
34850      A3(i) = (A3d1(i) + A3d3(i))/2.0
34900      B1(i) = (B1d2(i) + B1d4(i))/2.0
34950      B2(i) = (B2d2d1(i) + B2d2d3(i) + B2d4d1(i)
35000      1      + B2d4d3(i)) / 4.0
35050      B3(i) = (B3d2(i) + B3d4(i)) / 2.0
35100      7  Continue
35150
35200      C  IF ONLY TWO DIFFERENTIAL CHANNELS ARE WORKING, USE:
35250      C  GO TO 3077
35300      A1(i) = A1d3(i)
35350      A2(i) = A2d3d2(i)
35400      A3(i) = A3d3(i)
35450      B1(i) = B1d2(i)
35500      B2(i) = B2d2d3(i)
35550      B3(i) = B3d2(i)
35600      3077  Continue
35650
35700
35750      C  Calculate MEAN direction for n=1,2,3
35800      THTA1(i) = atan2(B1(i),A1(i)) * 180./3.14159
35850      THTA2(i) = atan2(B2(i),A2(i)) * 180./3.14159
35900      THTA3(i) = atan2(B3(i),A3(i)) * 180./3.14159
35950
36000      511  Continue
```

```
48050
48100      Return
48150      End
48200
48250
48300
48350
48400      Subroutine SCAN(X,N,NGAGE,AVG,DXINCH)
48450
48500      Dimension X(4100), HIGH(1000)
48550      Real LOW(1000), LOLIM
48600      Integer HISTOP
48650
48700      C Calculates the mean and std.deviation (N-1 weighting)
48750      C for the record.
48800
48850
48900
48950      RUN = 0.0
49000      SUM = 0.0
49050      DO 119 I=1,N
49100      119      SUM = X(I) + sum
49150      AVG = SUM/N
49200
49250      DO 130 I=1,N
49300      130      RUN = (X(I)-AVG)**2 + RUN
49350      DEV = sqrt(RUN/(N-1))
49400
49450      C Reduce those points beyond 3 std.deviations to
49500      C 3 std. deviations beyond record mean or the
49550      C average of neighboring points.
49600
49650
49700      HILIM = AVG + 3.0*DEV
49750      LOLIM = AVG - 3.0*DEV
49800      Khi = 0
49850      Klo = 0
49900      X(1) = AVG
49950      DO 300 I=2,N
50000      IF(X(I).LE.HILIM .and. X(I).GT.LOLIM) GO TO 300
50050      IF(X(I).GT.HILIM) GO TO 150
50100      IF(X(I).LT.LOLIM) Klo = Klo + 1
50150      LOW(Klo) = X(I)
50200      IF(X(i-1).lt.LOLIM.or.X(i+1).lt.LOLIM)
50250      1      X(I) = LOLIM
50300      IF(X(i-1).ge.LOLIM.or.X(i+1).ge.LOLIM)
50350      1      X(I) = (X(i-1)+X(i+1))/2.0
50400      GO TO 300
50450      150      Khi = Khi + 1
50500      HIGH(Khi) = X(I)
50550      IF(X(i-1).gt.HILIM.or.X(i+1).gt.HILIM)
50600      1      X(I) = HILIM
50650      IF(X(i-1).le.HILIM.or.X(i+1).le.HILIM)
50700      1      X(I) = (X(i-1)+X(i+1))/2.0
50750      300      Continue
50800
50850
50900
50950      C Print out truncated points
51000
```

```
51050      LOW(Klo+1) = 900.
51100      HIGH(Khi+1) = 900.
51150      LOSTOP = 0
51200      HISTOP = 0
51250
51300      WRITE(4,875) NGAGE
51350      WRITE(4,890) Klo,Khi,Avg,Dev,Lolim,Hilim
51400      C      WRITE(4,900)
51450
51500      GO TO 400
51550      DO 400 I=1,N
51600      IF(LOW(i).eq.900.) LOSTOP=1
51650      IF(HIGH(i).eq.900.) HISTOP=1
51700      IF(LOSTOP.eq.0 .and. HISTOP.eq.0)
51750      1      WRITE(4,901) LOW(i),HIGH(i)
51800      1      IF(LOSTOP.eq.1 .and. HISTOP.eq.0)
51850      1      WRITE(4,902) HIGH(i)
51900      1      IF(LOSTOP.eq.0 .and. HISTOP.eq.1)
51950      1      WRITE(4,903) LOW(i)
52000      1      IF(LOSTOP.eq.1 .and. HISTOP.eq.1)
52050      1      GO TO 410
52100      400  Continue
52150      410  CONTINUE
52200
52250      C      Average 2 adjacent points to halve the record size.
52300      N2 = N/2
52350      DO 480 I=1,N2
52400      J=I*2-1
52450      X(i) = (X(j)+X(j+1))/2.0
52500      480  CONTINUE
52550
52600      C      Re-calculate mean.
52650
52700      405  SUM = 0.0
52750      DO 440 I=1,N2
52800      440  SUM = X(i) + SUM
52850      AVG = SUM/N2
52900
52950      C      Subtract mean from record and convert from volts
53000      C      to PSI. Divide diff records by distance between
53050      C      sensing points to give pressure differential
53100      C      per length of arm.
53150
53200      DO 450 I=1,N
53250      IF(NGAGE.ne.5) X(i) = ((X(i)-AVG)/5.0)/DXINCH
53300      IF(NGAGE.eq.5) X(i) = (X(i)-avg) * 10.0
53350      450  Continue
53400
53450      875  Format(/,10x,'GAUGE NUMBER',12)
53500      890  Format(16,' LOW truncations',16,' HIGH truncations',/,
53550      1      4x,'Mean=',f6.3,' S.Dev=',f8.5,' Lower Limit=',
53600      2      f6.3,' Upper Limit=',f6.3)
53650      900  Format(4x,'LOW',7x,'HIGH')
53700      901  Format(F8.2,F10.2)
53750      902  Format(8x,F10.2)
53800      903  Format(F8.2)
53850
53900      Return
53950      End
54000
```

```
54050 C
54100
54150
54200      SUBROUTINE BLOCK(n,X,maxblk,blk)
54250      DIMENSION X(4100)
54300      INTEGER BLK,STOP
54350
54400      STOP = (N-BLK)
54450      NM = 1
54500
54550      DO 100 IJ=2,stop,blk
54600      SUM=0.0
54650      MJ=IJ+BLK-1
54700      KJ=IJ
54750      DO 130 KKJ=kj,mj
54800      130      SUM=SUM + X(kkj)
54850      X(nm) = SUM/BLK
54900      NM=NM+1
54950      100 Continue
55000
55050      SUM=0.0
55100      DO 140 kkj=ij,n
55150      140      SUM=SUM + X(kkj)
55200      X(nm) = SUM/(n-mj)
55250
55300      MAXBLK=nm
55350
55400      Return
55450
55500
55550
55600      SUBROUTINE SURF2(ab,d1,d2,d3,d4,ang1,ang2,ang3,ang4,icut,
55650                  wvnr,blk,orient)
55700
55750      1      DIMENSION ab(2050),d1(2050),d2(2050),d3(2050),d4(2050),
55800      1      ang1(400),ang2(400),ang3(400),ang4(400),
55850      2      wvnr(2050)
55900      1      INTEGER blk
55950
56000      C Estimates direction using only absolute gage and one
56050      C differential channel at a time.
56100
56150      pi = 3.14159
56200
56250      DO 300 j=2,icut
56300      z = 1./wvnr(j) * sqrt(d1(j)/ab(j))
56350      IF(Z.LE.1.)ANG1(j)=ORIENT-acos(Z)*180./pi
56400      z = 1./wvnr(j) * sqrt(d1(j)/ab(j))
56450      IF(Z.LE.1.)ANG2(j)=ORIENT-asin(Z)*180./pi
56500      z = 1./wvnr(j) * sqrt(d3(j)/ab(j))
56550      IF(Z.LE.1.)ANG3(j)=ORIENT-acos(Z)*180./pi
56600      z = 1./wvnr(j) * sqrt(d4(j)/ab(j))
56650      IF(Z.LE.1.)ANG4(j)=ORIENT-asin(Z)*180./pi
56700
56750      IF(ang1(j).lt.0.)ang1(j)=ang1(j)+360.0
56800      IF(ang2(j).lt.0.)ang2(j)=ang2(j)+360.0
56850      IF(ang3(j).lt.0.)ang3(j)=ang3(j)+360.0
56900      IF(ang4(j).lt.0.)ang4(j)=ang4(j)+360.0
56950
57000      300 Continue
```

```
57050      CALL BLOCK(icut,ang1,maxblk,blk)
57100      CALL BLOCK(icut,ang2,maxblk,blk)
57150      CALL BLOCK(icut,ang3,maxblk,blk)
57200      CALL BLOCK(icut,ang4,maxblk,blk)
57250
57300      Return
57400      End
57450
57500  C
```

---



Bodge, Kevin R.

The design, development, and evaluation of a differential pressure gauge directional wave monitor / by Kevin R. Bodge.--Fort Belvoir, Va. : U.S. Army, Corps of Engineers, Coastal Engineering Research Center ; Springfield, Va. : available from NTIS, 1982.

[227] p. : ill. : 28 cm.--(Miscellaneous report--U.S. Coastal Engineering Research Center; no. 82-11)

Cover title.

"October 1982."

Report presents a new technique and instrument, the differential pressure gage (DPG), to obtain directional wave data for use in coastal engineering design. DPG data is compared with radar and Baylor gage data, and recommendations for future investigations and development of the DPG system are discussed.

1. Waves. 2. Wave spectra. 3. Wave direction. 4. Wave gage.

I. Title. II. Coastal Engineering Research Center (U.S.).

III. Series: Miscellaneous report (Coastal Engineering Research Center (U.S.)); no. 82-11.

TC203

no. 82-11

627

627

Bodge, Kevin R.

The design, development, and evaluation of a differential pressure gauge directional wave monitor / by Kevin R. Bodge.--Fort Belvoir, Va. : U.S. Army, Corps of Engineers, Coastal Engineering Research Center ; Springfield, Va. : available from NTIS, 1982.

[227] p. : ill. : 28 cm.--(Miscellaneous report--U.S. Coastal Engineering Research Center; no. 82-11)

Cover title.

"October 1982."

Report presents a new technique and instrument, the differential pressure gage (DPG), to obtain directional wave data for use in coastal engineering design. DPG data is compared with radar and Baylor gage data, and recommendations for future investigations and development of the DPG system are discussed.

1. Waves. 2. Wave spectra. 3. Wave direction. 4. Wave gage.

I. Title. II. Coastal Engineering Research Center (U.S.).

III. Series: Miscellaneous report (Coastal Engineering Research Center (U.S.)); no. 82-11.

TC203

no. 82-11

627

Bodge, Kevin R.

The design, development, and evaluation of a differential pressure gauge directional wave monitor / by Kevin R. Bodge.--Fort Belvoir, Va. : U.S. Army, Corps of Engineers, Coastal Engineering Research Center ; Springfield, Va. : available from NTIS, 1982.

[227] p. : ill. : 28 cm.--(Miscellaneous report--U.S. Coastal Engineering Research Center; no. 82-11)

Cover title.

"October 1982."

Report presents a new technique and instrument, the differential pressure gage (DPG), to obtain directional wave data for use in coastal engineering design. DPG data is compared with radar and Baylor gage data, and recommendations for future investigations and development of the DPG system are discussed.

1. Waves. 2. Wave spectra. 3. Wave direction. 4. Wave gage.

I. Title. II. Coastal Engineering Research Center (U.S.).

III. Series: Miscellaneous report (Coastal Engineering Research Center (U.S.)); no. 82-11.

TC203

no. 82-11

627

627

Bodge, Kevin R.

The design, development, and evaluation of a differential pressure gauge directional wave monitor / by Kevin R. Bodge.--Fort Belvoir, Va. : U.S. Army, Corps of Engineers, Coastal Engineering Research Center ; Springfield, Va. : available from NTIS, 1982.

[227] p. : ill. : 28 cm.--(Miscellaneous report--U.S. Coastal Engineering Research Center; no. 82-11)

Cover title.

"October 1982."

Report presents a new technique and instrument, the differential pressure gage (DPG), to obtain directional wave data for use in coastal engineering design. DPG data is compared with radar and Baylor gage data, and recommendations for future investigations and development of the DPG system are discussed.

1. Waves. 2. Wave spectra. 3. Wave direction. 4. Wave gage.

I. Title. II. Coastal Engineering Research Center (U.S.).

III. Series: Miscellaneous report (Coastal Engineering Research Center (U.S.)); no. 82-11.

TC203

no. 82-11

627

no. 82-11

TC203

no. 82-11

627

no. 82-11

627





{  
}{  
}